NASA Contractor Report 181639

ATMOSPHERIC ELECTRICAL MODELING IN SUPPORT

OF THE NASA F-106 STORM HAZARDS PROJECT

John H. Helsdon, Jr.

SOUTH DAKOTA SCHOOL OF MINES AND TECHNOLOGY
Institute of Atmospheric Sciences
Rapid City, South Dakota

NASA

National Aeronautics and
Space Administration

Langley Research Center
Hampton, Virginia 23665

TABLE OF CONTENTS

TABLE OF CONTENTS (continued)

LIST OF FIGURES

LIST OF FIGURES (continued)

LIST OF TABLES

1. INTRODUCTION

With the use of composite (non-metallic) materials and microelectronics becoming more prevalent in the construction of both military and commercial aircraft, the control systems have become more susceptible to damage or failure from electromagnetic transients. One source of such transients is the lightning discharge. In order to study the effects of the lightning discharge on the vital components of an aircraft, NASA Langley Research Center undertook a Storm Hazards Program in which a specially instrumented F106B jet aircraft was flown into active thunderstorms with the intention of being struck by lightning. The overall purpose of the program was to enhance the capability of detecting and avoiding the hazards associated with severe storms and improving design capabilities to protect aircraft systems from unavoidable hazards.

One of the specific purposes of the program was to quantify the environmental conditions which are conducive to aircraft lightning strikes. To this end, the F106 made over 1400 thunderstorm penetrations at altitudes ranging from 3.1 km up to 12.2 km (temperatures from +5°C to -55°C) and obtained at least 690 direct strikes to the airframe (Fisher et al., 1986). Most of the strikes occurred at altitudes in excess of 6 km and temperatures colder than -20°C. Thus, a good data base was established for the study of lightning interaction and environment at higher (colder) altitudes (temperatures). Analysis of these data has shown that the greatest risk of a lightning strike to an airplane occurs at altitudes between 11 and 11.6 km (-40 to -45°C) where turbulence and precipitation intensities were classified as light (Fisher and Plumer, 1984). Analysis of UHF radar observations made during flight operations has indicated that these high altitude lightning strikes were triggered by the aircraft (Mazur et al., 1984).

The results from the Storm Hazards Program are in conflict with compilations of data concerning inadvertent lightning strikes to aircraft which show that most reported strikes occur in the vicinity of 4.5 km altitude, which has been very near the freezing level. Fisher and Plumer (1984) also state that the nature of the high altitude lightning strikes encountered (triggered) by the F106 have been generally of a low amplitude current nature, consistent with the known characteristics of intracloud lightning discharges (although some of the time-resolved characteristics appear to be different than anticipated). The need for a larger data base for the analysis of lightning strike characteristics at lower altitudes where these characteristics are anticipated to be somewhat different became evident. The primary difficulty during the F106 program was the paucity of lightning strikes at altitudes below 6 km. Through 1985, only 75 direct strikes to the aircraft were recorded below 6 km, 11% of the total, with 41 of these 75 occurring in the 1985 field season alone. Virtually all of these strikes occurred in the altitude range from 4.3 to 6 km

(temperatures colder than 0°C) and were apparently triggered by the aircraft (a deduction based on the on-board sensors and UHF-band radar data).

Given the need of obtaining a better data base on lower altitude lightning strikes, an effort was undertaken to determine possible methods of directing the F106 into lower altitude regions of thunderstorms where the probability of a lightning strike would be maximized. This effort involved the work of two organizations, the Institute of Atmospheric Sciences (IAS) at the South Dakota School of Mines and Technology and Electro Magnetic Applications, Inc. (EMA) of Denver, Colorado. As the project evolved, additional interests arose in the triggering capacity of the aircraft and what effect in-cloud environmental characteristics had on the triggering phenomenon. Also, the characteristics of the lightning discharge itself and its interaction with the storm environment were investigated. This report summarizes the results of this scientific investigation during its funding period from 15 March 1984 through 14 June 1987.

2. OBJECTIVES

The objectives of this research program involved the use of the IAS two-dimensional, Storm Electrification Model (SEM) to simulate the thunderstorm environment in which the F106 was operating. The results of the model simulations were initially used in two ways. The first use of the model results was to provide EMA with data on the time evolution and spatial patterns of the electric fields, small ion concentrations, electric charges on cloud and precipitation particles, and the total charge patterns in the simulated cloud. EMA personnel then used these data as initial and boundary values in their modeling studies of the aircraft lightning environment.

The main use of the IAS model simulations was to analyze the results with an emphasis on looking for relationships between the electrical structure of the storm and the basic cloud structure. The intent of this analysis was to determine what observable characteristics of the cloud correlated with strong electric field regions at lower altitudes in the hope of devising a scheme for vectoring the F106 into such regions to increase the lightning strike probability.

An additional objective of the research effort was to develop a lightning parameterization scheme for incorporation into the SEM. The SEM, in its original configuration, was only capable of simulating the development of the electrical aspects of a thunderstorm up to the time of first lightning. Without a scheme for simulating lightning, the buildup of the electric fields and charges would continue without limit, reaching unrealistic values and causing the simulation to terminate because of the necessity of reducing the model time step in order to maintain numerical stability of the electrical transport equations in these high electric fields. In nature, the electrical stresses that build up as the charge separation processes proceed, and the electric field increases, are relieved by the charge transfer that accompanies the lightning discharge. It was felt that an analogue to the lightning discharge needed to be incorporated in the model in order to accomplish the charge transfer and relief of electric stress so that simulations could continue into the mature and decaying stages of thunderstorm evolution. Only in this fashion could the complete evolution of a thunderstorm be studied dynamically, microphysically, and electrically.

In the following sections, the model will be described in detail and the results of the various model experiments will be described.

3. MODEL DESCRIPTION

3.1 The Base Model

The theoretical framework is a deep-convection, slab-symmetric, two-dimensional, time-dependent (2DTD) cloud model which has been applied in the past to several atmospheric convective situations. Atmospheric wind, potential temperature, water vapor, cloud liquid and ice, rain, snow, and graupel/hail (in the form of ice pellets, frozen rain, graupel, and small hail) are the main dependent variables. The model has been developed from the works of Orville (1965), Liu and Orville (1969), Wisner et al. (1972), Orville and Kopp (1977), and Lin et al. (1983). A density-weighted stream function has been used to extend the model to deep convection.

The nonlinear partial differential equations constituting the base model include the first and third equations of motion (from which a vorticity equation is derived), a thermodynamic equation, and water conservation equations (for the three phases). The model has been designed such that mesoscale convergence can be superimposed in the lower levels and divergence in the upper levels. The manner in which such convergence is applied to the model and further details of the hydrodynamic equations can be found in Chen and Orville (1980).

The bulk-water parameterization used in this model divides water and ice hydrometeors into five classes: cloud water, cloud ice, rain, snow, and high density precipitating ice (graupel/hail) with exponential size distributions hypothesized for the three precipitating classes. Figure 1 with an accompanying key in Table 1 shows the primary cloud microphysical processes simulated in the model. Briefly, the production of rain from cloud water is simulated using equations based on the works of Kessler (1969) and Berry (1968). Graupel/hail is generated by the aggregation of snow, by the capture of snow or cloud ice by raindrops (contact freezing), or by the probabilistic freezing of raindrops (Bigg, 1953) due to the inherent ice nuclei content of a specific volume of water at suitably cold temperatures. An approximation to the Bergeron-Findeisen process is used to transform some of the cloud water to snow. Growth of hail is governed by equations for wet and dry growth (Musil, 1970) and shedding of rain from hail is included. Cloud water may be transformed to cloud ice in the region between 0°C and -40°C using an equation developed by Saunders (1957). Natural cloud ice is normally initiated at temperatures of -20°C and colder, using an equation after Fletcher (1962) for the number of natural ice nuclei active. Homogeneous freezing occurs at -40°C. Accretional processes (including riming) involving the various forms of liquid and solid hydrometeors are simulated.

Rain, snow, and graupel/hail have appreciable terminal fall velocities, while cloud water and cloud ice have zero terminal velocity and, hence, follow the airflow. Evaporation of all forms of hydrometeors

(THIS PAGE INTENTIONALLY LEFT BLANK)

TABLE 1

Key to Figure 1

ORIGINAL PAGE IS
OF POOR QUALITY

Symbol	Meaning
P_{IMLT}	Melting of cloud ice to form cloud water, $T \geq T_0$.
P_{IDW}	Depositional growth of cloud ice at expense of cloud water.
P_{IHOM}	Homogeneous freezing of cloud water to form cloud ice.
P_{IACR}	Accretion of rain by cloud ice; produces snow or graupel depending on the amount of rain.
P_{RACI}	Accretion of cloud ice by rain; produces snow or graupel depending on the amount of rain.
P_{RAUT}	Autoconversion of cloud water to form rain.
P_{RACW}	Accretion of cloud water by rain.
P_{REVP}	Evaporation of rain.
P_{RACS}	Accretion of snow by rain; produces graupel if rain or snow exceeds threshold and $T < T_0$.
P_{SACW}	Accretion of cloud water by snow; produces snow if $T < T_0$ or rain if $T \geq T_0$. Also enhances snow melting for $T \geq T_0$.
P_{SACR}	Accretion of rain by snow. For $T < T_0$, produces graupel if rain or snow exceeds threshold; if not, produces snow. For $T \geq T_0$, the accreted water enhances snow melting.
P_{SACI}	Accretion of cloud ice by snow.
P_{SAUT}	Autoconversion (aggregation) of cloud ice to form snow.
P_{SFW}	Bergeron process (deposition and riming) - transfer of cloud water to form snow.
P_{SFI}	Transfer rate of cloud ice to snow through growth of Bergeron process embryos.
P_{SDEP}	Depositional growth of snow.
P_{SSUB}	Sublimation of snow.
P_{SMLT}	Melting of snow to form rain, $T \geq T_0$.
P_{GAUT}	Autoconversion (aggregation) of snow to form graupel.
P_{GFR}	Probabilistic freezing of rain to form graupel.
P_{GACW}	Accretion of cloud water by graupel.
P_{GACI}	Accretion of cloud ice by graupel.
P_{GACR}	Accretion of rain by graupel.
P_{GACS}	Accretion of snow by graupel.
P_{GSUB}	Sublimation of graupel.
P_{GMLT}	Melting of graupel to form rain, $T \geq T_0$. (In this regime, P_{GACW} is assumed to be shed as rain.)
P_{GWET}	Wet growth of graupel; may involve P_{GACS} and P_{GACI} and must include P_{GACW} or P_{GACR}, or both. The amount of P_{GACW} which is not able to freeze is shed to rain.

PRECEDING PAGE BLANK NOT FILMED
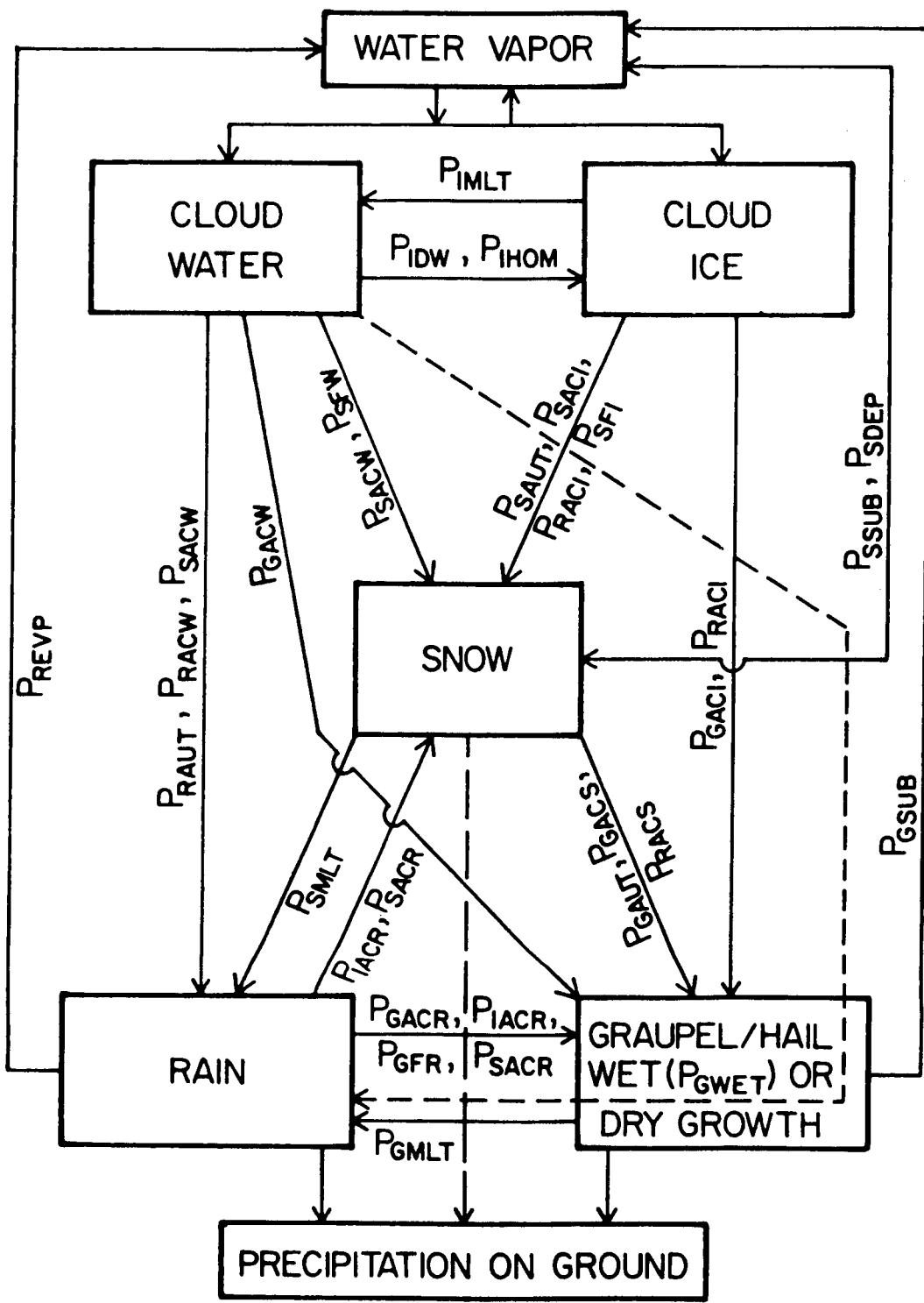
Fig. 1: Cloud physics processes simulated in the model. See Table 1 for an explanation of the symbols.

and the melting of snow and graupel/hail are also simulated. For a more detailed discussion of this base model, the reader is referred particularly to Orville and Kopp (1977) and Lin et al. (1983).

3.2 The Electrical Model

This base model has been modified to include various processes involved in thundercloud electrification. These modifications involved the coupling of the electro-microphysical processes which account for the charge exchange between interacting particles within the cloud domain. The means of coupling the electro-microphysics to the dynamics and microphysics of the base model are based on ideas from Chiu (1978), Helsdon (1980), and Kuettner et al. (1981). Each of the five classes of hydrometeors is allowed to have a charge associated with it. This charge is then transported with the species of hydrometeor according to the general equation

$$\frac{\partial Q}{\partial t} = -\vec{V} \cdot \nabla Q + \frac{1}{\rho_a} \frac{\partial}{\partial z} (U_t Q \rho_a) + \nabla \cdot K_m \nabla Q \pm \left(\frac{\delta Q}{\delta t}\right)_{inter} , \qquad (1)$$

where Q represents the charge density (C m^{-3}) carried by the hydrometeor class (positive or negative), $\vec{V}$ is the 2D velocity vector, ρ_a is the air density, U_t is the mass-weighted mean terminal fall speed of the hydrometeor class, K_m is the nonlinear eddy coefficient and $(\delta Q/\delta t)_{inter}$ represents the charge exchanged between classes of hydrometeors due to interactions. The first term on the right is the advection term, the second is the fallout term (zero for cloud water and cloud ice charge, which are assumed to move with the airflow), and the third is the eddy mixing term. The last term in (1) will be discussed below.

The model framework accounts for the presence of small ions as well. The equation governing the number concentration of small ions is

$$\frac{\partial n_{1,2}}{\partial t} = -\nabla \cdot [n_{1,2}\vec{V} \pm n_{1,2}\mu_{1,2}\vec{E} - K_m \nabla n_{1,2}] + G - \alpha n_1 n_2 + Src - Sink. \qquad (2)$$

Here $n_{1,2}$ is the concentration of small ions (the subscript 1 representing positive ions and 2 the negative ions); μ is the small ion mobility (m^2 V^{-1} sec^{-1}, pressure dependent); $\vec{E}$ is the 2D electric field vector; G is the ion generation rate due to cosmic ray ionization (ions m^{-3} sec^{-1}, dependent on height); α is the ion-ion recombination coefficient (1.6 x 10^{-12} m^3 sec^{-1}); Src is the source term for small ions from processes other than cosmic ray ionization; and $Sink$ is the sink term for small ions from processes other than recombination. An example of a source process for small ions would be the

evaporation of a charged hydrometeor, while a sink process would be Wilson capture (ion attachment to hydrometeors).

With the various types of charges accounted for in the model, a total charge density can be diagnosed at each grid point from

$$\rho = e(n_1-n_2) + \Sigma Q \quad , \tag{3}$$

where ρ is the total charge density (C m^{-3}) and e is the electronic charge (1.6 x 10^{-19} C). The first term represents the net charge due to the difference in small ion concentrations and the last term represents the net charge on the five classes of hydrometeors. With the net charge determined, we then use Poisson's equation

$$\nabla^2\phi = \rho/\epsilon \tag{4}$$

to determine the scalar electric potential, ϕ (Volts). In (4), ϵ is the electrical permittivity of air (8.86 x 10^{-12} kg^{-1} m^{-2} sec^2 C^2). Finally, the 2D electric field vector can be determined from the potential via Gauss's law

$$\vec{E} = -\nabla\phi \quad . \tag{5}$$

The last term in (1) represents the charge exchanged between any two classes of hydrometeors during an interaction between those two classes. Such interactions may be accretional or non-accretional in nature. It should be noted that, in such interactions as P_{iacr} in Fig. 1 (Table 1), where cloud ice is nucleating rain to form snow, the charge on the cloud ice and rain are summed and the total is introduced into the snow charge resulting in a three bodied type of transfer.

In the collisional process where a finite separation probability exists, two types of electrical interactions are possible: inductive processes, where the ambient electric field strength and its orientation with respect to the particles influence the magnitude and sign of the charge transfer; and non-inductive processes, where the ambient field exerts no influence, but such factors as temperature, liquid water content, and impact speed determine the charge transfer. The model has been configured to allow for the accounting of both inductive and non-inductive processes either individually or in concert. This is accomplished by starting with the following representation of the charge transferred between two interacting particles,

$$\Delta q = \Delta Q + 4\pi\epsilon\gamma_1 |\vec{E}| \cos(\vec{E}, \vec{r}_{LS}) r_s^2 + Aq_L - Bq_S \quad , \tag{6}$$

where ΔQ is the charge transferred due to any <u>non-inductive</u> process, γ_1 is a dimensionless variable which depends on the ratio of the radii of the two interacting particles, $\vec{r}_{LS}$ is the vector along the line joining the centers of the two particles at the time of impact, r_s is the radius of the smaller particle, q_L (q_S) is the charge already existing on the large (small) particle, and A (=1-B) is a dimensionless variable which depends on the radius ratio of the two hydrometeors. The first term, then, represents the non-inductive charge transfer, while the second term represents the inductive transfer. The last two terms account for the effect of charge already residing on the hydrometeors. Switches are used to activate/deactivate either process.

A single large hydrometeor may interact with many smaller particles in a unit time, so we integrate over the volume swept out by the large particle

$$\frac{\partial q_L}{\partial t} = \int E_f |\vec{V}_{SL}| N_S \Delta q S(\alpha) dA \tag{7}$$

to obtain the charge acquired per unit time by the large particle. In (7), E_f is the collision efficiency between the two particles, $|V_{SL}|$ is the relative impact speed, N_S is the number concentration of the smaller particles, Δq comes from (6), and $S(\alpha)$ is the angle-dependent separation probability. The integration results in three possible charging rates for the larger hydrometeor depending on which charge transfer mechanisms are active

$$\frac{\delta q_L}{\delta t} = C_1 \left\{ C_2 + Bq_S - Aq_L \right\} \quad , \tag{8}$$

where $C_1 = E_f |\vec{V}_{SL}| N_S \pi r_L^2 <S>$ (r_L being the radius of the large particle and $<S>$ is the mean separation probability) and

$$C_2 = \begin{cases} -\Delta Q & \text{non-inductive,} \\ 4\pi\epsilon\gamma_1 |\vec{E}| \cos(\vec{E}, \vec{V}_{SL}) r_s^2 <\cos\alpha> & \text{inductive,} \\ 4\pi\epsilon\gamma_1 |\vec{E}| \cos(\vec{E}, \vec{V}_{SL}) r_s^2 <\cos\alpha> - \Delta Q & \text{combined.} \end{cases} \tag{9}$$

Note that in (9) there are two important angles influencing the charge exchange: 1) the angle between the electric field vector and relative velocity vector of the two particles $[\cos(\vec{E},\vec{V}_{SL})]$; and 2) the average collision contact angle ($<\cos\alpha>$). For all practical purposes, the quantity $|\vec{E}| \cos(\vec{E},\vec{V}_{SL})$ is adequately approximated by $-E_z$, the negative of the vertical electric field component.

Since (8) implies that multiple charging interactions are possible for a precipitating hydrometeor per unit time of fall, and since the charge on the large particle appears on the right-hand side of the equation, it is not safe, a priori, to assume that $\delta q_L/\delta t$ is constant over a given time step. To account for this, we integrate (8) over the length of a time step, Δt, to obtain the charge transferred to the larger particle assuming that all quantities on the right-hand side are constant except q_L. This may seem like a contradiction at first since both the electric field, $|\vec{E}|$, and the charge on the small particles, q_s, appear on the right-hand side and would seem to be subject to time variation as well. It is safe to assume the constancy of q_s, since it is highly unlikely that any one cloud droplet or ice crystal will undergo more than one non-accretional collision per time step. In the case of the electric field strength, it is a much more macroscopic quantity, being determined by the entire charged volume of the cloud and not so significantly by the local charge changes exhibited by individual particles, although the effects of local volumes dominate. In spite of this, we do admit that the field can change rapidly on a local scale, but one other factor exists to help substantiate our locally steady assumption. This is the fact that the time step in the model is dependent on the electric field strength through the field's interaction with the small ion flux term. In order to maintain the stability of the ion transport equations, the time step must be reduced as the field strength increases. By the time the electric field has reached significant levels, the time step has been reduced to values of one second or less. Thus, we apply the steady field assumption with some confidence.

Carrying out the integration of (8) results in the following expression for the charge accumulated by a precipitating hydrometeor during a time step Δt,

$$\Delta q_L = (Q_m - q_{L0}) \left(1 - e^{-\Delta t/\tau_1}\right) \quad , \tag{10}$$

where q_{L0} is the initial charge on the large particle, and the parameters Q_m and τ_1 are given by

$$Q_m = \begin{cases} (-\Delta Q + Bq_s)/A & \text{non-inductive,} \\[2ex] (4\pi\epsilon\gamma_1\cos(\vec{E},\vec{V}_{LS})r_s^2\langle\cos\alpha\rangle + Bq_s)/A & \text{inductive,} \\[2ex] (4\pi\epsilon\gamma_1\cos(\vec{E},\vec{V}_{SL})r_s^2\langle\cos\alpha\rangle - \Delta Q + Bq_s)/A & \text{combined,} \end{cases} \quad (11)$$

and

$$\tau_1 = (E_f|\vec{V}_{SL}|N_s\pi r_L^2\langle S\rangle A)^{-1} \quad . \quad\quad (12)$$

Finally, the charge accumulated by one precipitating hydrometeor is multiplied by N_L, the number concentration of the large particles, in order to arrive at the total charge density created by interactions, which appears as part of the last term in (1). The other components of the last term in (1) include the accretional terms, evaporational processes, and ion attachment processes. Examples of the formulation of the attachment and accretional processes are available in Chiu (1978) and Helsdon (1980).

3.2.1 Charging processes

A great deal of laboratory and theoretical work has been, and continues to be done to investigate possible mechanisms of charge separation. A non-exhaustive list of possible mechanisms includes: 1) selective ion capture (Wilson, 1929); 2) convective charging (Vonnegut, 1955); 3) induction charging involving non-accretional collisions between various classes of particles in the electric field (Sartor, 1961, 1967, 1981; Muller-Hillebrand, 1954; Paluch and Sartor, 1973); 4) effects of freezing potentials during wet growth of hail or splashing collisions between graupel and raindrops (Workman and Reynolds, 1948, 1950; Latham and Warwicker, 1980; Shewchuk and Iribarne, 1971); 5) non-inductive charging during the riming of graupel (Reynolds et al., 1957; Buser and Aufdermaur, 1977; Takahashi, 1978; Gaskell and Illingworth, 1980; Jayaratne et al., 1983); 6) riming of graupel followed by splintering (Latham and Mason, 1961; Hallett and Saunders, 1979); and 7) evaporative charging of ice crystals in penetrative downdrafts (Telford and Wagner, 1979). It is entirely possible that all of these mechanisms (or some as yet undiscovered mechanism) are active to one degree or another in various thunderstorm situations. However, in order to minimize the degree of complexity involved in the modeling work, it was necessary to limit the mechanisms included in the model to a workable set.

The basic charge separation mechanisms included within the model can be broken down into four basic categories:

1) Graupel interacting with particles in a dry growth mode.

2) Graupel interacting with particles in a wet growth mode.

3) Rain interacting with cloud droplets.

4) Small ions interacting with all classes of hydrometeors.

Within these various categories, the two types of electrical interactions discussed above may be possible, i.e., inductive and/or non-inductive transfers.

The inductive water-water charge transfer interaction is generally believed to be ineffective in producing electrification typical of thunderstorm conditions on its own. Jennings (1975) has shown that such a process is capable of producing early electrification in clouds with fields up to 30 kV/m being possible. After this threshold is reached, the mechanism extinguishes itself due to the presence of such a field causing all collisions to result in permanent coalescence. This ability to generate early electrification well below thunderstorm values, but significantly above the background fair weather field, may affect the nature of other electrification mechanisms which must await the formation of ice particles for their initiation.

The charge separation resulting from the interaction of liquid drops and ice particles may be of a non-inductive or inductive nature. Kuettner et al. (1981) have summarized the controversy regarding the action of a non-inductive, ice-water charging mechanism. They chose to include such a process in their model (using conservative values for the charge transferred per collision) based on the lack of conclusive evidence for eliminating the mechanism and the fact that the riming process is a well established microphysical phenomenon in thunderclouds.

The non-inductive, ice-ice process is the subject of as much controversy as the water-ice mechanism; however, the controversy does not center around whether the process is effective, but rather exactly what physical mechanism is responsible for the charge exchange and, to a lesser degree, the magnitude of the charge transferred. Results have been summarized and assessed by Gross (1982).

The inductive mechanisms involving water-ice and ice-ice interactions have been argued as being ineffective in nature because only grazing collisions near the electrical equator result in separation of particles and charge in the ice-water case, and because of a relaxation time limitation on charge migration in the ice-ice case. In the ice-water case, it is true that grazing collisions will result in minimal charge separation; however, Sartor (1981) has shown that, due to the surface roughness of graupel particles, cloud droplets can bounce off of such rough particles from almost any impact angle negating the above restriction. In addition, the results of Tzur and Levin (1981) and Kuettner et al. (1981) have indicated that the combination of inductive and non-inductive mechanisms involving the ice phase yield the most realistic results.

-13-

With this discussion in mind and referring to Fig. 1 and Table 1 for the interactions listed below, the model in its present configuration can account for both inductive and non-inductive charge transfers when rain (P_{gacr}), cloud ice (P_{gaci}), and snow (P_{gacs}) interact with graupel in category (1). In category (2), graupel can interact with rain and cloud water (P_{gacr} and P_{gacw} through P_{gwet}) with the result that excess water is shed as rain (the wet growth process). In this category, only inductive charge transfers are accounted for due to uncertainty about the actual microphysical interactions taking place. In category (3), a limited inductive mode transfer is allowed. In addition, both inductive and non-inductive charge transfers are allowed when cloud ice interacts with snow. The category (4) interactions involving small ions have been described above.

3.3 Initialization

3.3.1 Environmental initialization

The base state of the atmosphere for this model is taken from a rawinsonde sounding typical of the type of day being studied. This sounding of temperature and moisture is, hopefully, representative of the atmosphere near the time of the formation of an observed cloud which may be compared with the model simulation, if such observations are available. The only modification made to the original sounding is to make the lowest layer adiabatic (if it is not already in such a state). The atmospheric winds are determined by projecting the winds from the sounding in the direction of the storm motion, since the model is two-dimensional. In addition, the winds determined by this procedure are frequently reduced to some percentage of their original value because the use of full winds has a tendency to propagate the simulated cloud off the grid too rapidly.

In order to initiate convection, we use a combination of random perturbations in temperature and water vapor in the lower 3 km of the grid (with maximum amplitude $\pm 0.5°C$ and $\pm 7\%$) and a warm bubble in the vicinity of the domain center. The bubble has a maximum deviation of $1.5°C$, is 4.8 km wide, and is present between 400 m and 2 km height.

3.3.2 Electrical initialization

We assume that an initial steady state exists with ion production due to cosmic ray generation, ion loss due to recombination, and ion transport due to conduction in the ambient electric field all balancing. We ignore ionic diffusion and invoke horizontal homogeneity so that the initial values of the variables are functions of height only. Then the aforementioned steady state balance can be described by

$$\frac{d}{dz} (\mu_1 n_1 E_z) = G(z) - \alpha n_1 n_2 \tag{13a}$$

and

$$\frac{-d}{dz} (\mu_2 n_2 E_z) = G(z) - \alpha n_1 n_2 \quad . \tag{13b}$$

The terms in these equations have been previously defined. E_z is the assumed fair weather electric field profile patterned after Gish (1944) which exhibits an exponential decrease with height such that

$$E_z = E_0[b_1 \exp(-a_1 z) + b_2 \exp(-a_2 z) + b_3 \exp(-a_3 z)] \quad . \tag{14}$$

In (14), the parameters E_0, b_i, and a_i are varied to adjust the vertical profile. This vertical electric field profile can be related to the small ion densities by the one-dimensional form of Gauss's law

$$\frac{dE_z}{dz} = \frac{e(n_1 - n_2)}{\epsilon} \quad . \tag{15}$$

We subtract Eq. (13b) from (13a) and integrate in the vertical to obtain

$$e(\mu_1 n_1 + \mu_2 n_2) = \lambda_T E_z = J_c \quad , \tag{16}$$

where λ_T is the total conductivity of the air and J_c (A m^{-2}) is the fair weather air-earth conduction current, which is assumed constant with height. Equations (15) and (16) can be solved simultaneously for n_1 and n_2 yielding

$$n_1 = \left(\frac{J_c}{E_z} + \mu_2 \epsilon E_z' \right) \frac{1}{e(\mu_1 + \mu_2)} \tag{17a}$$

and

$$n_2 = n_1 - \frac{\varepsilon E_z'}{e} \quad . \tag{17b}$$

If we assume, following Shreve (1970), that the polar ionic mobilities vary exponentially with height such that

$$\mu_{1,2} = c_{1,2} \exp(\beta z) \quad , \tag{18}$$

where $c_1 = 1.4 \times 10^{-4}$ and $c_2 = 1.9 \times 10^{-4}$ m^2 V^{-1} sec^{-1}, and $\beta = 1.4 \times 10^{-4}$ m^{-1}, then (17a) and (17b) define the initial profiles for positive and negative small ions. Finally, either (13a) or (13b) may be solved for the galactic cosmic ray generation function $G(z)$ which, after some algebraic manipulation, yields

$$G(z) = \frac{\mu_1 \mu_2 \varepsilon}{e(\mu_1 + \mu_2)} [\beta E_z E_z' + (E_z')^2 + E_z E_z''] + \alpha n_1 n_2 \quad . \tag{19}$$

The initial fair weather electrical state of the atmosphere is determined from Eqs. (14) and (17) - (19) by choosing appropriate values of E_0, a_i, b_i, and J_c. Since there are generally no specific observations upon which to base the selection of these parameters, values are chosen that produce profiles which are consistent with historical measurements.

3.4 Boundary Conditions

The top boundary is assumed to be rigid with all variables held constant. The vorticity, vertical velocity, rain, snow, graupel, cloud water, and cloud ice as well as their associated charges are all set to zero. The stream function, entropy, water vapor mixing ratio, small ion concentration, and electric potential are maintained undisturbed at their initial values. The potential at the top of the model is obtained by integrating (5) over the depth of the domain and employing (14) for the electric field profile.

At the lower boundary, the vertical velocity, vorticity, and stream function are set to zero. The electric potential is also set to zero, consistent with the assumption that the earth's surface is a conducting plane. Evaporation and heating rates at the surface are prescribed as functions of time. Heat and water vapor are allowed to diffuse into the lower boundary. Clouds are not permitted to form at the surface, but precipitation is allowed to fall through the surface level. Cloud shadow effects (on heating) are also simulated at the lower boundary.

At the lateral boundaries, the horizontal gradients of the stream function and the potential are assumed to be zero. Diffusional transport also assumes horizontal gradients of zero for all variables at the lateral boundaries. Both inflow and outflow from the domain are allowed. The constraints on the potential at the various boundaries result in the electric field components $E_x = 0$ at all boundaries and E_z being calculated at all boundaries.

3.5 Numerical Techniques

The equations are solved over a 19.2 km x 19.2 km or a 30 km x 20 km domain with a 200 m grid interval in both the X and Z directions. The advection technique used is that of Crowley (1968), which is first-order accurate in time and second-order in space. A two-step advection scheme is used (Leith, 1965) with vertical advection calculated first, followed by horizontal advection. Model variables are held constant at lateral inflow boundaries, whereas extrapolation via upstream differencing is employed at outflow boundaries. The general purpose Helmholtz solver in Cartesian coordinates (from the NCAR program library) is used to solve the Poisson-type equations for stream function and electrical potential. Centered differences are used throughout except at the upper and lower boundaries where second order, one-sided differences are used.

3.6 Final Considerations

The lightning parameterization has been developed as part of the model structure, but will be described later in the context of its historical development within the overall framework of this research. The following section will enumerate the results of the research.

4. RESEARCH RESULTS

4.1 Wallops Island Simulation

The first use of the SEM in connection with the Storm Hazards project was to simulate the 12 September 1983 operational flight of the F106 (flight 83-053) which experienced two lightning events near 28 kft during separate cloud penetrations. This simulation is termed a blind case because there were no specific observations with which the model results could be compared for verification.

The SEM was initiated using the Wallops Island, Virginia, 00Z sounding from 13 September 1983, shown in Fig. 2, which was near the time of the flight operations (2215-2258 GMT) and was considered characteristic of the atmospheric state in which the storms were developing. The temperature has been modified in the lowest hundred millibars to make the profile adiabatic, as described in Section 3.3.1. Examination of the sounding shows that the Lifted Index is -6.7 and the K Index is 42.1, indicating a very high potential for strong thunderstorms on that day. In fact, severe thunderstorms might have been expected except for the fact that the upper level winds were quite light and exhibited little shear. Much convective activity was actually observed on that day. With this sounding as input for the model, we expected strong convection to develop.

Figure 3 shows the characteristics of the modeled storm resulting from the simulation at two different simulation times: 15 and 22.5 min. The left column contains plots at 15 min, while the right column shows the same plots at 22.5 min. The plots from top to bottom represent the dynamical and microphysical character of the cloud (see plot caption for details), radar reflectivity, vertical velocity, total charge density, vertical electric field component, and the horizontal electric field component. As is evident from Fig. 3, the model simulation of this warm-based (~16°C), maritime type storm showed a very rapid development with rain formation proceeding via the stochastic coalescence process, well before the ice phase became significant. Note the nearly vertical development of the storm due to the lack of wind shear.

The early charge distribution and resulting weak electric fields were a result of the limited inductive interactions between raindrops and cloud droplets. Once the ice phase appeared, the charge separation processes became more vigorous and, in the course of a few minutes, charge densities reached the order of 10's of nanocoulombs per cubic meter, accompanied by electric field strengths in excess of 400 kV/m, a value near that necessary to produce lightning breakdown. The "classic" thunderstorm dipole structure (positive charge above negative) was produced in the simulation with a lower positive charge region also in evidence, although there were no observations upon which to judge the correctness of these results.

Dry adiabats

Saturation
adiabats

Temperature (°C)

Pressure (mbars)

Saturation/mixing
ratio (g/km)

Temperature (°C)

Fig. 2: Wallops Island, VA (WAL) sounding for 00Z, 13 September 1983.
Solid curve is temperature. Dashed curve is dewpoint.
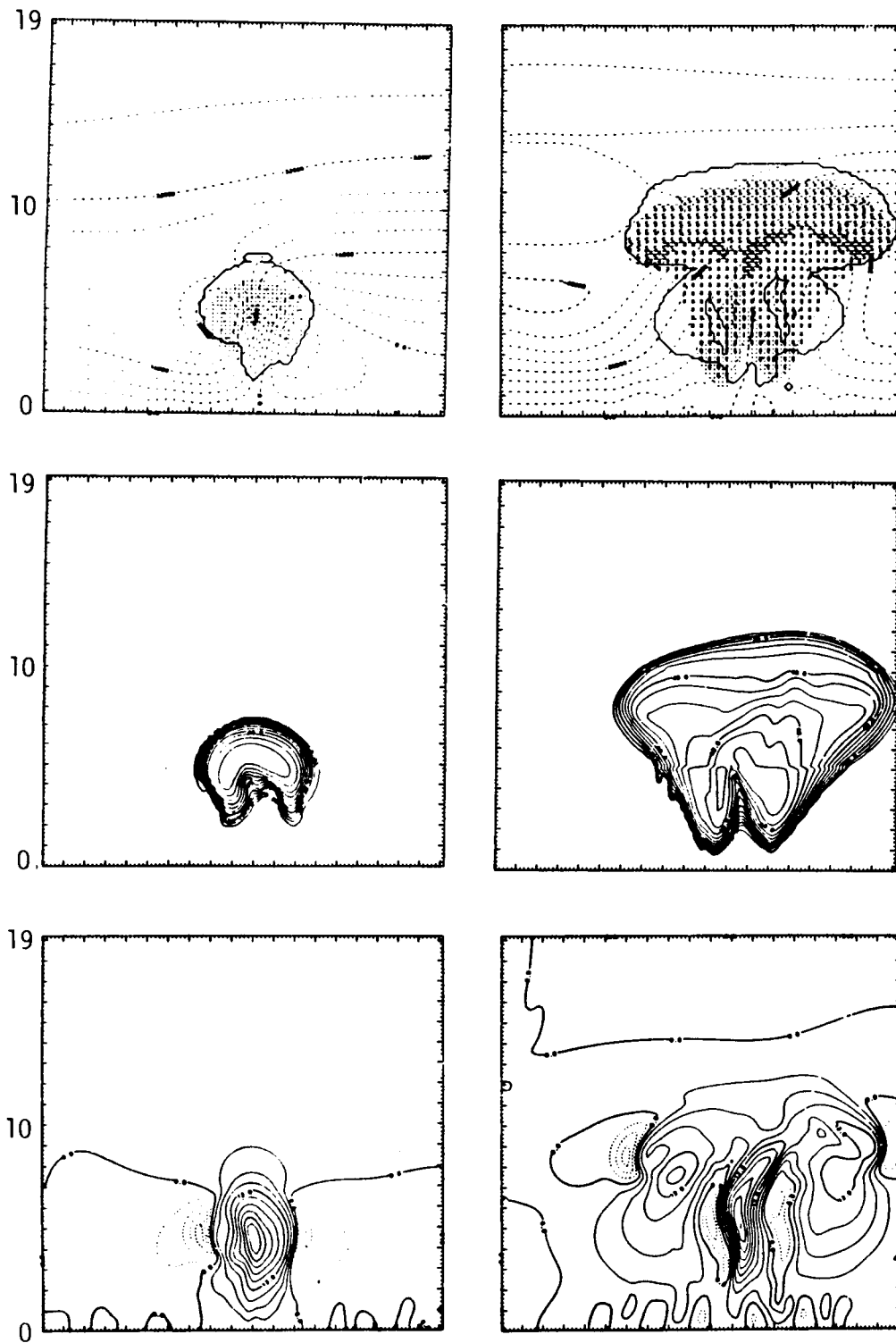
Fig. 3: Characteristics of the Wallops case for two different simulation times: left column, 15 min; and right column, 22.5 min. Reading from top to bottom, the plots represent: 1) storm dynamical and microphysical character including airflow streamlines (dashed lines), cloud boundary (solid line), and presence of snow (S), graupel (*), rain (•), and cloud ice (-) in amounts greater than a threshold value; 2) radar reflectivity in dBz (absolute values systematically too high, but structure is representative, contour interval 4 dB at 15 min, 5 dB at 22.5 min;
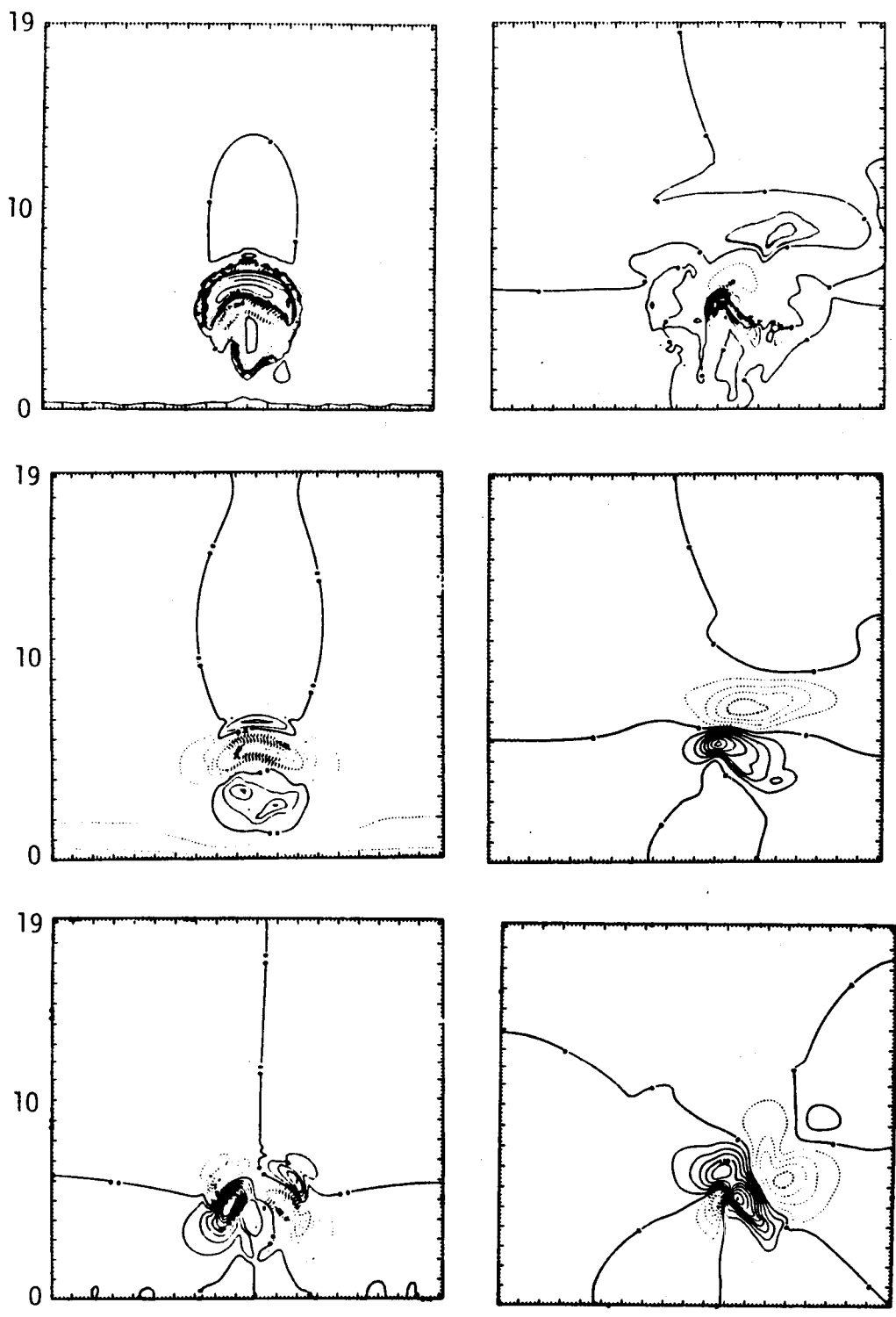
Fig. 3 (continued):
3) vertical velocity in m sec^{-1} (updraft-solid, downdraft-dashed, contour interval 3 m sec^{-1}); 4) total charge density in C m^{-3} (positive-solid, negative-dashed, contour intervals 0.9 pC.m^{-3} at 15 min, 1 nC m^{-3} at 22.5 min); 5) vertical electric field in V m^{-1} at 15 min, 60 kV m^{-1} at 22.5 min); 6) horizontal electric field (as per the vertical field, contour intervals 20 V m^{-1} at 15 min; 30 kV m^{-1} at 22.5 min).

The model run for this Wallops Island case had to be terminated after 22.5 minutes of simulated real time due to the continued buildup of the electric fields and the resulting prohibitively small time steps necessary to maintain computational stability of the ion transport equations. A simulation without the electrical processes active was run much longer in time. The inclusion of the lightning discharge in the model is necessary to overcome this early termination problem.

Although the electrical simulation had to be terminated prematurely, the outputs provided information on the electrical environment which might be expected during the early stages of thunderstorm development. These data in a form similar to Figs. 3 and 4, including electric fields, particle densities and charges, and ion densities at various altitudes and times within the simulated thunderstorm, were sent to EMA for use in conjunction with their 3D interaction model (Rudolph et al., 1984). The plots in Fig. 4 represent measurements which an instrumented aircraft would record if it made a level pass through the model storm at a given altitude. From these plots, EMA scientists were able to extract information considered representative of the environment in which the F106 might have operated.

Part of their work involved a determination of the shape factors due to the aircraft necessary to interpret the electric field mill data which is recorded during each F106 flight. Another aspect of their research was to do a parameter study of the aircraft under various electrical initial conditions using data from the SEM simulation, where appropriate. Their results (Rudolph and Perala, 1985), analyzing the data from the electric field mills at the time of a lightning strike to the aircraft during flight 83-053, showed that the field was predominantly vertical and negative in value. From examination of Fig. 4 at 22.5 min, the model predicts an environment in the neighborhood of 28,000 ft which is approaching conditions suitable for lightning activity (electric fields in excess of 300 kV/m), indicating that the model is capable of generating an environment which is similar to that which was observed.

The investigation of the low altitude strike problem is aided by looking at some of the model results. Figure 5 shows contour plots of the vertical electric field component (left panel) with solid contours indicating an upwardly directed (positive) field and dotted contours representing downwardly directed (negative) fields. The interval of each contour is 60 kV/m with the zero line indicated. The right panel represents the mixing ratio of graupel in the cloud in grams of graupel per kilogram of dry air. The contour interval in this panel is 1 g/kg. These plots represent the state of these two model variables for the Wallops Island simulation at 22.5 minutes after the initiation of the run.

The three horizontal lines drawn through the contour plots represent three possible flight altitudes for the F106. The dashed
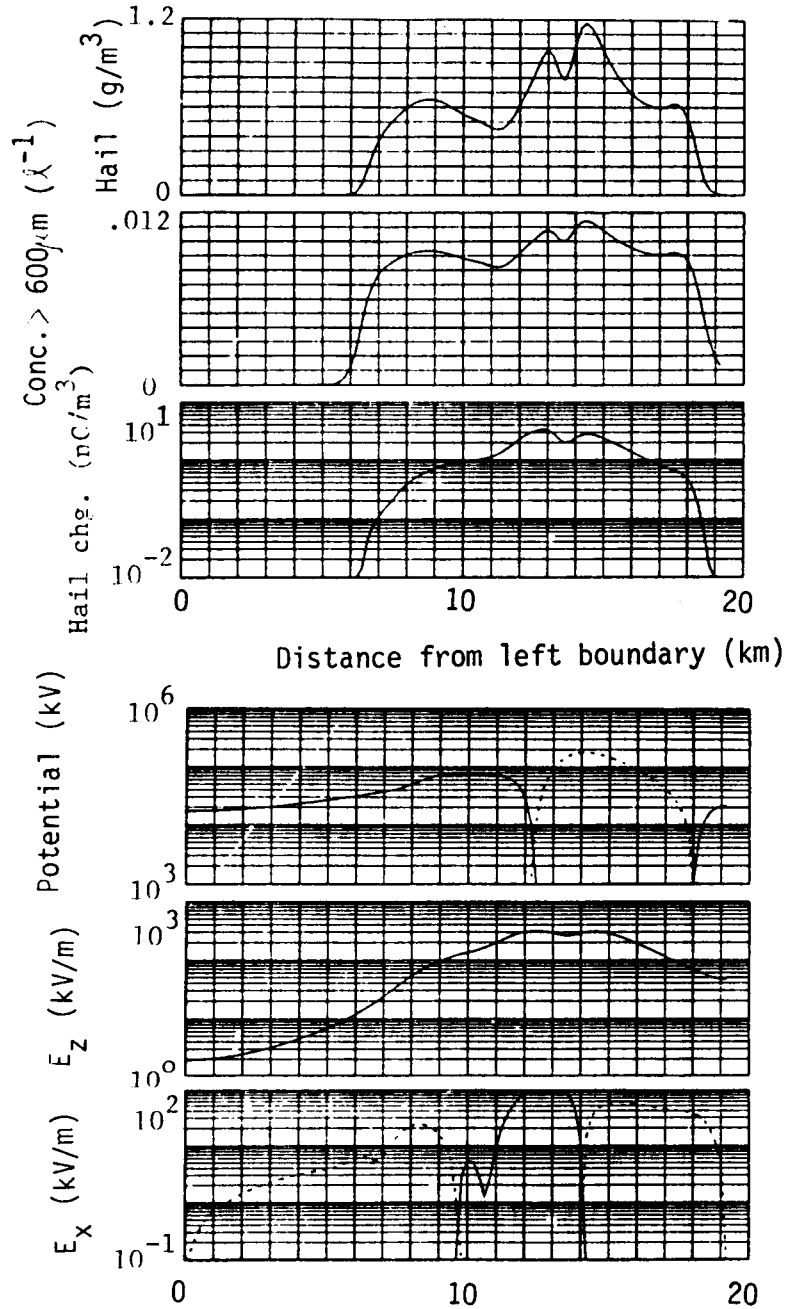
Fig. 4: Examples of measurements which would be recorded by an instrumented aircraft flying a horizontal path through the modeled storm at 8.4 km AGL and 22.5 min simulation time. Top plot: hail (graupel) content in g m^{-3}, number of graupel particles ℓ^{-1} with diameters > 600 μm, and charge on the graupel particles in nC m^{-3} (positive charge-solid line, negative charge-dashed line). Bottom plot: potential above ground in kV, vertical electric field component (E$_z$) in kV m^{-1} (positive-solid, negative-dashed), and horizontal field component (E$_x$) in kV m^{-1}.
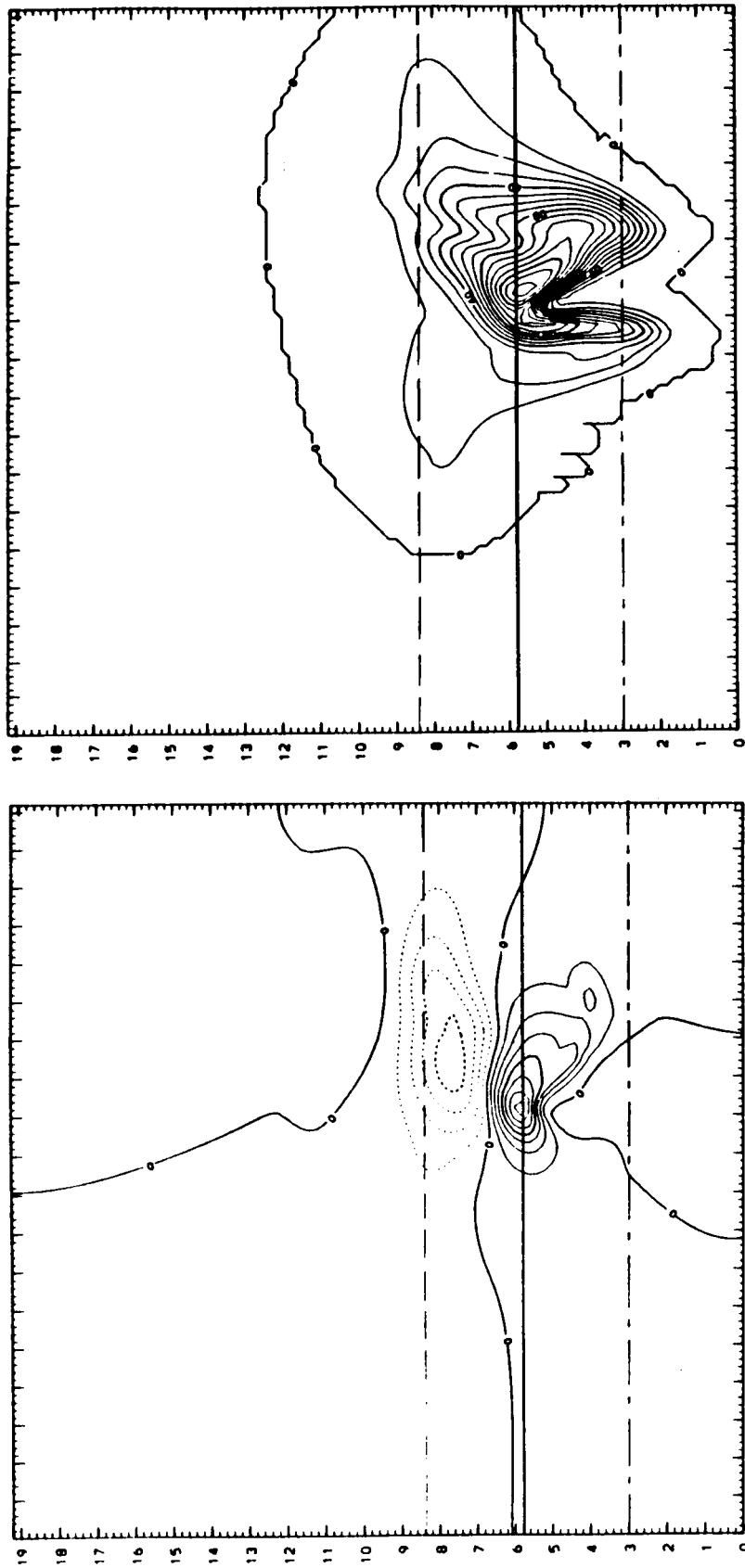
Fig. 5: Plots from the Wallops Island simulation at 22.5 minutes showing vertical electric field component (left panel) and graupel mixing ratio (right panel) over the model domain (19.2 x 19.2 km). In the left panel, downwardly directed fields are indicated by a dotted line and upwardly directed fields are contoured with a solid line. The contour interval is 60 kV/m and the zero line is marked. In the right panel, the contour lines represent mixing ratios in grams of graupel per kilogram of dry air and the contour interval is 1 g/kg. Also represented are possible flight altitudes of the F106 at 10 kft (3 km), 19 kft (5.8 km) and 27 kft (8.4 km) [see text].

line at 8.4 km represents the altitude at which the aircraft was operating at the time of the lightning strikes. The dash-dot line represents a flight level of approximately 10 kft, and the solid line, a level of around 19 kft. (The major tick marks on the horizontal and vertical axes represent distance in kilometers.) These two lower altitudes are in the region considered by NASA personnel to constitute the low altitude lightning environment (<20 kft).

Examination of the figure reveals that, at the altitude at which the aircraft was operating on that day, a high electric field environment would have been encountered (if the model is adequately simulating the cloud which was penetrated). The model results further indicate that had the F106 been operating in the vicinity of 10 kft, it would have encountered relatively low field strengths and probably not have been able to trigger a discharge (the triggering process seems to predominate at high altitudes). On the other hand, the flight level around 19 kft shows that a very concentrated and intense region of electric field in excess of 400 kV/m might have been encountered by the F106 had it been flying at that altitude. This result seems to indicate that lower level, high field regions could exist in the types of clouds penetrated during the project; however, examination of the right panel in the figure shows that this high field region is coincident with the maximum hail content of the storm (mixing ratio in excess of 14 g/kg). In addition, examination of Fig. 3 shows that this high field region also corresponds to a region of strong updraft and a sharp updraft/downdraft boundary, indicating the possibility of strong turbulence. Therefore, while a volume favorable to the initiation of lightning by the F106 in the low altitude region may be present, the simulation of this one case indicates that the aircraft would have to purposely avoid such a region for safety considerations. It is also interesting to note that the majority of the low altitude strikes that occurred during the 1985 field season were in the 15-20 kft region. This leads one to speculate that the low altitude, high field region may be a reasonably frequent feature of the storms encountered by the F106 and is not always associated with adverse flying conditions. More simulations of the electrical evolution of such clouds during their mature and dissipating stages would help to clarify this question.

These results brought to light several questions and limitations which resulted in additional research. First of all, while the model seemed to be producing realistic simulations of the storm conditions within which the F106 was operating and the data provided to EMA was useful in their analyses, we had no way of knowing whether or not the simulations were actually correct. The only way to verify the ability of a model to simulate nature is to have actual observations against which to compare the model results. The comparison between the F106 field mill data and the model output done by EMA scientists was encouraging, but was not a sufficient test. Such a test has been done on the model for a cold-based continental type storm (Helsdon and Farley, 1987a,b), giving us confidence that the model can correctly

simulate cloud development and its attendant electrification. However, there are significant differences between cold-based, continental clouds and the warm-based, maritime type clouds found along the east coast. These differences are such that we do not feel it is safe to assume that, because one type of cloud is well modeled, a different type of cloud will be equally well modeled.

Another, and even more important, consideration involves the inability of the model to simulate the electrical development of a cloud beyond its early stages. As noted above, the Wallops Island simulation had to be terminated after 22.5 minutes simulation time because of the constant buildup of the electric field strength. There is no mechanism within the model to relax the ever increasing electrical stresses. Nature takes care of the problem by initiating a lightning discharge. In order to be consistent, we realized that it was necessary for the model to be able to simulate a lightning discharge and its effects on the local charges and fields. Only when this capability was in place would the model be able to provide simulations of the mature and dissipating stages of a storm's electrical life.

As a result of the Wallops Island simulation, and through discussions with other project personnel, a plan was devised to aid in the increase of low altitude strikes to the F106. It was suggested that situations be sought where a line of storms was present with fairly high reflectivity cores. The F106 should then be directed to fly a course parallel to the storm line and upwind of the reflectivity maximum in the altitude range from 15 to 20 kft. Based on the Wallops simulation, this might put the airplane in the vicinity of the low level high field region, but out of the high graupel hazard region. Although this recommendation was speculative due to the uncertainty of the storm charge structure during the mature stage, it was adopted by project personnel.

4.2 Lightning Parameterization

The difficulties with electric field buildup led to investigating the question of incorporating (parameterizing) the lightning discharge in the SEM. We had two types of lightning to deal with; cloud-to-ground and intracloud. While intracloud lightning is the less well studied, it is also the most frequent to occur during a storm. It also seems, intuitively, to be the less complicated of the two to incorporate in the model and therefore was chosen to be examined first.

Without going into the arguments pro and con, we chose to adopt the philosophy of Kasemir (1960, 1984) whereby the overall intracloud lightning channel is electrically neutral. The charges that exist on the channel are the result of ionization along the channel and are not "gathered" from the surrounding cloud volume. When one deals with the simulation of the lightning discharge, which is a subgrid scale process

in the SEM, four basic criteria must be established in order to account for the process: 1) initiation; 2) direction of propagation; 3) termination; and 4) charge redistribution. In attempting a first order approximation to the lightning discharge, the idea is to keep the processes involved as simple as possible while still trying to maintain a physically reasonable approach to the problem. Simplicity is also advisable because the physical mechanisms involved in determining these criteria are poorly understood at this point. Thus, we have basically employed a single parameter approach to the first three processes mentioned above.

Recently Williams et al. (1985) have made a study of electrical discharges in polymethlymethacrylate (PMMA) which had been injected with electrons to form various space charge configurations. They found adequate scaled correlations to be able to relate the observed behavior of the discharges in the PMMA blocks to lightning discharges in thunderclouds. Their paper focused on the local electric field strength and the space charge distribution as the factors controlling the extent and direction of propagation of the discharge channel. While the extent and magnitude of the space charge cloud were important in the morphology of the laboratory discharges, they identified the local electrostatic field as the single most important parameter in controlling such discharges. And although there is no direct justification for extrapolating their results to what takes place in thunderclouds, a scaling approach and the application of their model to specific thunderstorm situations argued in favor of accepting a possible correlation. As a result of their work and the concept of maintaining simplicity in the initial approach to the lightning parameterization, it was decided to use the local electric field as the parameter controlling the first three criteria in the above list.

As an initiation criterion, a threshold electric field was chosen with a value of 400 kV/m. Williams et al. (1985) quote a value of 500-1000 kV/m for a breakdown field in their Table 1. It has frequently been mentioned that the in-cloud breakdown field must be in the vicinity of 400 kV/m since the highest reliable in-cloud field measurements have peaked near that value. We feel that using this value in the model is reasonable because the value at a grid point represents the average value of the quantity within a grid box 200 m on a side (for this model) and this average would most likely consist of both higher and lower values.

The termination criterion was selected to be a critical field strength of 150 kV/m based on work done by Griffiths and Phelps (1976) involving the propagation of positive streamers in the laboratory. While serious questions can be raised about the appropriateness of extrapolating such a laboratory value to the atmosphere, we feel that it represents a reasonable threshold to use in the first approximation. It is true that the stepped leader which precedes a cloud-to-ground discharge appears to propagate through regions where the field strength does not exceed a few kilovolts per meter and such an extinction

criterion as proposed above would not seem to be applicable; however, we are only dealing with the intracloud discharge at present.

In keeping with our single parameter formulation for the discharge process, we have chosen to use the electric field vector in determining the direction of the propagation path. Because the model domain is composed of grid points in a rectangular pattern, the lightning path is constrained to move either along the side of a grid box or along its diagonal, depending upon the direction of the electric field vector at that point. An algorithm has been developed which computes the angle of the field vector with respect to the vertical direction and determines whether the path should be taken along the diagonal or the side. Even though the vector may be (and usually is) canted with respect to the vertical, the diagonal path is not chosen unless the canting exceeds a value of 22.5°. Because of these geometric constraints created by the use of a rectangular grid, the resulting lightning channel will probably be artificially relegated to a more vertical propagation path than would normally be observed in nature; however, for a first approximation, this seemed to be a reasonable approach which could be improved upon as experience and increased knowledge dictated. For example, we recognized that the electric field vector at the tip of the propagating leader is important in determining the propagation direction; however, this was beyond the scope of a first order approximation and was relegated to consideration as a subsequent improvement. Finally, since the initiation point of the channel was the point of highest electric field strength, the channel propagation was made bi-directional from that point, moving both parallel and anti-parallel to the field vector and terminating when the field strength along each segment fell below the cutoff threshold.

In order to evaluate the effectiveness of these criteria, a test was conducted using model output from a simulation of the 19 July 1981 cloud which was observed in the vicinity of Miles City, MT, and produced a single intracloud lightning discharge (inferred from the electric field measurements of the NCAR/NOAA sailplane; see Dye et al., 1986). The initiation, propagation, and termination criteria as outlined above were applied to the model predicted state of the cloud at a time when the electric field was sufficient at some point in the domain to exceed the initiation threshold. From this point, the discharge path was computed in two directions following the electric field vector. The upward and downward paths continued until their termination thresholds were reached, at which point the discharge in that direction was stopped.

The results of this process are shown in Fig. 6 which depicts the model calculated lightning channel superimposed on the ambient charge distribution (left panel) and the vertical electric field component (right panel). We can see that the discharge originates in the region of maximum vertical electric field, which corresponds to a region of low net charge density. The discharge path is basically vertical
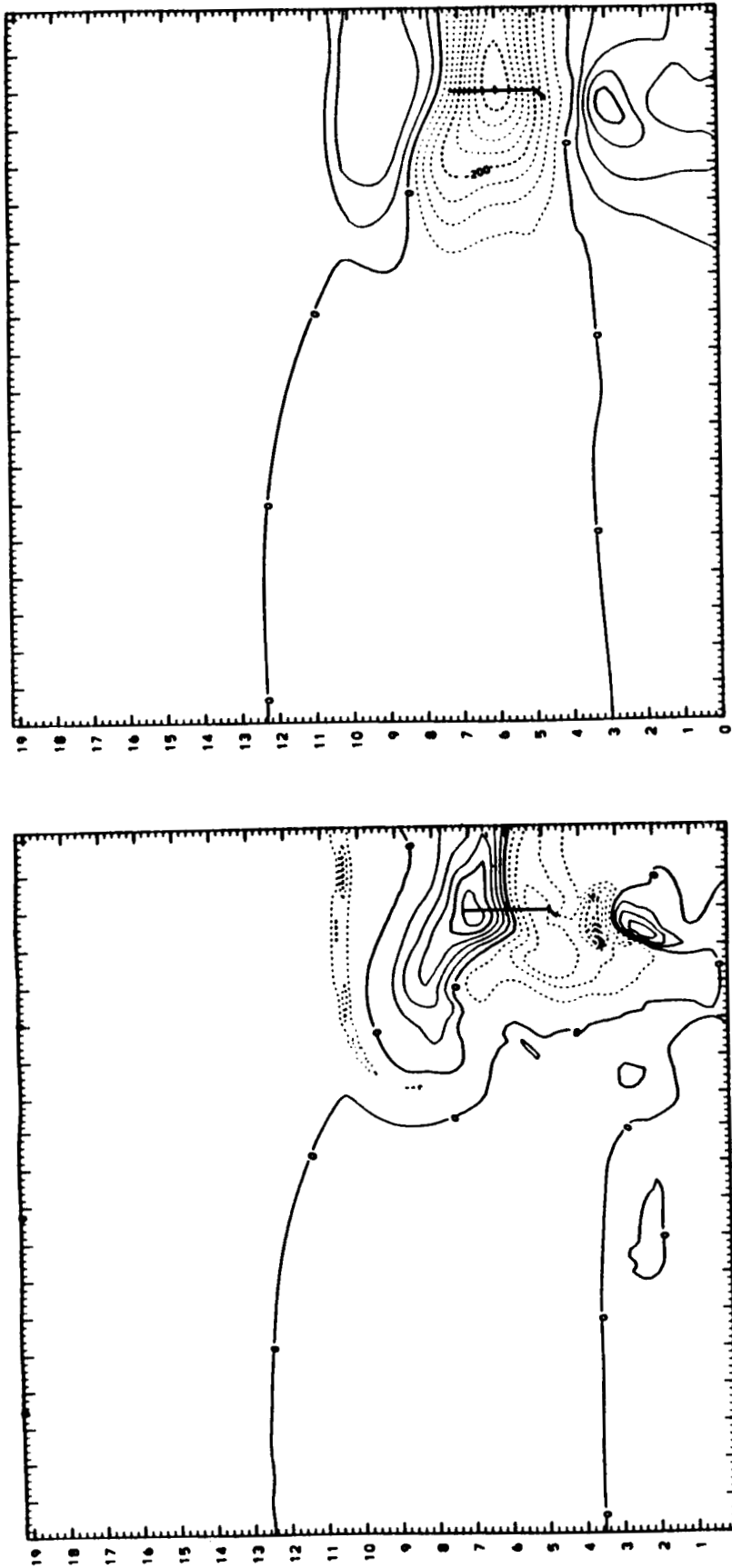
Fig. 6: Plots from the 19 July 1981 CCOPE case showing the model generated lightning channel superimposed on the model predicted net charge distribution (left panel) and vertical electric field component (right panel). The model domain is the same as in Fig. 1. The lightning channel is depicted as a vertical line segment centered at 6 km altitude and located 17 km from the left boundary. Note that the lower segment of the channel deviates from the vertical. In the left panel, the solid contours represent net positive charge and the dotted contours net negative charge. The contour interval is 0.9 nC/m^3 with the zero line indicated. In the right panel, the solid contours represent an upwardly directed electric field while the dotted contours represent a downwardly directed field. The contour interval is 50 kV/m and, again, the zero line is displayed.

following the dominant vertical electric field component and penetrates both the positive (upper) and negative (lower) charge centers. One should note, however, that the effect of the horizontal component of the electric field vector (not shown) becomes sufficient in the vicinity of the downward propagating part of the path so that the channel is deflected to the left as termination takes place. The total path length of the discharge channel in this instance was 2682 meters.

The parameterization of the lightning process was completed by specifying the manner in which the charge created along the channel is redistributed into the environment. This aspect of the problem was approached in the following manner. Using ideas from Kasemir (1960, 1984), we assume that the lightning channel is going to be electrically neutral over its entire length, indicating the deposition of equal amounts of positive and negative charge along the two portions of the simulated discharge. In the model, this charge deposition is accomplished by assuming that the charge density per unit length along the channel is proportional to the difference between the ambient potential, ϕ (in Volts), at the grid point in question and the potential, ϕ_0, at the initiation point of the discharge. Thus

$$Q_0 = -k(\phi-\phi_0) \tag{20}$$

where Q_0 is the linear charge density at a point along the channel, and k is a proportionality constant (farads/m). The negative sign assures that the charge deposited along that portion of the channel is basically opposite in sign to the ambient net charge in that grid volume, since the sign of the potential and the charge responsible for that potential are generally the same.

The application of Eq. (20) results in a charge distribution along the channel similar to that shown in Fig. 7 between +1.2 and -1.5 km. The two tails extending beyond these points in Fig. 7 will be explained subsequently. Since we are working with a discrete grid and the termination criterion forces the channel path to stop at a specific grid point (not at the exact place where this criterion is just met), charge neutrality which is required by theory is not guaranteed by this process. In order to overcome this difficulty, we arbitrarily extend the channel path four grid points beyond the designated termination point at each end. We first integrate over the channel path to find the total charge deposited on the sections of opposite polarity. We then compare these two and, at the end of the path segment having the greatest total charge magnitude, we cause an exponentially decreasing amount of charge to be deposited over the four additional grid points using the following expression

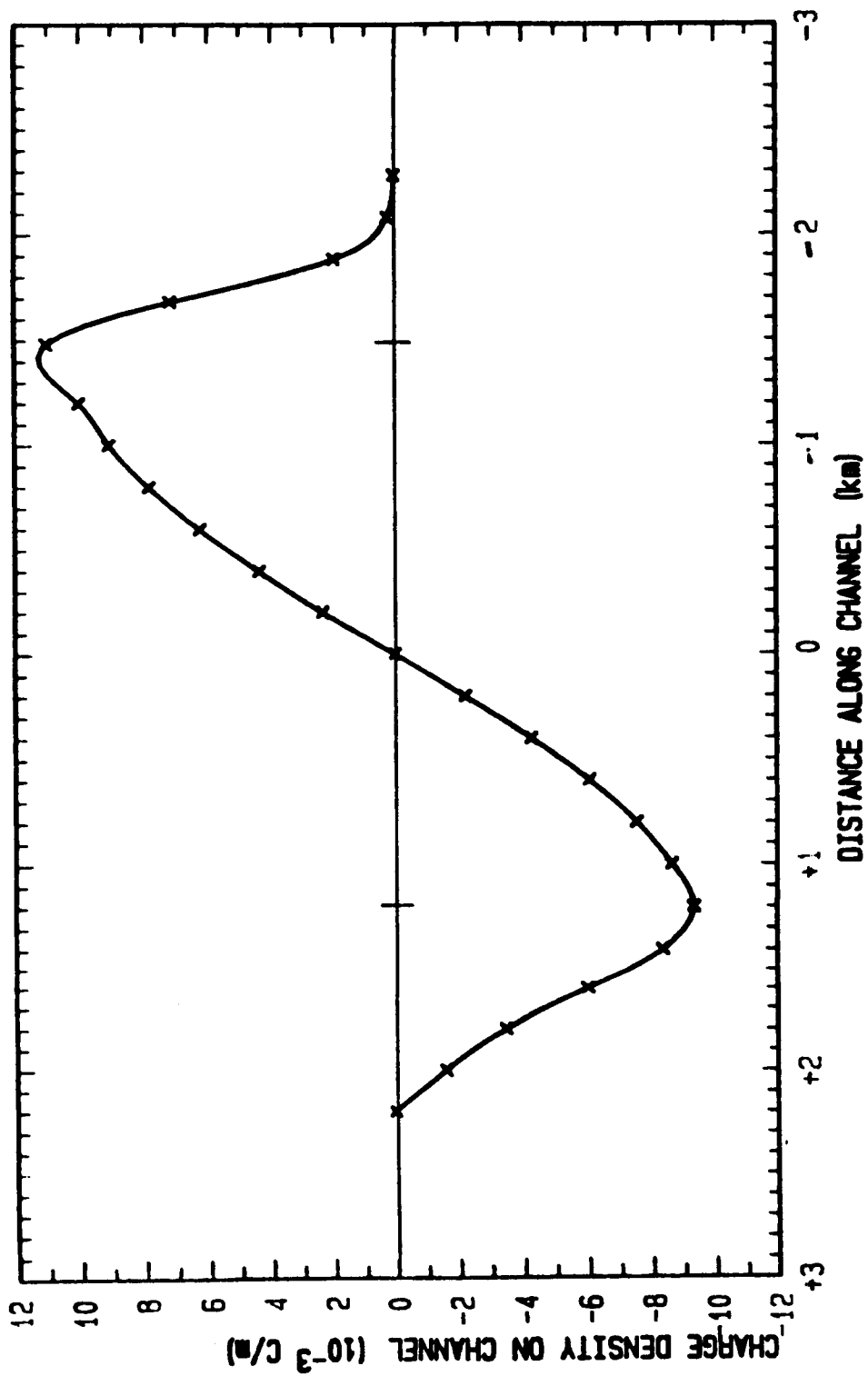$$Q_j = Q_n exp(-k\{[j-n]\Delta\}^2) \tag{21}$$

Fig. 7: Linear charge density along the channel path using Eq. (20) and a value of $k = \underline{2.5} \times 10^{-11}$ F/m. The original channel is delineated by the vertical bars on the horizontal axis.

where $j = n\pm1,\ldots,n\pm4$, Q_n is the linear charge density (C/m) at the termination point of that segment [as determined by Eq. (20)], Δ is the grid spacing, and k is chosen such that $Q_{n\pm4} = Q_n/1000$. This new segment of charge density is integrated to obtain the total charge deposited along the segment of that polarity. We then calculate the absolute difference between the charge residing on the completed segment and the charge residing on the segment of opposite polarity. This difference is used as a basis for calculating a charge density decrease over the four grid points at the end of the remaining segment.

As with the charge calculations on the initial channel, a trapezoidal integration is performed using Eq. (21) to represent the charge decrease over the four grid points. An iterative process (Newton-Raphson) is used on the integration scheme with the exponential factor k being the unknown quantity. By varying k, the rate of decrease of charge density away from the initial endpoint of the segment is controlled and the total additional charge distributed off the end of the segment can be set so that the total charge of that segment just balances the total charge on the other segment. By this procedure, the neutrality of the discharge channel is obtained over the discrete grid.

Figure 7 shows the linear charge density calculated along the channel using Eq. (20) and a value of $k = 2.5 \times 10^{-11}$ farads/m. The original channel is delineated by the 2 vertical bars on the horizontal axis. The effect of the charge balancing procedure is evident at the 2 tails. The total channel length is nearly 4.5 km. For this particular discharge (value of k), the total charge transferred is 12 C. This may be a bit high for an intracloud discharge; however, it is not an unreasonable value.

To this point, we have the lightning discharge represented as a path on the discrete grid with a linear charge density at every grid point along the path. In order to allow this discharge to interact with the other model parameters, we need to make some further modifications. The discrete discharge path represents a line (1D) source in the 2D model. Because of the numerical methods employed in the model calculations, the sudden appearance of a line source of ions would represent a shock which the model could not accommodate. In order to make the channel ion production tractable for the model numerics, the charge must be distributed to some of the grid points adjacent to the channel path. A minimum of three grid points must be involved for numerical stability, the channel path itself and one grid point on each side. We have chosen to employ a total of 9 grid points (the path grid point plus four on each side) to represent the charge distribution. An expression identical to Eq. (21) is used to specify the decay of the magnitude as a function of distance away from the channel, again with $Q_{n\pm4} = Q_n/1000$. For either a vertical or diagonal path orientation, the charge spreading is done in a horizontal direction.

One additional consideration must be made. The charge density along the channel is expressed in terms of C/m. This must ultimately be converted into an ion density (ions/m^3). The linear charge density, expressed by Q_n, represents the charge density through a grid volume which surrounds the grid point and, therefore, can be converted to an equivalent volumetric charge density, assuming that the charge is distributed uniformly throughout the grid volume in question. In addition, when we undertake to distribute the line charge laterally away from the discharge path, we would artificially create charge if we do not take steps to maintain charge conservation. However, charge conservation can be accomplished during the spreading by adopting the following procedure.

Figure 8 is a representation of the charge conservation concept. Q_n represents the linear charge density at a particular grid point along the discharge path. Assuming that Q_n represents the charge distribution in the grid volume $\Delta x \Delta y \Delta z$ surrounding the grid point, then the total charge in the grid volume is

$$Q_T = Q_n \Delta l \tag{22}$$

where Δl is the length of the discharge path segment for that grid volume. Because we are using a two-dimensional model, we must generate a fictitious volume with which to work. Although, in a strict sense, the adoption of slab symmetry for the 2D model implies an infinite extension to all model features in the y-direction, we choose here to adopt a concept of infinity which encompasses only the range of influence of the process being considered. Since we are employing a 9 grid point spreading procedure in the x-direction, we hypothesize a 9 grid point spreading in the y-direction also to comprise the influence volume.

In Fig. 8, the rectangular volume at the center represents the total charge associated with the grid volume in question. The two Gaussian type curves represent the redistribution of that charge over the 9x9 rectangular grid array surrounding the grid point where the total charge in both distributions is the same.

Mathematically the procedure is developed as follows. The total charge under the two distributions is equated such that

$$Q_T = Q_n \Delta l = Q' \int_0^{\Delta l} \int_{-4\Delta y}^{4\Delta y} \int_{-4\Delta x}^{4\Delta x} e^{-k_1 x^2} e^{-k_2 y^2} dx\,dy\,dz \tag{23}$$

which becomes
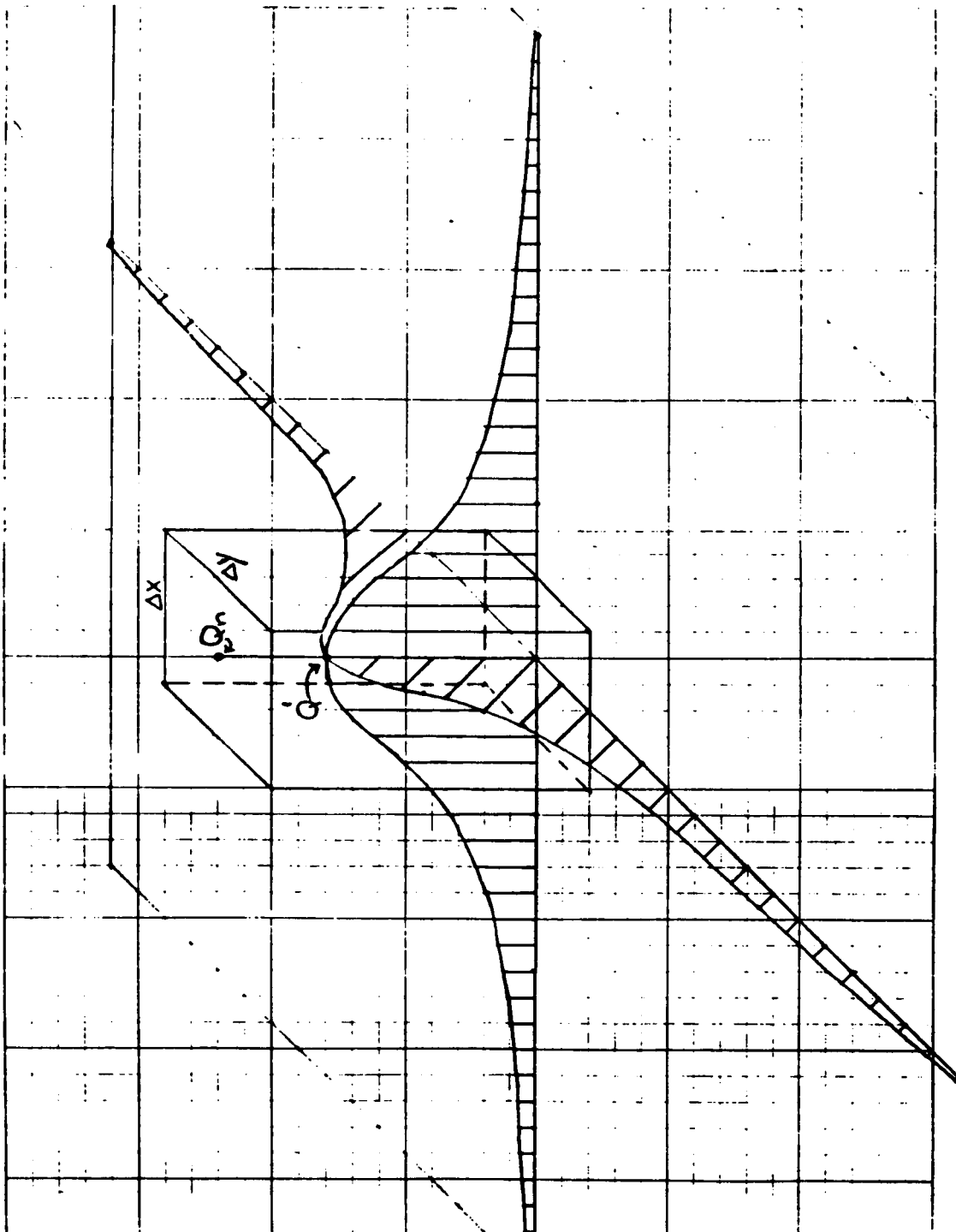
Fig. 8: Depiction of the three-dimensional charge spreading procedure. The total charge in the rectangular volume and under the surface defined by the Gaussian curves are equal.

$$Q_T = Q_n\Delta l = 4Q'\Delta l \int_0^{4\Delta y} \int_0^{4\Delta x} e^{-k_1 x^2} e^{-k_2 y^2} dx dy \qquad (24)$$

which can be separated to yield

$$Q_T = Q_n\Delta l = 4Q'\Delta l \int_0^{4\Delta y} e^{-k_2 y^2} dy \int_0^{4\Delta x} e^{-k_1 x^2} dx \qquad (25)$$

Here, Q' is the magnitude of the charge density (C/m^3) at the grid point under consideration which will result in the same total charge, Q_T, when distributed under the exponential distribution rule.

The two integrals are evaluated using 6 point Gauss-Legendre Quadrature with $k_1 = k_2$, yielding a fall off to 1/1000 of the central point value at the 4th grid point [see discussion following Eq. (21)]. The result of this integration yields a relationship between Q' and Q_n such that $Q' = Q_n/2.909 \times 10^5$. Therefore, the linear charge density at a grid point may easily be converted to a volumetric charge density spread out laterally away from the discharge path in a manner identical to Eq. (21), but with Q' replacing Q_n. Figure 9 shows the results of the horizontal spreading of the charge distribution depicted in Fig. 8. Because of the exponential fall off, most of the charge is concentrated nearest to the main channel. The upper portion of the channel contains negative charge and the lower portion is positive. This process conserves the original total charge transferred by the discharge.

Each calculated grid point charge density must be converted to an equivalent ion density. This is accomplished by dividing each charge magnitude by the electronic charge, $e = 1.6 \times 10^{-19}$ C/electron, assuming that all the ions produced are singly charged. The ions resulting from the redistribution process are then added into the ambient ion fields as they exist at that point in the simulation. With the ion fields modified, a new total charge density is calculated, then Poisson's equation is employed to diagnose a new potential field from which the modified electric field components are calculated. This completes the discharge process in the model and the time marching is resumed. The ions which were injected into the cloud along the discharge path interact with the charged hydrometeors in subsequent time steps and continue to modify the charge distribution and the resulting electric fields.

Fig. 9: Horizontal distribution of the linear charge in Fig. 7 after applying the procedure in Fig. 8.

4.3 Experiments with the Lightning Parameterization

4.3.1 Charge transfer parameter study

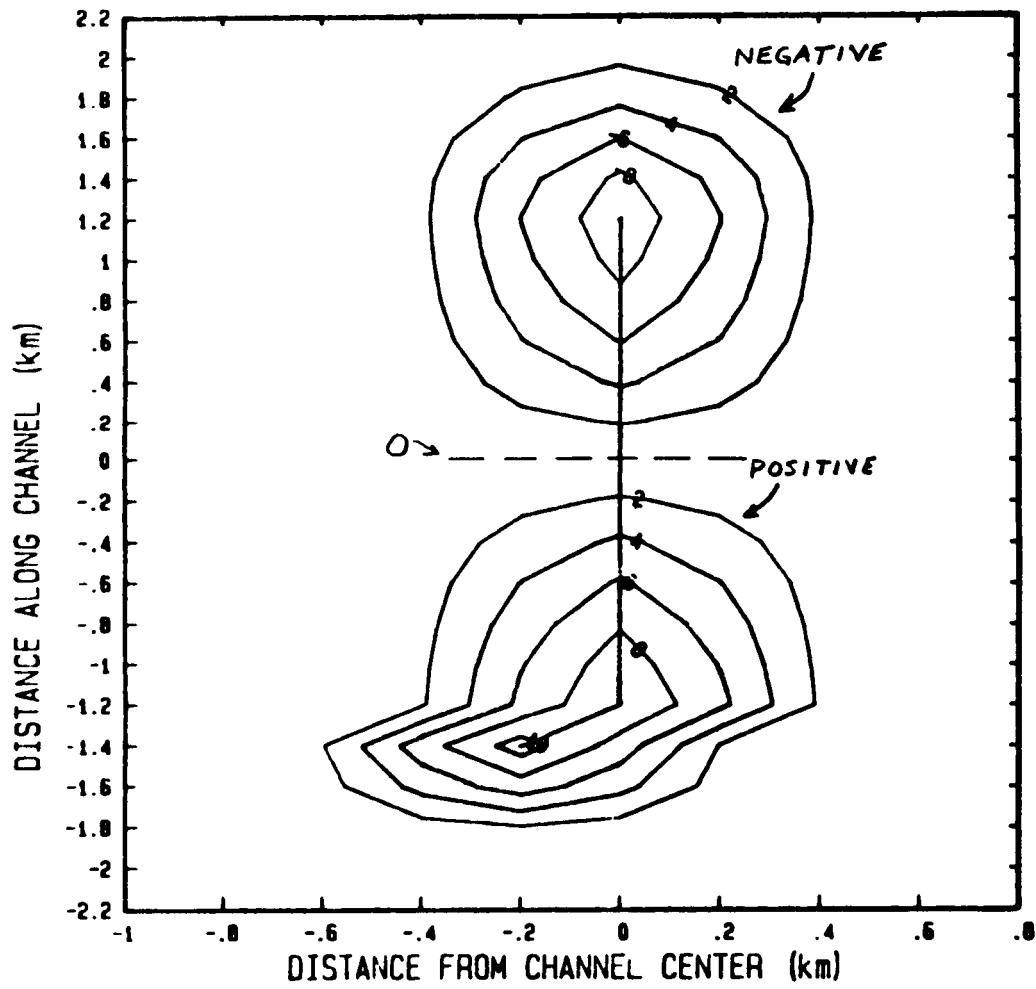The first experiment performed with the parameterization scheme used the value of k referred to above and resulted in a very strong influence on the subsequent electrification. Because of this, we decided to try a series of k values to see how differing amounts of charge transfer affected the electrical behavior. Using 10 values of k ranging from 2.5×10^{-12} (weak charge transfer) to 2.5×10^{-11} (strong charge transfer), we found a vastly different character to the electrical structure of the cloud. These results ranged from a minor perturbation for the weak cases to a complete domination of the charge structure and electrical evolution for the strongest cases. The 19 July CCOPE simulation was used as the framework for these experiments.

For demonstration purposes, some aspects of four of the cases have been chosen to illustrate these differences. In the following graphs, the numerical labels represent the following values of k [in Eq. (20)] and amounts of charge transferred:

$$1 \rightarrow k = 2.5 \times 10^{-11}, \ 12 \ \text{Coul}$$

$$2 \rightarrow k = 2.5 \times 10^{-12}, \ 1.2 \ \text{Coul}$$

$$5 \rightarrow k = 1.0 \times 10^{-11}, \ 4.8 \ \text{Coul}$$

$$7 \rightarrow k = 1.5 \times 10^{-11}, \ 7.2 \ \text{Coul}.$$

Figure 10 shows the variation of the maximum snow charge density (a), the maximum negative vertical (b), and maximum negative horizontal (c) electric field strengths for a period of 30 seconds following the time of the simulated lightning discharge for each of the four cases listed above. The majority of the snow in the simulated cloud is charged positively as a result of riming electrification. The lightning discharge occurs in the region of maximum snow charge density with both positive and negative ions being deposited amongst the positively charged snow. The negative lightning ions are formed in the region of maximally charged snow. Figure 11 shows the snow charge density before and after the discharge for case 5. Figure 10a shows that, in all four cases, the negative ions attach to the snow particles to reduce the maximum charge density. For the weakest case (2), the effect is very small and the electrical processes tend to return to their previous state. For the intermediate cases (5 and 7), there are sufficient negative ions for the attachment process to continue to erode the charge on the snow. For the strongest case (1), the trend is the same initially, but then shows a large increase in the snow charge. Because the data used to make up this plot are the domain maximum values, this large increase represents the effect of the attachment of positive ions from the lower portion of the channel to snow particles lower in the cloud. While the original maximum charge region has been eroded by the negative
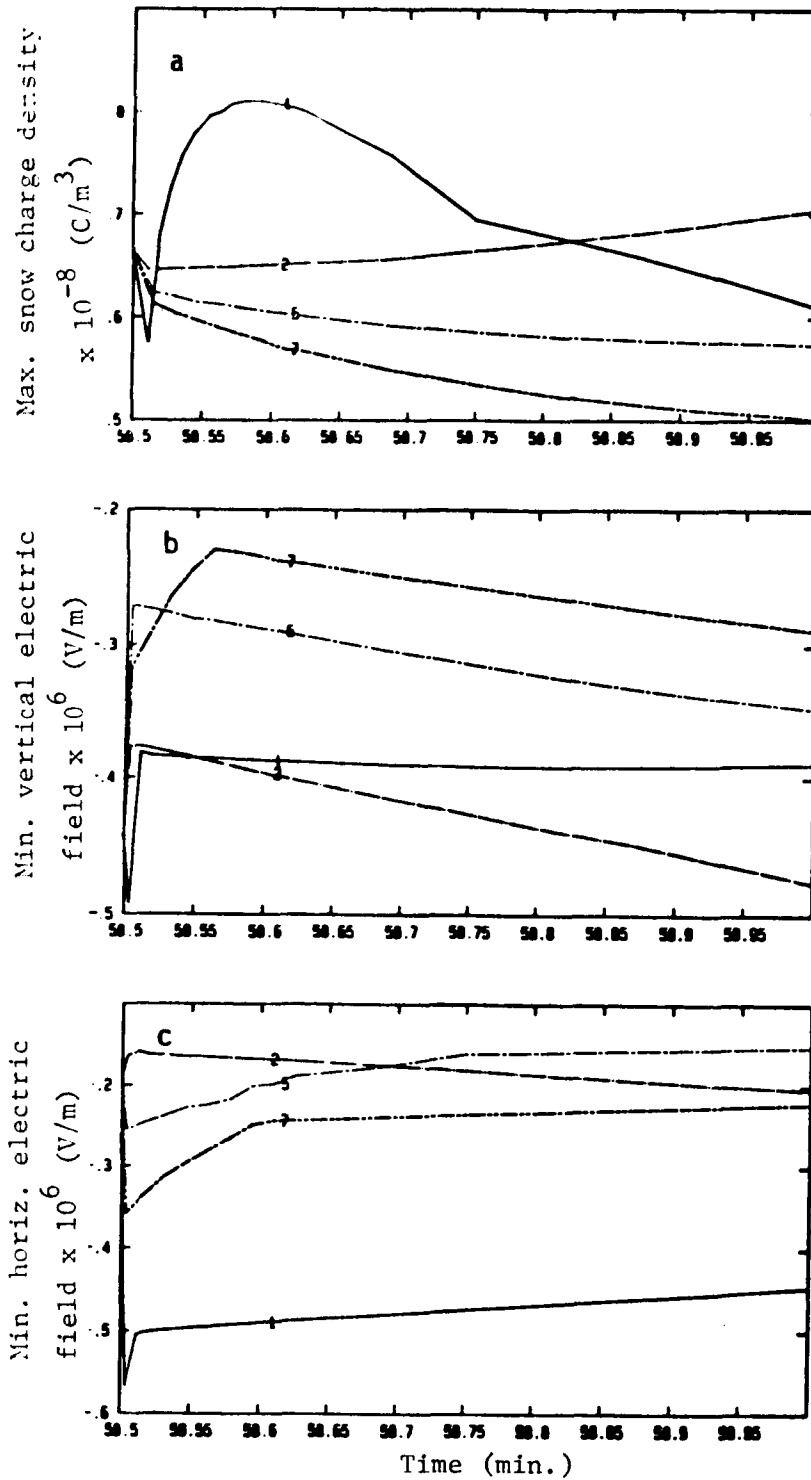
Fig. 10: Domain maximum positive snow charge density (a), maximum negative vertical electric field (b), and maximum negative horizontal electric field (c) for 30 sec following the discharge for four experiments.
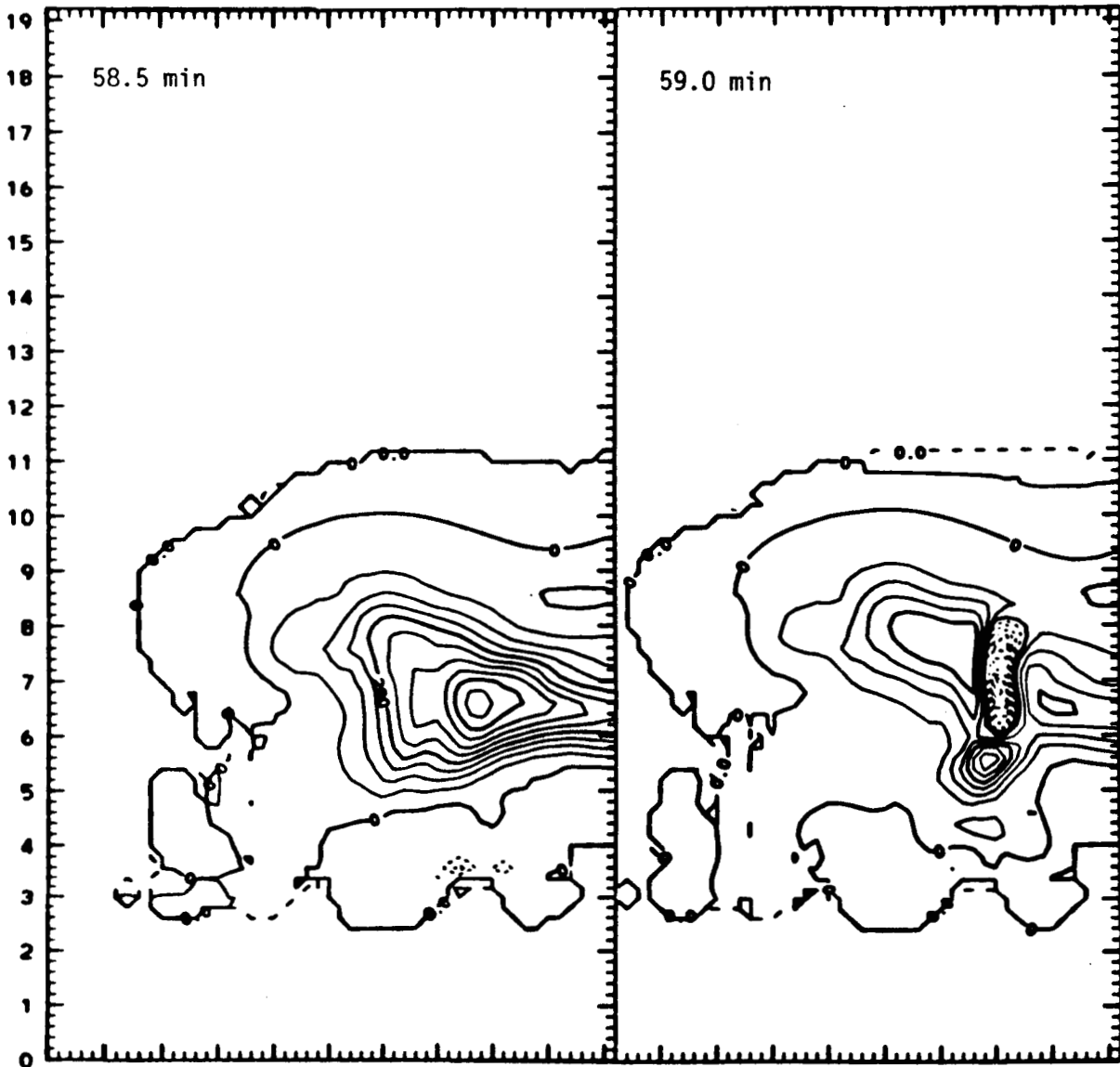
Fig. 11: Snow charge density at 58.5 min (before lightning) and 59.0 min (30 sec after lightning). Solid lines represent positive charge and dashed lines, negative charge. The attachment of lightning produces ions (both positive and negative) is apparent.

ions, a new region of positive maximum has been created. Figure 11 shows the results of the discharge ion injection on the snow charge after 30 seconds.

Figure 10b shows the effect of the discharge ions on the maximum negative vertical electric field component. The weak and intermediate discharges all exhibit a tendency to reduce the field strength, with stronger discharges exhibiting the stronger tendency. This seems intuitively satisfying because we tend to think of lightning as acting to reduce the electrical stress in a cloud. For the strong case, however, the results are somewhat unexpected. Here there is an initial increase in the magnitude of the negative field component followed by a return to a near steady state at almost the initial value. Examination of the structure of the vertical field component for cases 2, 5, and 7 shows that the lightning causes an ever increasing perturbation on that structure; however, for case 1 an entirely different structure is established by the discharge.

Figure 10c, which shows the maximum negative horizontal electric field component, further demonstrates the transition from perturbation to domination. Here, only the weak case shows a decrease in the field strength with a rapid return to the slow field buildup. The two intermediate cases both show an increase in the field strength immediately following the discharge; however, case 5 then shows a field reduction below the initial value, while case 7 continues to maintain field strengths greater than the initial value. The strong case shows a dramatic increase in this field component and maintains the increased magnitudes.

4.3.2 Comparison with lightning induced electric field changes

These widely varying results led us to conclude that there was a great deal that we did not understand about how the lightning discharge operates in nature. Therefore, we saw that there was a need to continue to study how the parameterization scheme worked within the context of the model and what the various results meant relative to an actual thunderstorm. Unfortunately, in order to interpret our results as to their meaning within the realm of actual storms, we needed to have actual observations for comparison. This is one of the problems confronting our investigations. There are very few actual in situ observations of lightning and its effects on the electrical structure of thunderstorms. Most of the measurements that are available are of the change in the electric field associated with lightning made by suitably equipped balloons or aircraft which happen to be flying in the vicinity of discharge. In the case of our use of the 19 July CCOPE case as a framework within which to develop the lightning parameterization, one such observation was available.

During the CCOPE experiment, the National Center for Atmospheric Research flew a sailplane equipped with a cylindrical field mill for measuring two components of the electric field. This sailplane took

measurements during an ascent in the updraft of the 19 July cloud and during two passes along the periphery of the cloud after exiting the updraft. One pass was made along the edge of the cloud at an altitude of 5.3 km MSL (4.5 km AGL in the model) and detected an apparent intracloud discharge. The electric field recorded by the sailplane during its pass along the cloud edge is shown in Fig. 12, which is reproduced from Fig. 9 of Dye et al. (1986). The sharp discontinuity in the horizontal field component just after 1637 MDT led them to infer the occurrence of an intracloud discharge.

In order to compare this observation with the model simulation, we had to establish a point in the model domain to use as a reference for extracting the electric field data. We assumed that the sailplane would fly perpendicular to the model plane (X-Z plane). We used the simulated cloud boundary for the horizontal position and an altitude of 4.4 km AGL for the vertical position of the sailplane. Just prior to the lightning discharge in the model, the sailplane would measure a horizontal electric field component of about 65 kV/m. The actual horizontal component measured by the sailplane just prior to the discharge was 7 kV/m. While the modeled and observed values differ by an order of magnitude, the horizontal position of the model sampling point was quite arbitrary and the field strengths vary rapidly in the horizontal. Thus, the discrepancy in the quantitative aspects of the comparison is not particularly significant. After the simulated intracloud discharge, the sailplane would measure a horizontal field component value of about 55 kV/m. The field change due to the simulated intracloud lightning was -10 kV/m. The actual horizontal electric field measured by the sailplane following the discharge was 2.5 kV/m, yielding an actual field change due to lightning of about -4.5 kV/m.

Figure 13 illustrates the time evolution of the modeled horizontal and vertical electric field components as might be measured by the sailplane at the time of the intracloud discharge. We can compare these with the actual curves shown in Fig. 12. Allowing for the difference in magnitudes, there is a high degree of similarity between the two curves representing the horizontal component. But we also note that, for the vertical field component, the model result does not compare well with the actual sailplane data. This discrepancy may be the result of model geometry. Since, in this two-dimensional model, we assume that the cloud is homogeneous and infinite in the Y direction, the cloud geometries are not equivalent. On the positive side we note that, in thunderclouds studied in New Mexico, balloon borne field mills have recorded simultaneous discontinuities similar to those in Fig. 13 for all three components of the electric field (cf. Weber et al., 1982).

4.3.3 Lightning ion interaction with cloud particles

In addition to the study of the effect of the lightning discharge on the electric field structure, another point of interest was how the
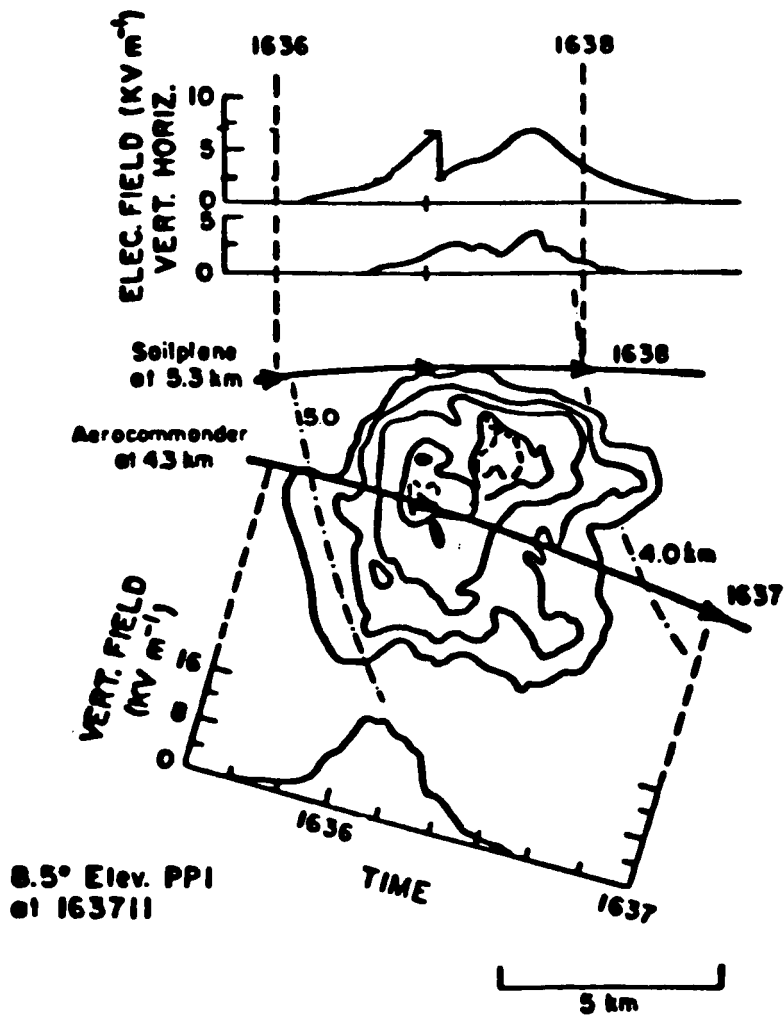
Fig. 12: Reflectivity contours near the time of the intracloud discharge with tracks of the NCAR sailplane and the Desert Research Institute Aerocommander superimposed. Arrowheads show the position of the aircraft on each minute. Sailplane measurements of electric field are shown above. The discontinuity in the horizontal field trace is evident. (Extracted from Dye et al., 1986, with permission).

-42-
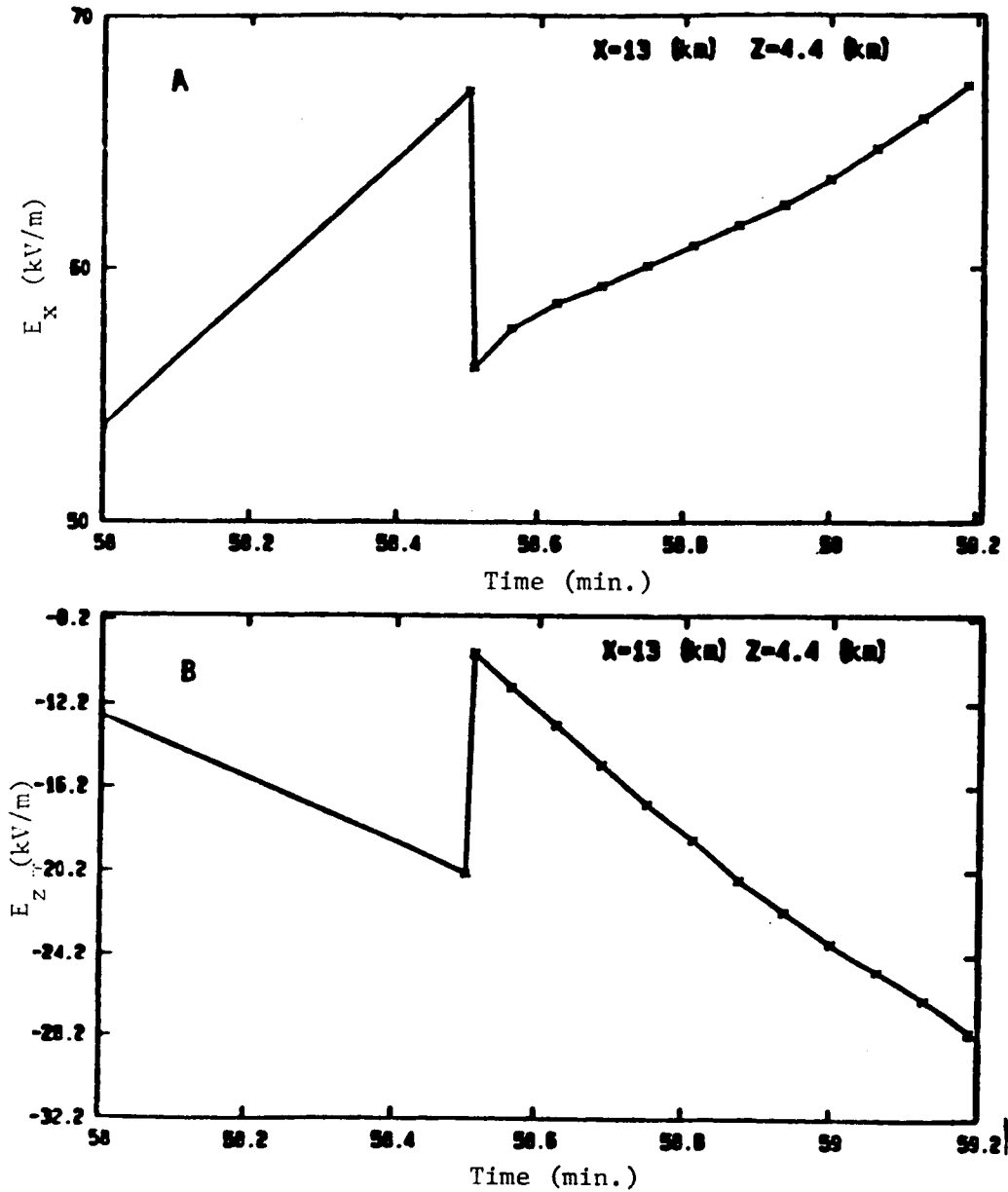
Fig. 13: Time evolution of the horizontal (A) and vertical (B) electric field components at the assumed sailplane position around the time of the lightning discharge.

ions produced by the lightning interacted with the hydrometeors in the cloud. This is an area in which little in the way of observational data are available, but which lends itself nicely to study within the model. To do this, we simulated a number of aircraft traverses through the storm at an altitude of z=4 km (AGL) and at 7.5 second time intervals. The 4 km height was near the lower termination point of the discharge channel. The results concerning the charge on the cloud droplets are shown in Fig. 14, while the charge on graupel particles is shown in Fig. 15.

Before the lightning, the cloud water charge has two positively charged regions (one located at x=13 km and the other at x=17 km) and two regions of negative charge centered at x=14 and x=16.5 km, respectively. For the graupel, there is a broad region of negative charge centered near x=16 km. The lightning discharge produces a large number of ions (depending on the amount of charge transferred by the channel) which can interact with hydrometeors in the vicinity by the ion attachment process (Wilson capture). In Fig. 14, we see that the region of strong negative cloud water charge density near the lightning channel at x=17 km is reduced rapidly, disappearing after 58.625 min, while the adjacent region of positive charge broadens and intensifies with time. Referring to Fig. 15, we see that the lightning induced change in the graupel charge distribution is initially apparent as a notch developing in the negative region at x=17 km, the channel axis. We note that the effect is small until the negative cloud water region has disappeared. After that time, the positive ions which were produced by the lightning channel interact more strongly with the negative graupel charge. At 59 min, the graupel charge distribution is characterized by two peaks. The adjacent region of positive cloud water charge becomes stronger during this time period, but more slowly. The cloud droplets are a more efficient sink for ions by the attachment process than are the graupel particles. This is because the total surface area associated with the cloud droplets is usually much larger than that associated with graupel even when the cloud water content is smaller than the water content contained in the graupel. The ion attachment process is dependent on the surface area of the attaching species.

4.3.4 Energy dissipation

Another way to check the consistency of the lightning parameterization is to look at the energy associated with the discharge. It is widely accepted that the energy for the lightning discharge is provided by the ambient electric field of the thundercloud environment as well as the electric field at the tip of the leader. The energy which is dissipated by the lightning is used for ionizing and heating the channel, producing electromagnetic radiation, building a magnetic field, producing acoustical waves, etc. In order for the parameterization scheme developed for the SEM to be valid, the electrical energy dissipated by the model channel should agree in order of magnitude with observed or theoretically estimated discharge energy dissipation.
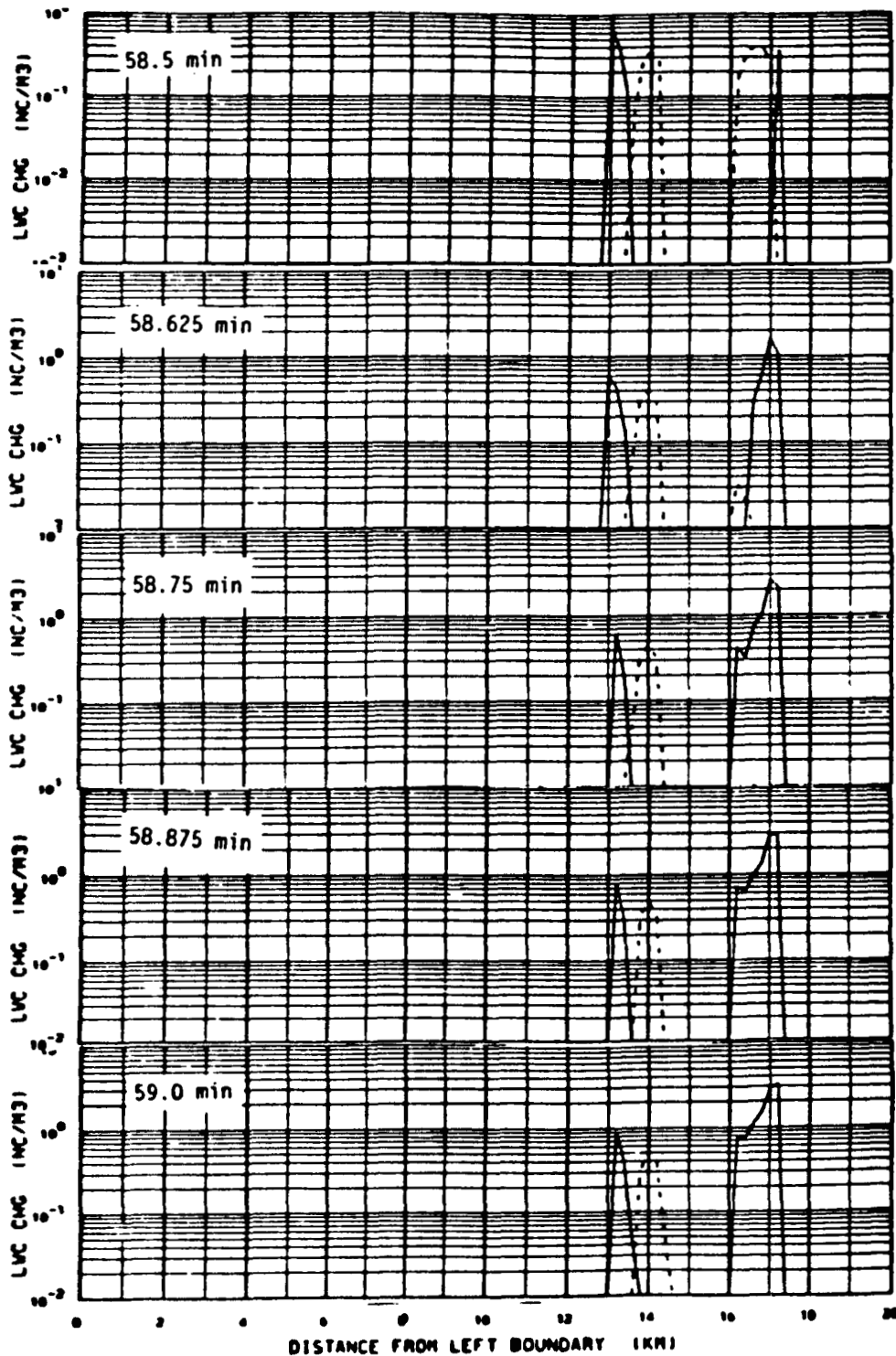
Fig. 14: Time evolution of the cloud water charge density at 4 km (AGL) following the lightning discharge. Solid lines represent positive charge while dashed lines represent negatively charged cloud droplets.
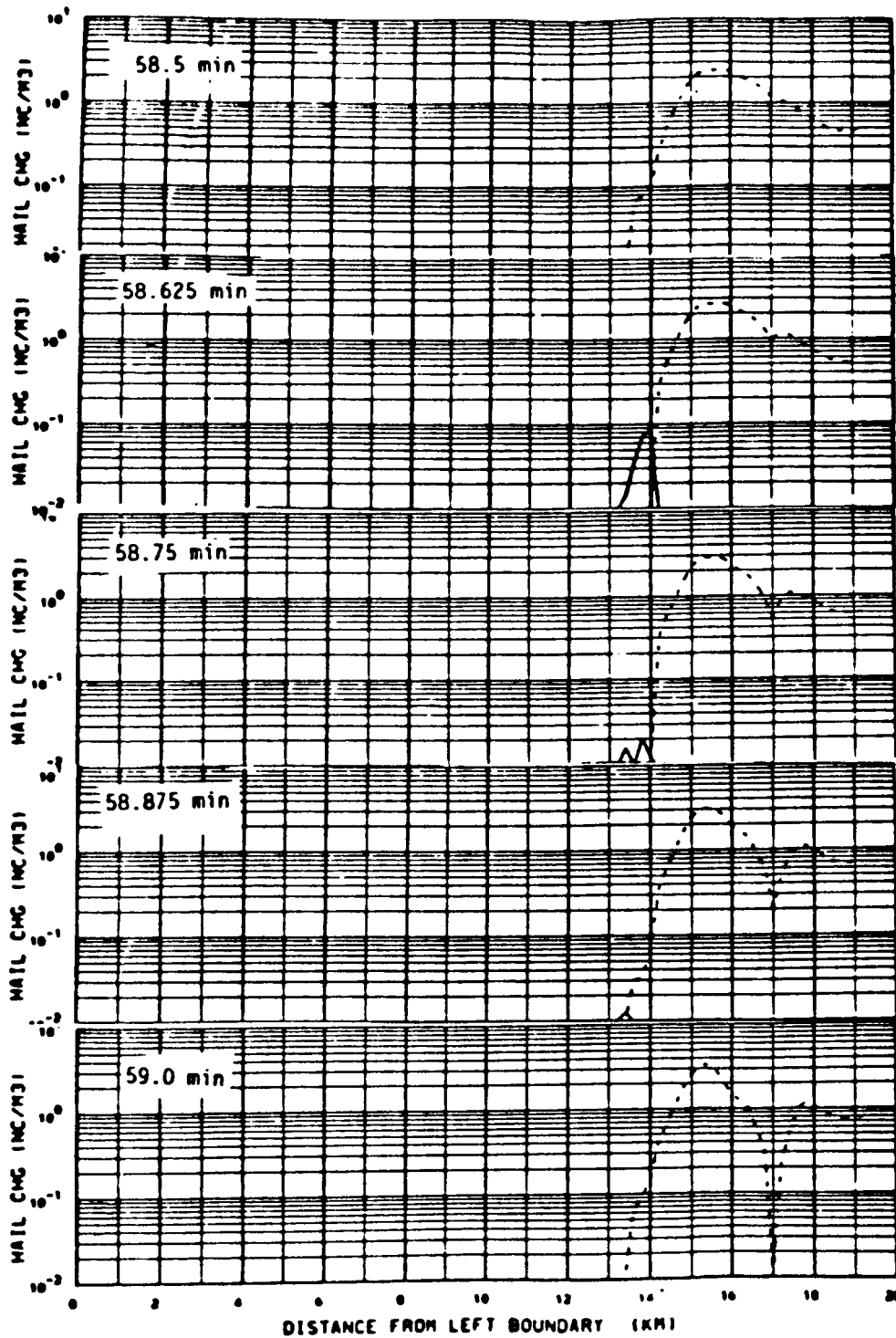
Fig. 15: Same as in Fig. 14 except for the charge on graupel particles.

We know that the energy density produced by the electric field can be calculated from the following equation

$$1 = \frac{1}{2} \epsilon_o E^2 \tag{26}$$

where $\epsilon_o = 8.86 \times 10^{-12}$ F/m is the permittivity of air. If we integrate this expression over the whole domain of the simulated cloud using a numerical integration scheme, we can get the total electrical energy at each simulation time. We did this for Case 5, which represents a charge transfer of 4.8 Coul. A calculation over the cloud volume before the lightning discharge resulted in a total electrical energy of 1.14×10^{10} J. The same calculation after the discharge gave a total energy of 9.4×10^9 J. Thus, the energy dissipated by the lightning channel is about 2×10^9 J. If we consider the total simulated lightning channel length to be 4280 meters (see Fig. 7) and assume that the energy dissipation along the channel is uniform, we calculate an energy dissipation along the channel of around 4.7×10^5 J/m.

Krider et al. (1968), based on observational data, inferred the energy dissipation along the lightning channel to be about 2.3×10^5 J/m. Hill (1971) and Plooster (1971) developed models of the detailed lightning channel itself. In these models, a portion of the plasma channel was simulated without considering any of the environmental influences. From their modeling they calculated lightning energy dissipations of 1.5×10^4 and 2.5×10^3 J/m, respectively. There is an unresolved debate about the discrepancy between these two model calculations and between the model calculations and the calculation made from laboratory simulation. Despite the simple numerical integration technique employed in our calculation and the assumption of constant energy dissipation along the channel, the model generated energy dissipation is in reasonable agreement with the work of Krider. Although the energy estimate does not agree so well with the works of Hill and Plooster, we find these initial estimates to be encouraging and add to our confidence in the parameterization scheme.

4.4 Cloud-to-Ground Discharge Parameterization

Having made these tests of the lightning parameterization scheme, we undertook a preliminary implementation of a cloud-to-ground discharge. Since our termination criterion of an electric field strength less than 150 kV/m would not allow a ground flash to occur in the 19 July simulation (and in fact no such ground discharge was observed by the lightning detection network installed for the project), we had to artificially force the intracloud discharge channel to go to ground by ignoring the lower termination criterion. The remaining initiation, propagation, and termination criteria were employed as for the intracloud discharge. The parameterization scheme has to be

modified somewhat, however, when the lightning channel makes contact with the ground, particularly with respect to the charge redistribution.

As our first order approximation, we assumed that Eqs. (20), (21), and (25) were all applicable because the physical concept of the cloud-to-ground discharge is the same as for the intracloud discharge. The key parameter in simulating a cloud-to-ground discharge is ϕ_1, the electric potential of the lightning channel. Because the lightning channel is a conductor, we have ϕ_1, ϕ_i, where ϕ_i is the potential of the initiation point of the lightning channel. Because the earth is a good conductor, as soon as the channel attaches to the ground, both the channel and earth should have the same value of potential. We choose the ground as the reference point (zero potential) for the potential field so the channel experiences a sudden change in potential when ground attachment occurs. The total charge transferred to the ground due to the cloud-to-ground discharge can be written as

$$Q_\ell = K \int_\ell \phi_i \, d\ell \qquad (27)$$

where the integral is taken along the channel path.

For this simulation, we chose $k=1.5 \times 10^{-11}$ F/m (case 7) as the framework within which to test the cloud-to-ground discharge. Using Eq. (27), we obtained a transfer of -1.5 C of charge to the ground. This is within the observed range of charge transfer values for a cloud-to-ground discharge. Figure 16 shows the time evolution of the total charge density and cloud water charge density for a one minute period following the simulated discharge. Figure 17 shows the same history for the horizontal and vertical electric field components.

As seen in Fig. 16, the lower part of the channel creates a large number of positive ions which attach to and reverse the polarity of a portion of the negative cloud water charge structure of the lower cloud. Initially, the total charge density field is dominated by the lightning produced ions, although over the course of the minute following the discharge, the original charge structure is seen to become more prevalent. Shortly after the simulated discharge, the original negative cloud charge nearly disappears and a new positive space charge is created on the cloud water. This positive charge accumulation strongly influences the vertical electric field component, as can be seen in Fig. 17. The positive vertical field region present beneath the cloud prior to the discharge disappears. A negative vertical field becomes dominant below the cloud after the lightning. The horizontal electric field component is also dramatically changed.

Observations typically show a reversal of the electric field (as measured at the ground) from foul weather (positive) values to fair weather (negative) values following a lightning discharge. This abrupt

field reversal is followed by a gradual recovery to foul weather values if no other lightning occurs near in time to the discharge responsible for the initial reversal. As can be seen from the maximum negative values of the vertical field component in Fig. 17, a recovery process is underway in the negative field region below the cloud. While this gives qualitative agreement with an observed characteristic of cloud-to-ground lightning, the magnitudes predicted by the model may not be comparable to those observed. However, we must keep in mind that, in this simulation, we forced a ground discharge. If one had been predicted to occur naturally, the results may have been more meaningful.

Another aspect of the parameterized discharge which appears in the simulation and has been observed to occur in actual thunderstorms is the creation or enhancement of the lower positive charge center following lightning. Holden et al. (1983) and Marshall and Winn (1982) reported on the creation of lower positive charge centers in thunderstorms in New Mexico following lightning discharges. They found that positive charge was deposited on precipitation falling from the base of the storms which subsequently fell to the ground. Their instrumentation was only capable of measuring the charge on precipitation-sized particles. In the model results shown in Fig. 16, we can clearly see the formation of this positive charge in the total charge density. Most of the charge is attached to the cloud particles (as noted above); however, there is also attachment of positive lightning ions to the rain falling in the vicinity of the discharge. This is further indication that the basic physical processes involved with the lightning discharge are being simulated in the model. The question of correct magnitudes remains to be investigated in more detail.

4.5 EMA Subcontract

During the third year of this investigation, we engaged Electro Magnetic Applications, Inc., of Denver, CO, under a subcontract to aid in improving two of the criteria used in developing the lightning parameterization scheme. The four criteria involved in the scheme include initiation, propagation, termination, and charge redistribution which have been described in Section 4.2. The first of EMA's efforts involved an attempt to improve the propagation scheme for the discharge. The second effort involved investigating the effect of thunderstorm particles on the initiation criterion.

4.5.1 The lightning propagation model

Under the subcontract, EMA developed a Lightning Discharge Propagation Model (LDPM) for incorporation into the SEM. The purpose of the LDPM is to account for the tortuous path that is usually followed by a lightning channel. One of the weaknesses of the SEM discharge parameterization scheme has been the propagation criterion which artificially constrains the channel to follow the side of a grid

-49-
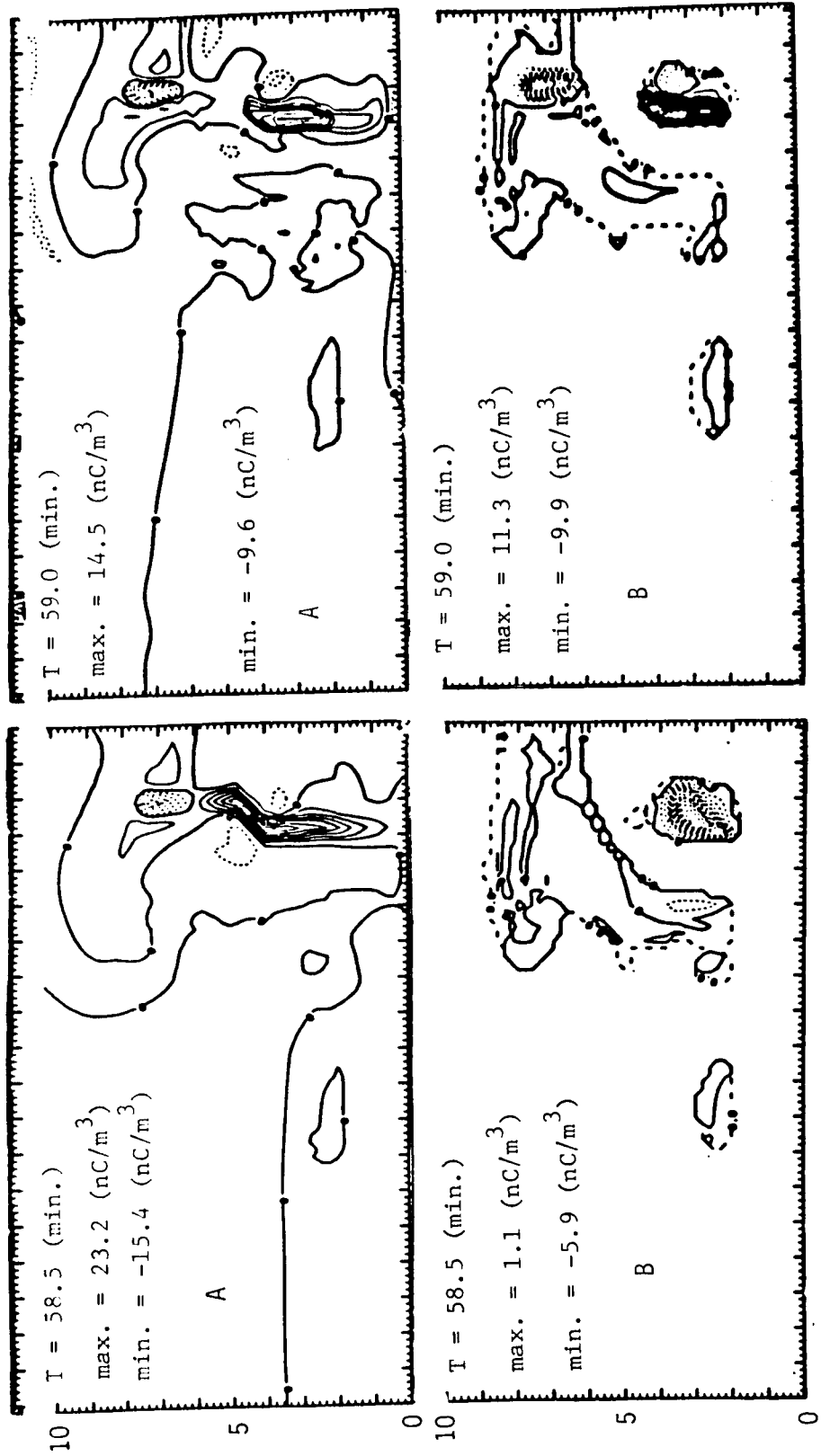
Fig. 16: Plots of the total charge density (A) and cloud water charge density (B) at various times following the cloud-to-ground discharge. Solid lines represent positive values and dashed lines, negative values. Maximum and minimum values are indicated on each plot.

T = 59.0 (min.)

max. = 14.5 (nC/m^3)

min. = -9.6 (nC/m^3)

A

T = 59.0 (min.)

max. = 11.3 (nC/m^3)

min. = -9.9 (nC/m^3)

B

T = 58.5 (min.)

max. = 23.2 (nC/m^3)

min. = -15.4 (nC/m^3)

A

T = 58.5 (min.)

max. = 1.1 (nC/m^3)

min. = -5.9 (nC/m^3)

B
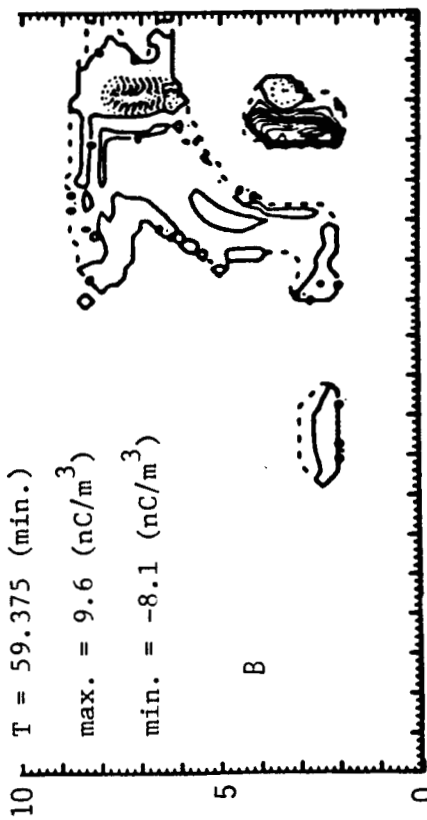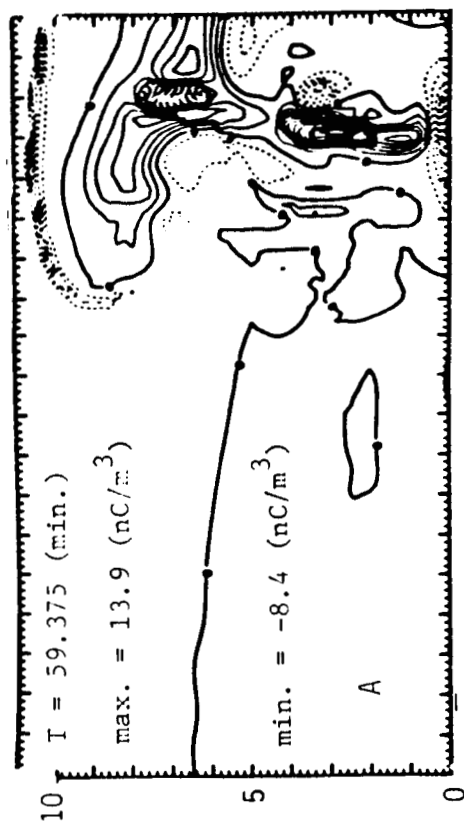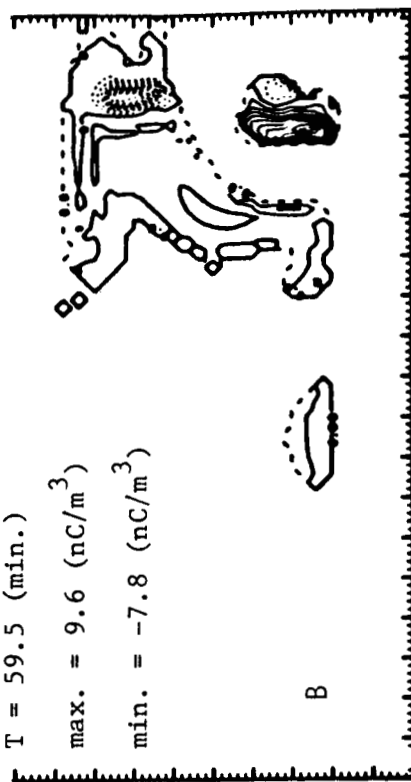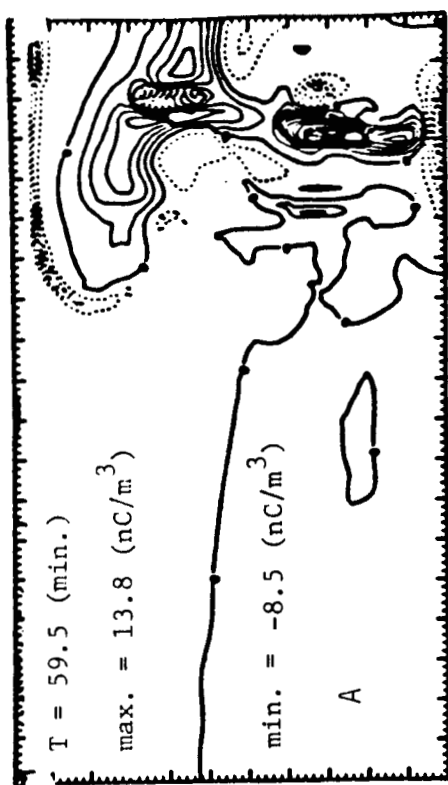
Fig. 16: (concluded.)
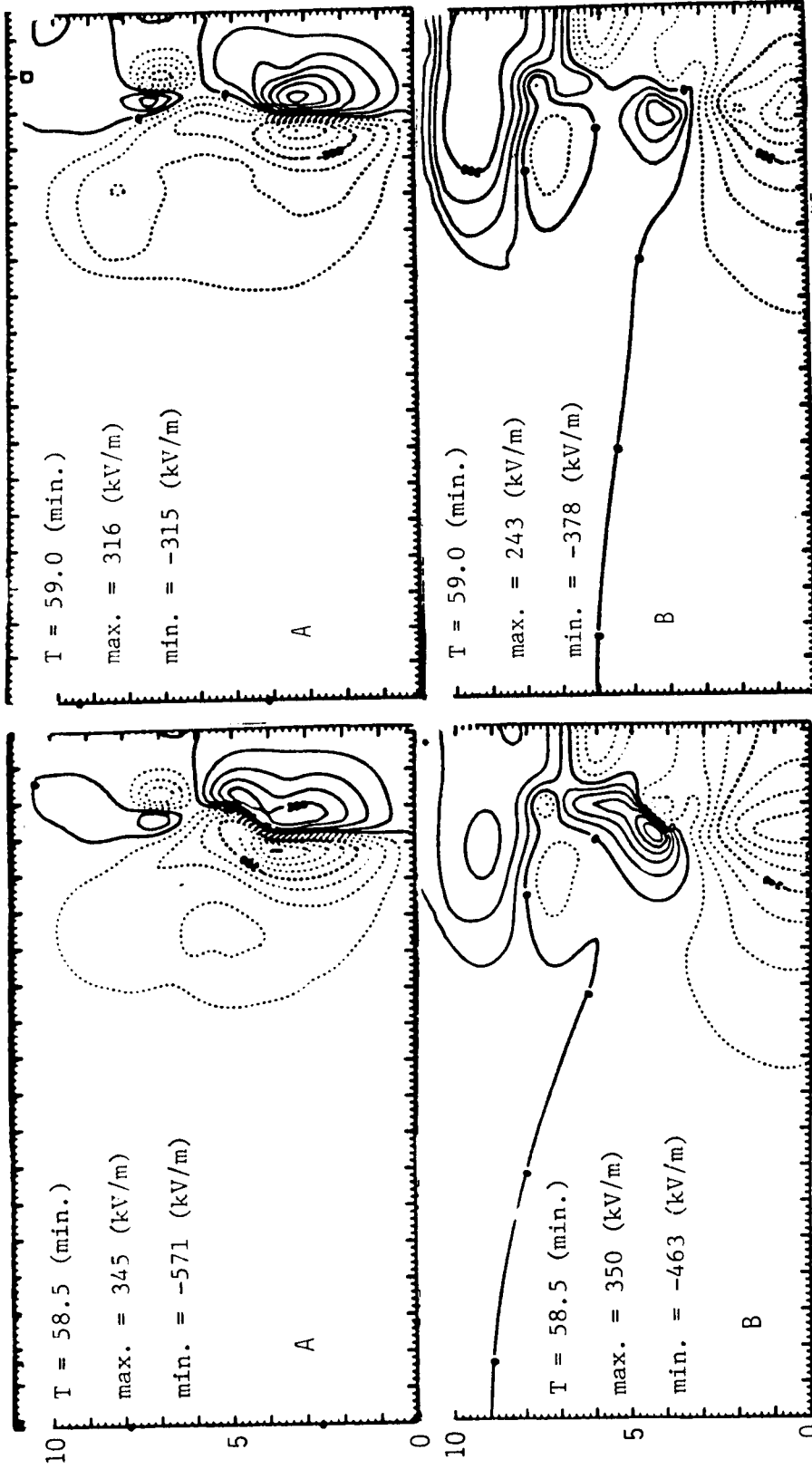
Fig. 17: Plots of the horizontal (A) and vertical (B) electric field components at various times following the cloud-to-ground discharge. Solid lines represent positive values and dashed lines negative values. Maximum and minimum values are indicated on each plot.

T = 59.0 (min.)

max. = 316 (kV/m)

min. = -315 (kV/m)

A

T = 59.0 (min.)

max. = 243 (kV/m)

min. = -378 (kV/m)

B

T = 58.5 (min.)

max. = 345 (kV/m)

min. = -571 (kV/m)

A

T = 58.5 (min.)

max. = 350 (kV/m)

min. = -463 (kV/m)

B

-52-

T = 59.5 (min.)

max. = 318 (kV/m)

min. = -295 (kV/m)

A

T = 59.5 (min.)

max. = 251 (kV/m)

min. = -311 (kV/m)

B

T = 59.375 (min.)

max. = 318 (kV/m)

min. = -306 (kV/m)

A

T = 59.375 (min.)

max. = 250 (kV/m)

min. = -327 (kV/m)

B
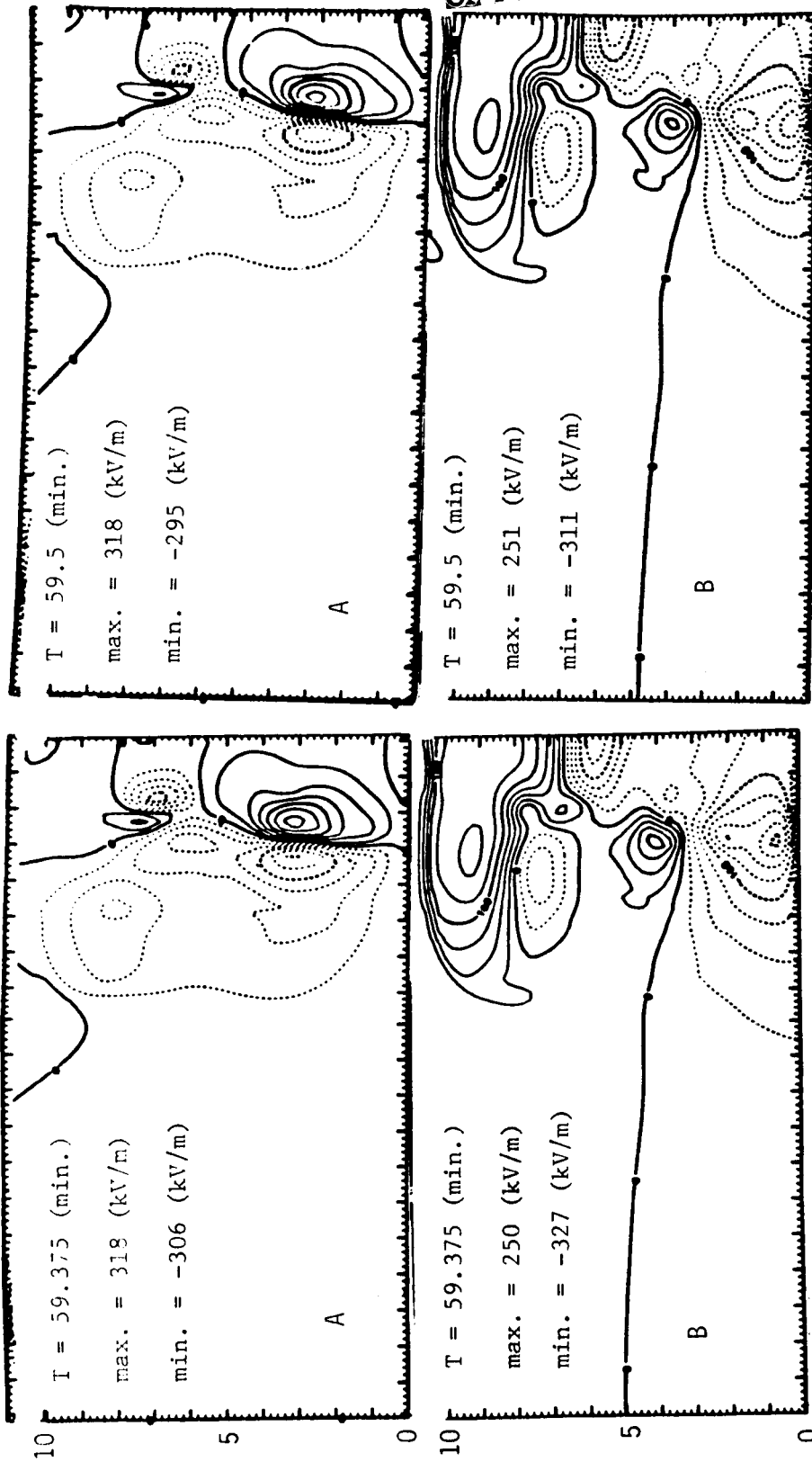
Fig. 17: (concluded.)

box, or its diagonal, depending on the ambient electric field direction. The LDPM scheme takes into account the electric fields created by the leader tip and the previous leader segment. Also included are the effects of random free electrons in the vicinity of the leader tip as an influence in determining the direction of propagation of the next segment.

The basic idea employed involves consideration of conditions in proximity to the leader tip. The leader tip contains a high concentration of charge. In the region around the tip, free electrons are randomly generated by the action of cosmic rays. These electrons are accelerated in the combined electric fields of the ambient thunderstorm and the leader. If the acceleration is strong enough, such electrons can collide with and ionize neutral air molecules creating secondary free electrons which are subsequently influenced by the field. As the process proceeds, an avalanche of electrons will occur and the air will become highly conductive in the avalanche region. The LDPM algorithm determines which free electrons will result in the conducting path that will become the next leader step. By using random seeds, the LDPM produces lightning channels which propagate in the same general direction as the original scheme used in the SEM, but show deviation from the path more reminiscent of actual lightning. The scheme has been included in the SEM but not as yet tested on an actual case. A report describing the LDPM in more detail is included in Appendix B. The report includes several figures which show the difference between the original propagation scheme and the improved scheme.

4.5.2 Particle effects on lightning initiation

The initiation criterion used for the SEM requires an electric field strength in excess of 400 kV/m in the cloud domain. In clear air at altitudes where we would expect to find lightning, the electric field required to initiate air breakdown would exceed 1000 kV/m. The model criterion of 400 kV/m is a rough estimate of what the actual breakdown field might be inside a thunderstorm based on observations of in-cloud electric fields that have rarely exceeded 400 kV/m. What the actual field strength is at the actual point of lightning initiation is an open question which may never be precisely answered. However, the evidence does suggest that the in-cloud breakdown field is considerably lower than the clear-air value. One of the most appealing explanations for this discrepancy is that the hydrometeors within a thunderstorm, particularly the ice particles, act to enhance the local thunderstorm field to the point where breakdown potential is achieved. This conjecture formed the basis for the EMA study of particle field enhancement.

Their study involved an examination of how the shape, size, and number density of particles at different altitudes altered the pure air breakdown value. They accomplished this by looking at how the electron avalanche rate was affected by the various particle parameters. Since

analytical solutions for the electric field enhancement around irregularly shaped particles such as snowflakes and ice crystals do not exist, they employed an approximation using the field distribution of a spherical conductor (dipole field) and modified it with additional enhancement factors determined from previous research. Their results showed that only the largest uncharged ice particles were capable of making significant reductions in the breakdown field. When these particles were charged, the reduction of the breakdown field showed a linear dependence with particle charge and the enhanced field became asymmetric, favoring one-sided corona. While not studied per se, the interactions of two or more particles in further enhancing the local field were noted and suggested as being in need of further research. A report covering this work is also included in Appendix C. A scheme for incorporating these results into the initiation criterion of the SEM will be worked out at some future time.

5. SUMMARY AND CONCLUSIONS

The results of this research have served two purposes. The first is gaining an insight into the low level strike environment for the F106 Storm Hazards Project and the second is the development, for the first time, of a lightning parameterization scheme within the context of a multidimensional cloud electrification model.

With regard to the low level strike environment, the simulation of the Wallops Island case has shown that, within the limitations of the model physics, a region of high electric field strength does occur in the 15-20 kft altitude range. In the early developmental stage of the storm, this high field region is associated with the presence of graupel, and possibly turbulence, making it a region where flight operations would have to be restricted. However, it is entirely possible that at a later time in the storm's life cycle, such a high field region would continue to exist without being accompanied by such threatening conditions. In addition, the Wallops Island simulation was characterized by little wind shear, leading to a nearly vertical development of the modeled storm. In a case where a stronger environmental shear were present, the high field region might not be concomitant with the presence of graupel or the graupel production might not be as heavy as in the case simulated. As a result of this investigation and complementary radar studies, an operational procedure based on these considerations was adopted for the 1986 field season.

The development of the lightning parameterization scheme has been pioneering in nature. The simulation of a lightning channel within the context of a numerical cloud model has not been attempted before. We accomplished this by establishing criteria for the initiation, propagation, termination and charge redistribution of a lightning channel. Even though the parameterization is crude and the lack of understanding of how the lightning mechanism acts in a cloud is great, the simulations and studies we have done with the scheme active in the model have yielded results which are qualitatively consistent with the observations which are available. Because of the nature of this aspect of the research, more questions have been raised than have been answered; however, it appears that we have made a positive first step upon which to build as our understanding of lightning improves. Much more research into the storm-lightning environment is needed. With the lightning parameterization and the improvements developed through the EMA collaboration included in the SEM, it should be possible to make a significant contribution to the understanding of the thunderstorm environment.

6. CONFERENCE PAPERS AND PUBLICATIONS

The following citations are for conference papers and refereed publications resulting from this research grant. Abstracts of the papers appear in Appendix A.

Helsdon, J. H., Jr., 1985: The parameterization of the lightning discharge in a two-dimensional, time-dependent electrical cloud model. Trans. Amer. Geophys. Union, 66, 837.

Helsdon, J. H., Jr., R. D. Farley and G. Wu, 1986: A lightning parameterization scheme in a two-dimensional, time-dependent storm electrification model. Preprints Conf. Cloud Physics, Snowmass, CO, Amer. Meteor. Soc., J273-J276.

Helsdon, J. H., Jr., and R. D. Farley, 1987: A numerical modeling study of a Montana thunderstorm: 2. Model results versus observations involving electrical aspects. J. Geophys. Res., 92, 5661-5675.

ACKNOWLEDGMENTS

7. REFERENCES

Berry, E. X, 1968: Modification of the warm rain process. Preprints First Natl. Conf. Wea. Modif., Albany, NY, Amer. Meteor. Soc., 81-88.

Bigg, E. K., 1953: The supercooling of water. Proc. Phys. Soc. London, B66, 688-694.

Buser, O., and A. N. Aufdermaur, 1977: Electrification by collisions of ice particles on ice or metal targets. Electrical Processes in Atmospheres (eds. H. Dolazalek and R. Reiter), Steinkopff-Verlag, Darmstadt, 294-301.

Chen, C-H., and H. D. Orville, 1980: Effects of mesoscale convergence on cloud convection. J. Appl. Meteor., 19, 256-274.

Chiu, C. S., 1978: Numerical study of cloud electrification in an axisymmetric, time-dependent cloud model. J. Geophys. Res., 83, 5025-5049.

Crowley, W. P., 1968: Numerical advection experiments. Mon. Wea. Rev., 96, 1-11.

Dye, J. E., J. J. Jones, W. P. Winn, T. A. Cerni, B. Gardiner, D. Lamb, R. L. Pitter, J. Hallett and C. P. R. Saunders, 1986: Early electrification and precipitation development in a small, isolated Montana cumulonimbus. J. Geophys. Res., 91, 1231-1247.

Fisher, B. D., and J. A. Plumer, 1984: Lightning attachment patterns and flight conditions experienced by the NASA F-106B airplane from 1980-1983. Presented at AIAA 22nd Aerospace Sciences Meeting, Reno, NV.

_____, P. W. Brown and J. A. Plumer, 1986: Summary of NASA storm hazards lightning research, 1980-1985. Presented at the Intnl. Conf. Lightning and Static Electricity, Dayton, OH.

Fletcher, N. H., 1962: The Physics of Rainclouds. Cambridge Univ. Press, NY. 390 pp.

Gaskell, W., and A. J. Illingworth, 1980: Charge transfer accompanying individual collisions between ice particles and its role in thunderstorm electrification. Quart. J. Roy. Meteor. Soc., 106, 841-854.

Gish, O. H., 1944: Evaluation and interpretation of the columnar resistance of the atmosphere. Terr. Magn. Atmos. Elect., 49, 159-168.

Griffiths, R. F., and C. T. Phelps, 1976: The effects of air pressure and water vapour content on the propagation of positive corona streamers and their implications to lightning initiation. Quart. J. Roy. Meteor. Soc., 102, 419.

Gross, G. W., 1982: Role of relaxation and contact times in charge separation during collisions of precipitation particles with ice targets. J. Geophys. Res., 87, 7170-7178.

Hallett, J., and C. P. R. Saunders, 1979: Charge separation associated with secondary ice crystal production. J. Atmos. Sci., 36, 2230-2235.

Helsdon, J. H., Jr., 1980: Chaff seeding effects in a dynamical-electrical cloud model. J. Appl. Meteor., 19, 1101-1125.

_____, and R. D. Farley, 1987a: A numerical modeling study of a Montana thunderstorm: 1. Model results versus observations involving nonelectrical aspects. J. Geophys. Res., 92, 5645-5659.

_____, and _____, 1987b: A numerical modeling study of a Montana thunderstorm: 2. Model results versus observations involving electrical aspects. J. Geophys. Res., 92, 5661-5675.

_____, _____, and H. D. Orville, 1984: A numerical modeling study of ice electrification mechanisms in a Montana cloud. Preprints VIIth Intnl. Conf. Atmos. Elec., Albany, NY, Amer. Meteor. Soc., 174-177.

Hill, R. D., 1971: Channel heating in return stroke lightning. J. Geophys. Res., 76, 637-645.

Holden, D. N., C. R. Holmes, C. B. Moore, W. P. Winn, J. W. Cobb, J. E. Griswold and D. M. Lytle, 1983: Local charge concentration in thunderclouds. Proc. in Atmospheric Electricity, L. H. Ruhnke and J. Latham, eds., A. Deepak, Hampton, VA, 179-183.

Jayaratne, E. R., C. P. R. Saunders and J. Hallett, 1983: Laboratory studies of the charging of soft-hail during ice crystal inter-actions. Quart. J. Roy. Meteor. Soc., 109, 609-630.

Jennings, S. G., 1975: Charge separation due to water drop and cloud droplet interactions in an electric field. Quart. J. Roy. Meteor. Soc., 101, 227-223.

Kasemir, H., 1960: A contribution to the electrostatic theory of a lightning discharge. J. Geophys. Res., 65, 1873-1878.

_____, 1984: Theoretical and experimental determination of field, charge, and current on an aircraft hit by natural or triggered lightning. Presented at the Intnl. Aerospace and Ground Conf. on Lightning and Static Electricity, Orlando, FL.

Kessler, E., 1969: On the distribution and continuity of water substance in atmospheric circulations. Meteor. Monogr., 10, No. 32. 84 pp.

Krider, E. P., G. A. Dawson and M. A. Uman, 1968: Peak power and energy dissipation in a single-stroke lightning flash. J. Geophys. Res., 73, 3335-3339.

Kuettner, J. P., Z. Levin and J. D. Sartor, 1981: Thunderstorm electrification--inductive or non-inductive? J. Atmos. Sci., 38, 2470-2484.

Latham, J., and B. J. Mason, 1961: Generation of electric charge associated with the formation of soft hail in thunderclouds. Proc. Roy. Soc., A260, 537-549.

_____, and R. Warwicker, 1980: Charge transfer accompanying the splashing of supercooled raindrops on hailstones. Quart. J. Roy. Meteor. Soc., 106, 559-568.

Leith, C. E., 1965: Numerical simulation of the earth's atmosphere. Methods in Computation Physics, Vol. 4, Applications in Hydrodynamics, Academic Press.

Lin, Y-L., R. D. Farley and H. D. Orville, 1983: Bulk parameterization of the snow field in a cloud model. J. Climate Appl. Meteor., 22, 1065-1092.

Liu, J. Y., and H. D. Orville, 1969: Numerical modeling of precipitation and cloud shadow effects on mountain-induced cumuli. J. Atmos. Sci., 26, 1283-1298.

Marshall, T. C., and W. P. Winn, 1982: Measurements of charged precipitation in a New Mexico thunderstorm: Lower positive charge centers. J. Geophys. Res., 87, 7141-7157.

Mazur, V., B. D. Fisher and J. C. Gerlach, 1984: Conditions for lightning strikes to an airplane in a thunderstorm. Presented at the AIAA 22nd Aerospace Sciences Meeting, Reno, NV.

Muller-Hillebrand, D., 1954: Charge generation in thunderstorms by collision of ice crystals with graupel falling through a vertical electric field. Tellus, 6, 367-381.

Musil, D. J., 1970: Computer modeling of hailstone growth in feeder clouds. J. Atmos. Sci., 27, 474-482.

Orville, H. D., 1965: A numerical study of the initiation of cumulus clouds over mountainous terrain. J. Atmos. Sci., 22, 684-699.

_____, and F. J. Kopp, 1977: Numerical simulation of the life history of a hailstorm. J. Atmos. Sci., 34, 1596-1618.

Paluch, I. R., and J. D. Sartor, 1973: Thunderstorm electrification by the inductive charging mechanism: I. Particle charges and electric fields. J. Atmos. Sci., 30, 1166-1173.

Plooster, M. N., 1971: Numerical model of return stroke of the lightning discharge. Phys. Fluids, 14, 2124-2133.

Reynolds, S. E., M. Brook and M. F. Gourley, 1957: Thunderstorm charge separation. J. Meteor., 14, 426-436.

Rudolph, T., and R. A. Perala, 1985: Studies in increasing the probability that the NASA F-106B thunderstorm research aircraft will intercept low altitude lightning strikes. Tech. Rpt. EMA-85-R-24. 101 pp.

_____, _____, P. M. McKenna and S. L. Parker, 1984: Investigations into the triggered lightning response of the F-106B thunderstorm research aircraft. Tech. Rpt. EMA-85-R-02.

Sartor, J. D., 1961: Calculations of cloud electrification based on a general charge separation mechanism. J. Geophys. Res., 66, 831-843.

_____, 1967: The role of particle interactions in the distribution of electricity in thunderstorms. J. Atmos. Sci., 24, 601-615.

_____, 1981: Induction charging of clouds. J. Atmos. Sci., 38, 218-220.

Saunders, P. M., 1957: The thermodynamics of saturated air: A contribution to the classical theory. Quart. J. Roy. Meteor. Soc., 83, 342-350.

Shewchuk, S. R., and J. V. Iribarne, 1971: Charge separation during splashing of large drops on ice. Quart. J. Roy. Meteor. Soc., 97, 272-282.

Shreve, E. L., 1970: Theoretical derivation of atmospheric ion concentrations, conductivity, space charge density, electric field and generation rate from 0 to 60 km. J. Atmos. Sci., 27, 1186-1194.

Takahashi, T., 1978: Riming electrification as a charge generation mechanism in thunderstorms. J. Atmos. Sci., 35, 1536-1548.

Telford, J. W., and P. B. Wagner, 1979: Electric charge separation in severe storms. Pure Appl. Geophys., 117, 891-903.

Tzur, I., and Z. Levin, 1981: Ions and precipitation charging in warm and cold clouds as simulated in a one-dimensional, time-dependent model. J. Atmos. Sci., 38, 2444-2461.

Vonnegut, B., 1955: Possible mechanism for the formation of electricity. Geophys. Res. Pap., No. 42, Air Force Cambridge Res. Center, MA, 169-181.

Weber, M. E., H. J. Christian, A. A. Few and M. F. Stewart, 1982: A thundercloud electric field sounding, charge distribution, and lightning. J. Geophys. Res., 87, 7158-7169.

Williams, E. R., C. M. Cooke and K. A. Wright, 1985: Electrical discharge propagation in and around space charge clouds. J. Geophys. Res., 90, 6059-6070.

Wilson, C. T. R., 1929: Some thundercloud problems. J. Franklin Inst., 208, 1-12.

Wisner, C. E., H. D. Orville and C. Myers, 1972: A numerical model of a hailbearing cloud. J. Atmos. Sci., 29, 1160-1181.

Workman, E. J., and S. E. Reynolds, 1948: A suggested mechanism for the generation of thunderstorm electricity. Phys. Rev., 74, 709.

_____, and _____, 1950: Electrical phenomena occurring during the freezing of dilute aqueous solutions and their possible relationship to thunderstorm electricity. Phys. Rev., 78, 254-259.

APPENDIX A

ABSTRACTS OF CONFERENCE PAPERS AND

PUBLICATIONS

APPENDIX A

THE PARAMETERIZATION OF THE LIGHTNING DISCHARGE IN A
TWO-DIMENSIONAL, TIME-DEPENDENT ELECTRICAL CLOUD MODEL

John H. Helsdon, Jr.

ABSTRACT

In order to extend the capabilities of thunderstorm electrification models to simulate all but the earliest stages of a storm, it is necessary that the electrical stresses created by an ever increasing electric field be relieved in some manner. In nature, it is the lightning discharge which fulfills this need. In keeping with the modeler's goal of attempting to simulate natural processes as faithfully as possible, it is necessary for the model, then, to contain some parameterization of the lightning discharge.

In this presentation, a first order attempt at simulating the intracloud lightning discharge within the context of a two-dimensional, time-dependent thunderstorm electrification model will be discussed. The criteria for the initiation, direction of propagation, termination, and redistribution of charge associated with the simulated channel will be presented. Finally, the effect of the parameterization in an actual simulation will be shown.

A LIGHTNING PARAMETERIZATION SCHEME IN A TWO-DIMENSIONAL, TIME-DEPENDENT STORM ELECTRIFICATION MODEL

John H. Helsdon, Jr., Richard D. Farley,
and Gang Wu

ABSTRACT

An important consideration in the modeling of thunderstorm electrification is the existence of lightning in nature. A model without lightning is only capable of simulating the development of a storm in its early stages (up to the time of first lightning). Since lightning accounts for significant charge rearrangement within a storm, it becomes necessary to include such processes in any modeling effort which hopes to shed light on the electrical evolution of such storms. In an attempt to make allowance for the lightning discharge in our Storm Electrification Model (SEM), we have developed a simplified parameterization scheme to simulate the lightning channel and its attendant charge redistribution.

This parameterization scheme has criteria for the initiation, propagation, termination, and charge redistribution associated with lightning. In order to simplify the scheme as much as possible, the first three criteria are all dependent on the strength and direction of the electric field vector. The propagation of the channel is calculated so as to maintain overall charge neutrality for an intracloud discharge. The charge deposited along the channel is then spread in a conservative manner laterally away from the channel over several grid points in order to maintain computational stability. This distribution of charges is then added to the small ion population and allowed to interact with the other charge carriers as the integration proceeds.

A simulation of the 19 July 1981 CCOPE case has been run with the lightning discharge included. A parametric study has been undertaken to determine the effects of different amounts of charge transfer on the subsequent electrical evolution. The results of these simulations will be discussed.

A NUMERICAL MODELING STUDY OF A MONTANA THUNDERSTORM: 2. MODEL RESULTS VERSUS OBSERVATIONS INVOLVING ELECTRICAL ASPECTS

John H. Helsdon, Jr., and Richard D. Farley

ABSTRACT

In this investigation, we compare the results of the Storm Electrification Model (SEM) simulation of the 19 July Cooperative Convective Precipitation Experiment (CCOPE) case study cloud against the actual observations with respect to the cloud's electrical characteristics, as deduced from the data of two aircraft. It is found that the SEM reproduces the basic charge and electric field structure of the cloud on a similar time scale to that observed. The comparability of the modeled and observed values of field strength and charge within the cloud is directly related to the proximity of the aircraft to the main active core of the cloud. The character of the electric field external to the cloud appears to be well modeled, at least at the time of observation. A feature which was not observed, but appears in the model, is a charge-screening layer at the top of the anvil. In addition, the model predicts electric field strengths sufficient to initiate a lightning discharge at approximately the same time in cloud evolution as that when an intracloud discharge was recorded.

EMA-86-R-55

A STOCHASTIC MODEL FOR THE TORTUOUS PROPAGATION OF A LIGHTNING STEPPED LEADER

by

Dale A. Steffen
Robert W. Haupt
Terence Rudolph

Prepared for:

September 1986

A STOCHASTIC MODEL FOR THE TORTUOUS PROPAGATION
OF A LIGHTNING STEPPED LEADER

The results of Task 1 produced by EMA for the referenced contract
"Completion of a Lightning Discharge Propagation Model (LDPM)" are discussed in
this report. A FORTRAN code has been written for this model which can be integrated
into the South Dakota School of Mines (SDSM) time-dependent Storm Electrification
Model (SEM). The LDPM has been structured to enable its use in either a two or
three-dimensional SEM with minor modifications.

1.   INTRODUCTION

The LDPM is an approximation of the tortuous path of a lightning channel in
a thunderstorm environment. Location and direction for the initial discharge point must
be supplied as input data to the model. The discharge channel is then established as
a series of connected stepped leader segments and propagates until certain
termination conditions are met. All leader segments are assumed to be the same
length and have equal charge densities. These parameters can be set to any
values desired. While testing the LDPM, parameter values of 50 meters and
1 millicoulomb/meter were used based on the average values published by Uman[1].

The primary parameter calculated in the model is the direction for a segment
of the stepped leader. This computation is based on the effects of random free
electrons in the vicinity of a leader segment tip which determine the direction of the
next stepped leader segment. The details of the direction parameters for a stepped
leader segment will be discussed in the next section. Once this direction is
established, position vectors for a segment can be calculated. The model is then able
to continue the computation of the positions and directions of following stepped leader
segments.

---

[1] Uman, M.A., "Lightning," McGraw-Hill, New York, 1969.

The remainder of this report discusses the calculations used in the LDPM, presents results obtained during the model tests, and provides a discussion on how the code is used. In addition, a listing of the code is provided.

2.   PHYSICAL CONSIDERATIONS

Uman[1] discusses several theories which have been presented since the late 1930's to explain observed stepped leader characteristics. Although basic differences exist between these theories, several fundamental issues are common for the theories and are listed below.

1.   A stepped leader has an inner conducting core wherein most of the current flows.

2.   The core is surrounded by a corona region in which the electric field exceeds the breakdown field of air (approximately 3×10^6 volts/meter for standard temperature and pressure at sea level).

3.   A mechanism exists which precedes the stepped leader to create an ionized channel in "virgin air" which provides continuation of the stepped leader propagation.

4.   As current flow increases into the ionized channel, a condition occurs whereby the conductivity increases until the channel becomes a new segment of the stepped leader and the end of the channel becomes the new tip of the leader.

These theories agree that stepped leader segment directions are randomly distributed. Based on lightning channel tortuosity studies by Hill[2] , the mean absolute direction change is nearly constant from flash-to-flash and on the order of 16 degrees. For purposes of the LDPM, it is assumed that the randomness of the stepped leader direction is related to the random creation of free electrons in air due to cosmic ray bombardment.

[2] Hill, R.D., "Analysis of the Irregular Paths of Lightning Channels," J. Geophys. Res., Vol. 73, 1968 (pp. 1897 - 1906).

Issue 3 is of primary concern for this model. The stepped leader propagation theories often vary when describing this mechanism. The process occurring which results in the formation of the ionization channel ahead of the stepped leader tip has been more recently described by Rudolph[3] from studies involving the interaction of lightning with aircraft in flight.

The leader tip is a region which contains a large charge density and high electric field levels. Free electrons (generated by cosmic rays) in the air are accelerated in this high field until they collide with a neutral atom or molecule. If the electron's kinetic energy is large enough at the time of the collision, the neutral particle can have an electron separated from it, producing a second free electron and a positive ion. The free electrons are then again accelerated by the field, possibly suffering more collisions and producing more free electrons and ions. If the rate of production of free electrons is larger than the rate of loss (by recombination, and attachment to form negative ions), an electron "avalanche" occurs, in which sufficient numbers of electrons and ions are produced and substantially alter the electrical conductivity of the air.

Figures 1 and 2 illustrate how the effects of avalanching result in the generation of a new leader step from an existing leader tip. Figures 1 and 2 also illustrate the ionization path mechanisms for a negatively charged and for a positively charged leader tip, respectively.

In Figure 1, a free electron (at time t_1) is accelerated by the electric field towards the leader tip. As avalanching occurs (time t_2), a net positive charge is formed in the region of the initial free electron position. This results from positive ions which have a much lower mobility or drift velocity than electrons. The net effect is neutralization of the electric field at the leader tip (time t_3). The conductivity in the region approaches the conductivity in the inner core of the stepped leader. Thus, the region in which positive ions were first produced becomes the new leader tip.

In Figure 2, a free electron (at time t_1) is accelerated by the electric field away from the leader tip. As avalanching occurs (time t_2), a net positive charge is

[3] Rudolph, T., and R.A. Perala, "Linear and Non-Linear Interpretation of the Direct Strike Lightning Response of the NASA F106B Thunderstorm Research Aircraft," Electro Magnetic Applications - Denver, EMA-83-R-21, March 21, 1983.
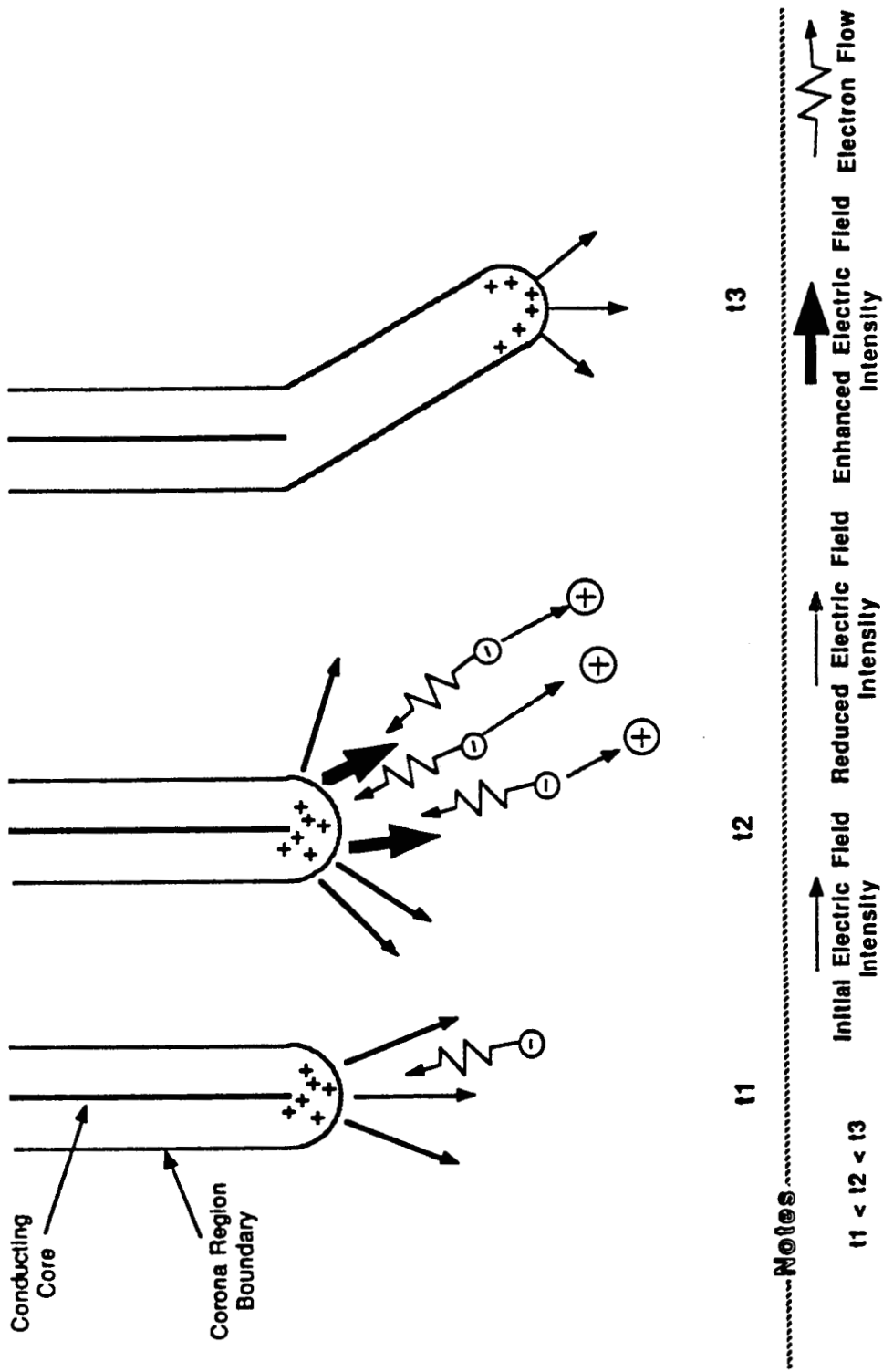
Figure 1. Time Scenario of Free Electron Avalanching for Positively Charged Leader Tip
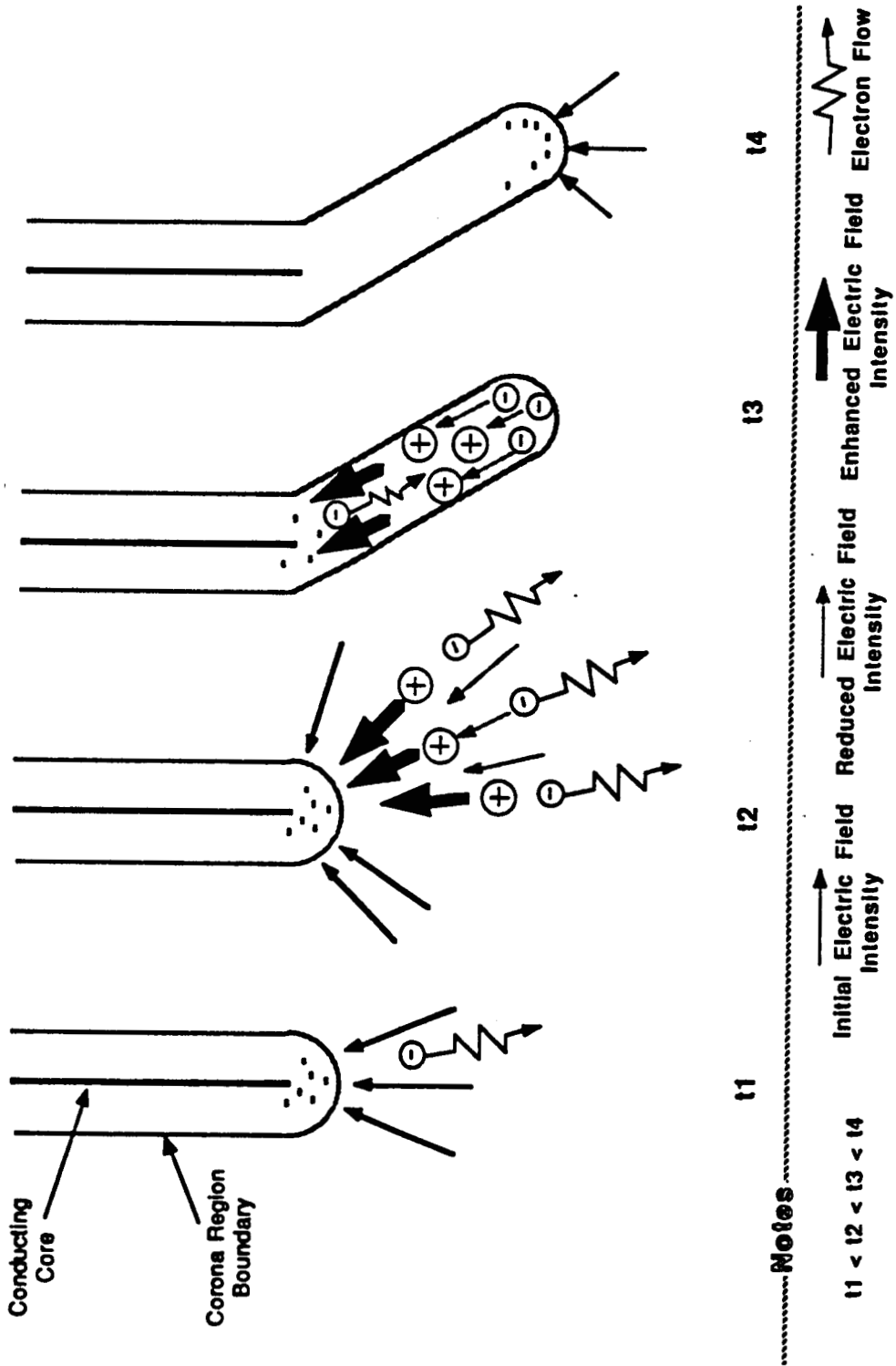
Figure 2. Time Scenario of Free Electron Avalanching for Negatively Charged Leader Tip

Conducting Core

Corona Region Boundary

Notes

t1 < t2 < t3 < t4

t1 — Initial Electric Field Intensity

t2 — Reduced Electric Field Intensity

t3 — Enhanced Electric Field Intensity

t4 — Electron Flow

formed in the region of the initial position of the free electron. Moreover, as the electrons move away from this region, a conducting channel is generated between the positive ions and electrons until the electric field between the two opposite charge regions is neutralized. However, the electric field is enhanced between the leader tip and the positive charge region and induces additional forces on the negative charge region around the tip. In addition, the breakdown region is extended toward the positive charge region. This effect is illustrated in Figure 2 at time t_3 as a new conductive region extends the stepped leader. The leader tip occurs at the negative charge region created by the electrons which were first accelerated away from the original free electron position.

The mechanism for extending the stepped leader is dependent on the location of free electrons which create a conductive channel to the leader tip. Thus, it is necessary to consider all free electrons and determine which one will initiate the first complete ionized path to the leader tip. Moreover, the algorithm used must determine which electron will initiate this complete ionized path in the minimum time (compared to other electrons).

A rigorous mathematical treatment of the mechanisms just discussed would require involved calculations for the avalanche process and resultant conductivity in the stepped leader tip vicinity. These calculations would also involve significant computer time when used in the SEM. A simplified algorithm which has similar dependencies on the position of random electrons and the electric field around the tip of a stepped leader segment was developed.

Since the drift velocities of the positive ions are significantly lower than those of electrons, the first simplification does not account for the mobility of resultant positive ions. The equation of motion for electrons generated by the avalanche is then given by:

$$\frac{d\vec{V_e}}{dt} = -\frac{q_e}{m_e}(\vec{E_T} + \vec{V_e} \times \vec{B}) - v\vec{V_e} \tag{1}$$

where: q_e = electron charge,
        m_e = electron mass,

$\vec{E}_T$ = total electric field,

$\vec{V}_e$ = electron velocity,

$\vec{B}$ = magnetic field, and

v = an approximate collision frequency.

To further simplify this equation, it is assumed that the creation of electrons due to avalanching has progressed to a level where a collision dominated, plasma region exists. In turn, the electron velocity is constant and equal to the drift velocity, and:

$$\frac{d\vec{V}_e}{dt} = 0 . \tag{2}$$

Thus,

$$\frac{q_e}{m_e} \vec{E} - v \vec{V}_d = 0, \quad \text{or} \quad \vec{V}_d = - \mu_e\vec{E} \tag{3}$$

where: μ_e = electron mobility, and

V_d = drift velocity.

It is assumed that the vector $\vec{r}_e$ between the leader tip and the electron position can be approximated by:

$$\vec{r}_e = \vec{V}_dt, \tag{4}$$

or the time necessary to create a channel can be approximated:

$$t = \frac{|\vec{r}_e|}{|\vec{V}_d|} \propto \frac{|\vec{r}_e|}{|\vec{E}_T|} . \tag{5}$$

It is assumed in the model that the ionized channel induced by the avalanching process (resulting from randomly occurring electrons) will initiate the next stepped leader segment in the same direction for either a positively or negatively

charged stepped leader segment. Thus, the model is independent of the leader tip charge. Based on these assumptions, the new stepped leader segment direction is determined by identifying the free electron in the vicinity of the previous stepped leader segment tip which will create an ionization path in a minimum time (compared to other free electrons).

The model requires the following computations which will be discussed in detail in the next sections.

a. Random generation of electrons in the vicinity of each stepped leader tip.

b. Total electric field strength and direction at each electron location.

c. The direction vector of the new stepped leader.

3. LIGHTNING DISCHARGE PROPAGATION MODEL CALCULATIONS

3.1 Description

The LDPM code was written to predict the tortuous path of a lightning channel based on the physical considerations in Section 2. The routine is programmed to calculate the parameters for each stepped leader segment.

3.1.1 Random Electron Generation

A Monte Carlo technique was used to generate the random locations of free electrons within a sphere around each leader segment tip. The ambient electron density is assumed to be .2 electrons/m^3. The size of the sphere is dependent upon the number of free electrons. Each model run in this report considered 500 random electrons around each tip. Thus, the sphere centered at the leader tip was required to have a radius of 8.419 meters.

A seed integer is also required for the Monte Carlo routine. This seed controls the random placement of electrons. Different seeds will produce different sets of electron locations.

3.1.2   Total Electric Field Calculation

The total electric field strength and direction was computed for each electron location generated by the Monte Carlo technique. The electric field at any electron location should be the resultant of the ambient field and the fields due to the previous leader segments. The model code was tested to incorporate the effects of the previous leader segments and the ambient field in the electric field calculation. It was observed that this calculation only required the ambient electric field and the electric field components due to the two leader segments closest to the electron. Electric fields caused by segments further away did not affect the modeled lightning path significantly. The total resultant electric field at a location (x,y,z) in the vicinity of the ith stepped leader segment is stated below:

$$E_{total}\ (x,y,z)\ =\ E_{ambient}\ (x,y,z)\ +\ E_{i\ segment}\ (x,y,z)\ +\ E_{i\text{-}1\ segment}\ (x,y,z)\ . \qquad (6)$$

The general equation for the electric field at any point in space due to a line charge is given below and is illustrated by Figure 3.

The electric field at any point in space due to the line charge element λdl is:

$$d\vec{E}\ =\ \frac{\lambda dl\ (\vec{r} - \vec{r}')}{4\pi\varepsilon_0\ |\vec{r} - \vec{r}'|^3}\ ;\ \lambda\ =\ \text{charge/unit length}\ . \qquad (7)$$

Thus, the electric field at point p due to the total line charge is:

$$\vec{E}\ =\ \frac{\lambda}{4\pi\varepsilon_0}\ \int_0^L\ \frac{\vec{r} - (\vec{R} + l\vec{u})}{|\vec{r} - (\vec{R} + l\vec{u})|^3}\ dl\ . \qquad (8)$$

B-10
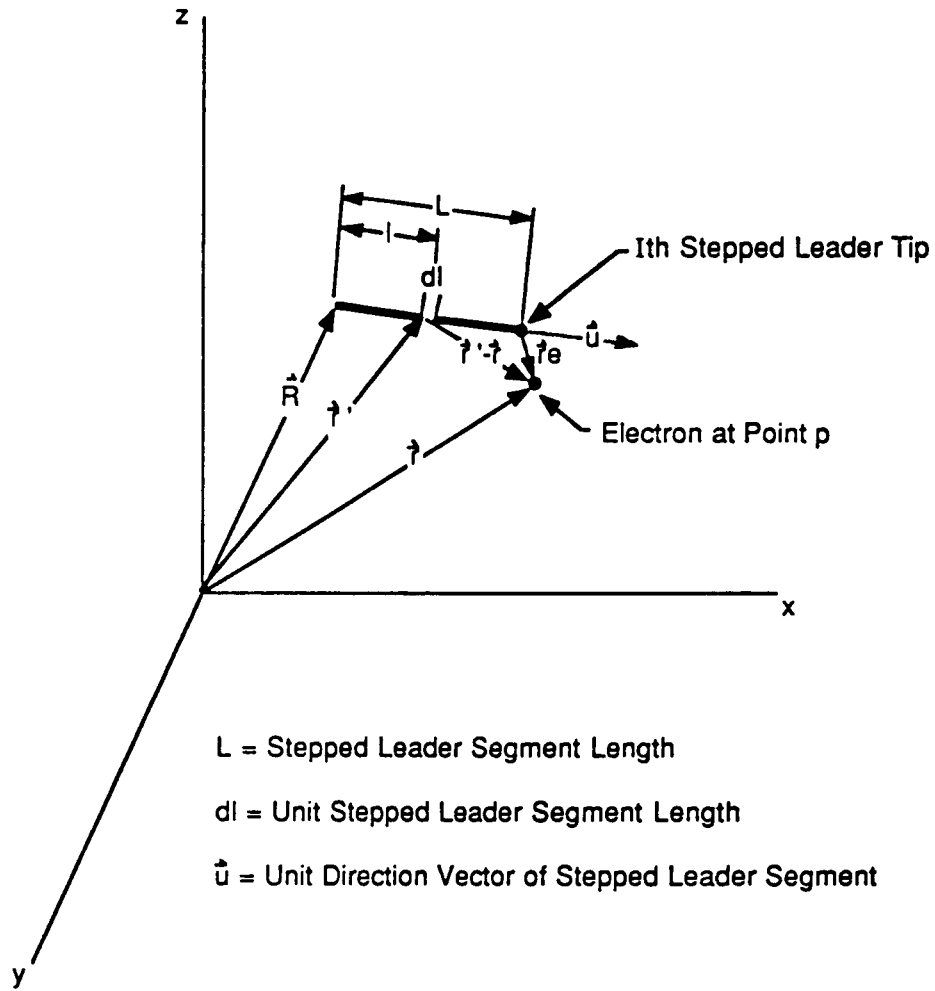
Figure 3. Stepped Leader Segment Line Charge and Its Parameters in World Coordinates

L = Stepped Leader Segment Length

dl = Unit Stepped Leader Segment Length

$\vec{u}$ = Unit Direction Vector of Stepped Leader Segment

The general world coordinate solution for the electric field due to the line charge becomes:

$$\vec{E} = \frac{\lambda}{4\pi\varepsilon_0 (A^2 - B^2)} \left\{ \left[\frac{\vec{A}(L - B) + \vec{u}(A^2 - BL)}{(A^2 - 2BL + L^2)^{1/2}} \right] - \left[\frac{A^2\vec{u} - \vec{A}B}{|A|} \right] \right\} \tag{9}$$

where: $\vec{A} = \vec{r} - \vec{R}$, and
         $B = \vec{A} \cdot \vec{u}$.

Figure 4 depicts the constant electric field contours due to a line charge. The arrows show the direction of the electric field.

3.1.3 Direction Vector of the New Stepped Leader Segment

Only one of the electrons generated in the vicinity of the leader tip will properly satisfy the model requirements and determine the direction of the new stepped leader segment. For simplification, each stepped leader segment is assumed to be positively charged (as discussed in Section 2) for the LDPM. The new stepped leader segment is assumed to be initiated by the ionized path formed in the least time. The time to generate the ionized path is proportional to the ratio formed from the distance of the leader tip to the electron (r_e) and the resultant electric field strength (E_T) at the electron location. This relationship was determined in Section 2 and is stated in Equation 5. Thus, the new stepped leader segment direction is chosen to be the electric field direction at the initial location of the free electron which initiates an ionized path in the minimum time (compared to other electrons).

If the angle θ_e, formed by the E_T and r_e vectors at the initial electron location is within a certain angle range, that electron will create an ionized channel to the leader tip along a "relatively" straight path. The time it takes to establish the ionization channel can be approximated using Equation (5). As θ_e increases beyond this certain angle range, the actual path of the ionization channel along electric field lines will deviate from a straight line. Therefore, the actual time it takes to establish the ionized channel to the leader tip may be significantly greater than the time approximated by Equation (5). In fact, if θ_e is large enough, the ionized path may not attach to the leader segment tip, but to some point behind the tip instead. The cosine of θ_e formed by E_T and r_e at any electron location is computed as follows:

$$\cos \theta_e = \frac{\vec{r_e} \cdot \vec{E_T}}{|\vec{r_e}| \, |\vec{E_T}|} . \tag{10}$$

A stepped leader segment is defined by the computer code as a finite length with its tip being a single point. In nature, the leader tip is not a single point but is actually defined as a volume. In terms of the LDPM, this volume exists around the
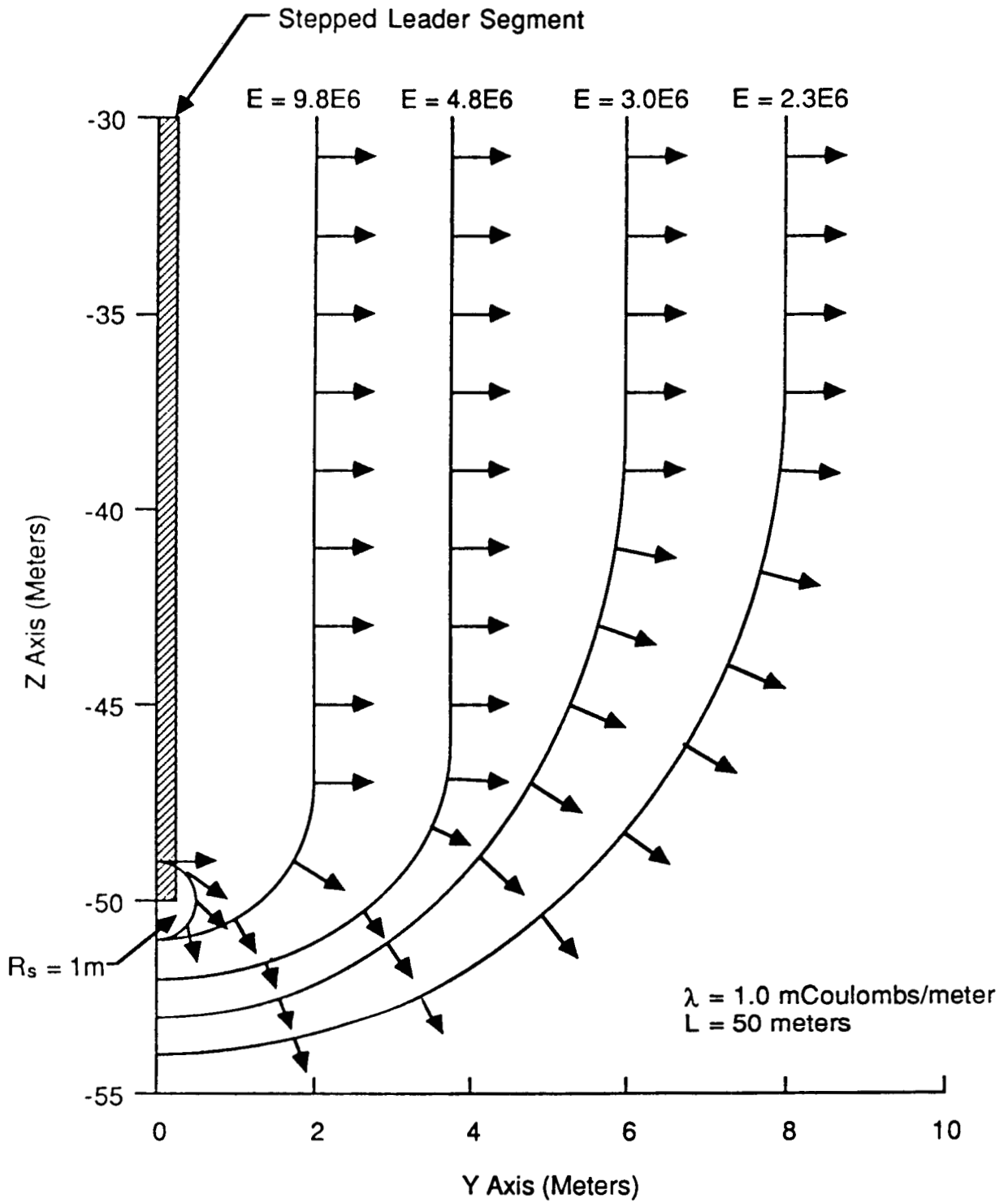
Figure 4. Constant Electric Field Amplitude Contours for Line Charge

leader tip point and has an electric field strength greater than 3×10^6 V/m everywhere inside.

Figure 5 depicts the above concepts. The angle range parameter is determined by the radius of the corona region. This radius is on the order of 2 meters and is assumed to be the same magnitude for all leader segments in the LDPM. The angle range parameter was adjusted to an absolute value of 12.5 degrees. This value appeared to allow the lightning channel path to be reasonably tortuous. The angle range parameter can be changed in the LDPM as desired. However, 12.5 degrees is recommended, since smaller angle parameter values limit the tortuousity, while larger angle parameter values result in erratic tortuousity which exceeds the findings of Hill[2].

Each of the 500 electrons generated by the Monte Carlo routine is tested in the code to determine which one is used to establish the direction of the new stepped leader segment. The one electron chosen must meet the following conditions:

1. The initial free electron which initiates an avalanche must originate in a location where the electric field strength is less than 3×10^6 V/m. (If the field was larger, the electron was assumed to be inside the corona region of the leader segment and was not considered).

2. The angle θ_e formed by E_T and r_e for an electron location must be less than the angle range parameter (absolute value of 12.5 degrees) (If θ_e was greater, the electron was not considered).

3. Of the remaining electrons, the electron which creates an ionization channel to the leader tip in the least time, t (as computed in Equation (5)) was identified and used to calculate the new direction.

The new stepped leader segment direction is then taken to be the direction of the total electric field at this "identified" electron location.

It is important to note that, if the Monte Carlo sphere is too small, most or all of the random electrons will lie in a region where the electric field strength is above 3×10^6 V/m. In turn, the model may not function properly. It was observed that a sphere containing 500 electrons and having a radius of 8.419 meters worked best

Ith Stepped Leader Segment

$\vec{E}_I$ = Electric field component due to the Ith leader segment line charge

$\vec{E}_T$ = Total resultant electric field

θ_e = Angle between $\vec{r}_e$ and $\vec{E}_T$

Ambient Electric Field

θ_e

$\vec{E}_I$ Ambient $\vec{E}$

$\vec{E}_T$

Electron "C" $\vec{r}_e$

Stepped Leader Tip Coordinate (LTP)

Corona Region Boundary

Avalanche Path

Monte Carlo Sphere (Contains Random Free Electrons)

$\vec{r}_e$

$\vec{r}_e$

Electron "B"   Ambient $\vec{E}$ Electron "A"

θ_e $\vec{E}_T$ $\vec{E}_I$ Ambient $\vec{E}$

$\vec{E}_I$ θ_e $\vec{E}_T$

θ_e

Ambient Electric Field

Electron "A" will be drawn to the leader tip in time, t.
t can be adequately approximated in equation [5] since θ_e <12.5°.

Electron "B" will be drawn to the leader tip along the path illustrated.
The time will be significantly greater than t computed by equation [5] since θ_e > 12.5°.

Electron "C" will not be drawn to the leader tip at all and equation [5] does not apply.
However, θ_e >12.5° and the electron will not be considered.

Figure 5.   Paths of Free Electrons In Vicinity of Stepped Leader Tip

during the LDPM development. This sphere size contained enough electrons in a region where the electric field was below breakdown and allowed the LDPM to function properly and efficiently.

3.2   Model Termination Conditions

The LDPM will terminate if any of the following conditions are met:

1.   The stepped leader enters a defined region (grid cell) with an ambient electric field less than 1.5×10^5 V/m. This termination criterion was based on work done by Griffiths[4] involving the propagation of positive streamers in the laboratory,

2.   The stepped leader propagates outside the designated problem space,

3.   (Optional) The stepped leader enters a defined charged region (Specified grid cell).

3.3   MODEL INPUT AND OUTPUT REQUIREMENTS

3.3.1   Input

The problem space is depicted as a rectangular grid either in two or three dimensions. The code is written to accommodate two or three-dimensional data. This version of the LDPM is adjusted for a two-dimensional SEM. Each grid cell has side lengths equal to 200 meters. This routine requires the number of grid cells along the x-axis (horizontal), along the z-axis (vertical), and the initial discharge coordinate (x,z). Ambient electric field components are required for each grid cell. The routine also requires a seed integer for the Monte Carlo scheme. These variables are:

1.   NCELX   Number of cells along the x-axis
       NCELZ   Number of cells along the z-axis,

---

4 Griffiths, R.F. and C.T. Phelps, "The Effects of Air Pressure and Water Vapor Content on the Propagation of Positive Corona Streamers and Their Implications to Lightning Initiation," Quart. J. Roy. Meteor. Soc., Vol 102, 1976 (p. 419).

2.	ICX, ICZ	Initial discharge point (x,z),
3.	FEX(K), FEZ(K)	One-dimensional array of x,z ambient field components, and
4.	ISEED	Monte Carlo seed integer; must be less than 32,000.

For the NCAR Electricity Model:

1. NCELX = 97;   NCELZ = 97
2. ICX = 86;   ICZ = 31
3. FEX(K), K = 1, 9409;   FEZ(K), K = 1, 9409

3.3.2   Output

The routine generates the (x,z) position in world coordinates for each stepped leader segment tip in the propagation path. The x and z arguments are written in the one-dimensional RX and RZ arrays. Coordinate values x and z are given in meters from the origin (x = 0, z = 0). These arguments can be passed back into the main program and are as follows:

1.	RX(NL), RZ(NL)	One-dimensional arrays of the x and z values in meters
		NL corresponds to the leader number (not the grid cell number), and
2.	NFL	Integer; total number of NL leader segments.

3.4   MODEL EXAMPLES

Several lightning discharge propagation paths were generated and are shown in Figures 6 through 8. Figure 6 shows the lightning paths modeled for the NCAR electricity data at 58.5 minutes. The solid and dashed lines are the models

Key
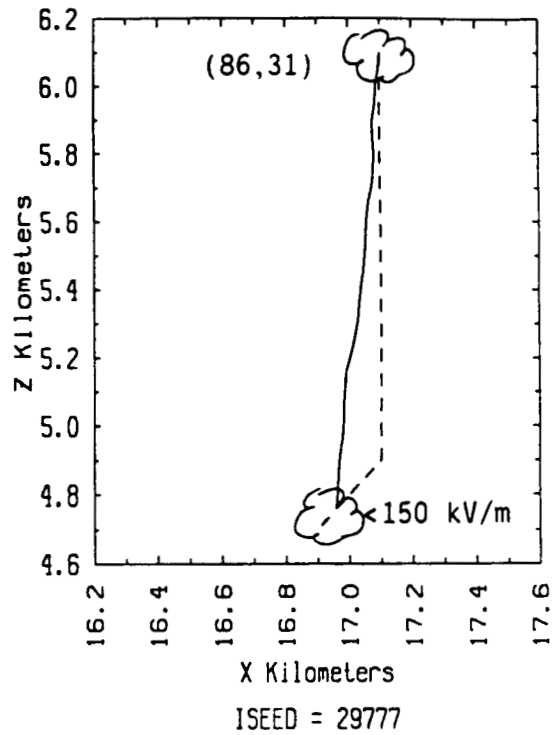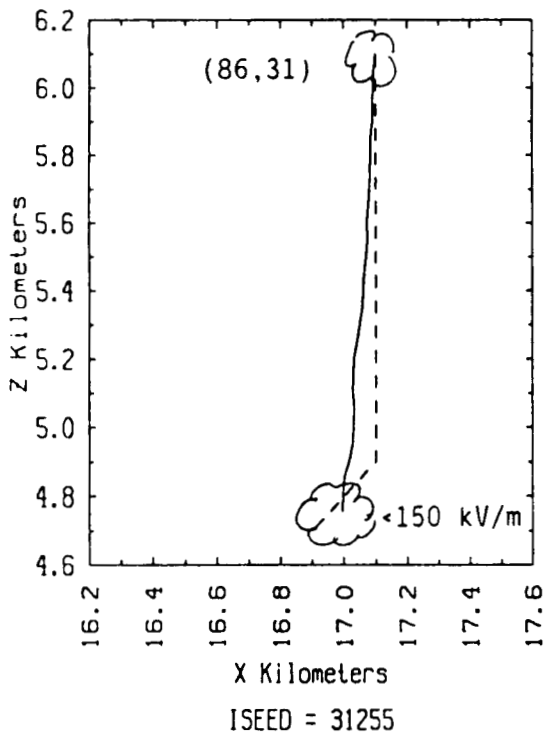
------ SDSM Algorithm
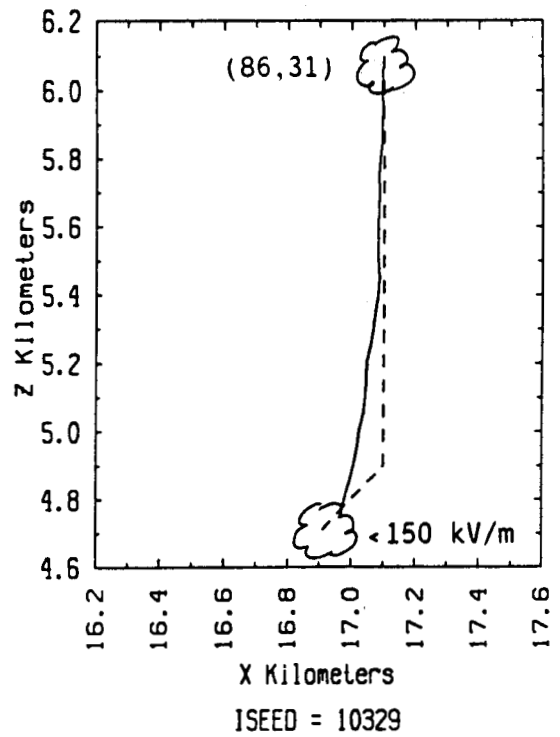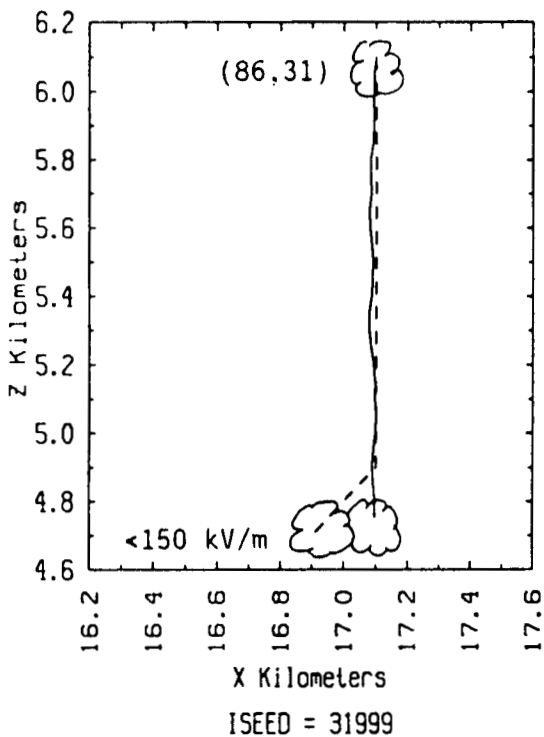
——— EMA Algorithm

**Figure 6. NCAR Electricity Model Data (58.5 Minutes)
(Comparison of Monte Carlo Seeds)**
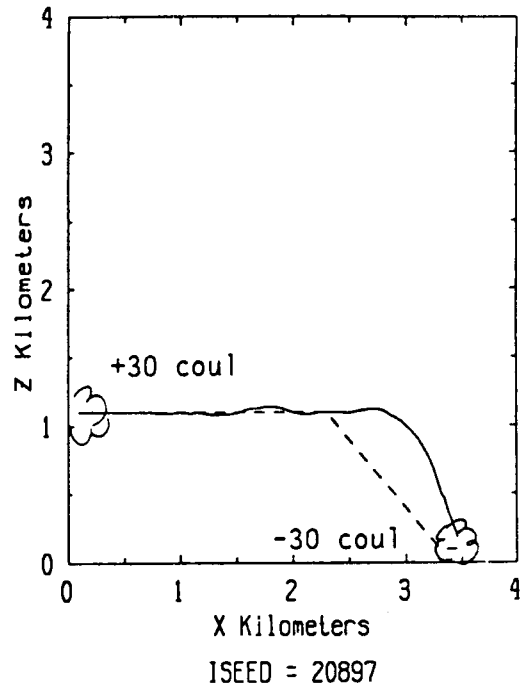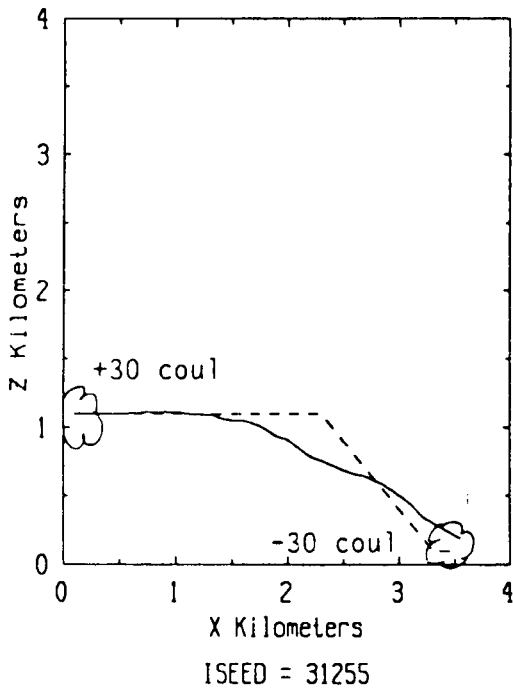
Figure 7. EMA Electricity Model Data - Initial Discharge
In the Positively Charged Grid Cell
(Comparison of Monte Carlo Seeds)

Key
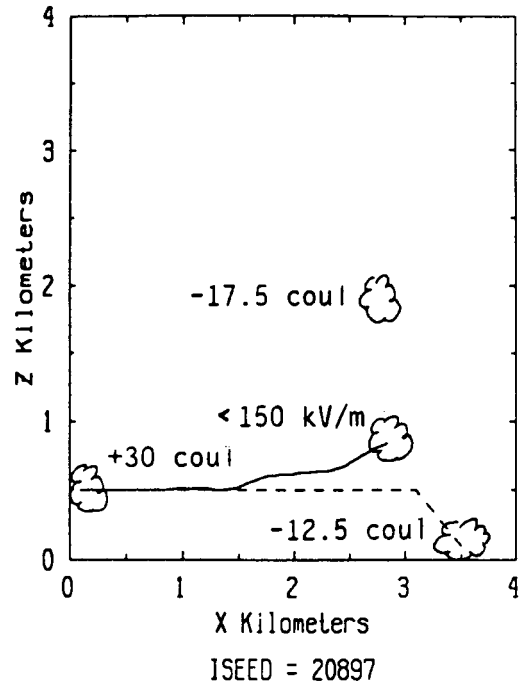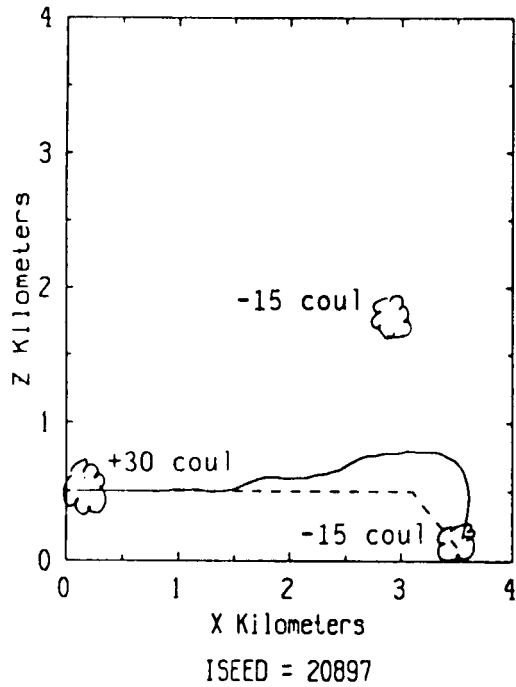
----- SDSM Algorithm
——— EMA Algorithm
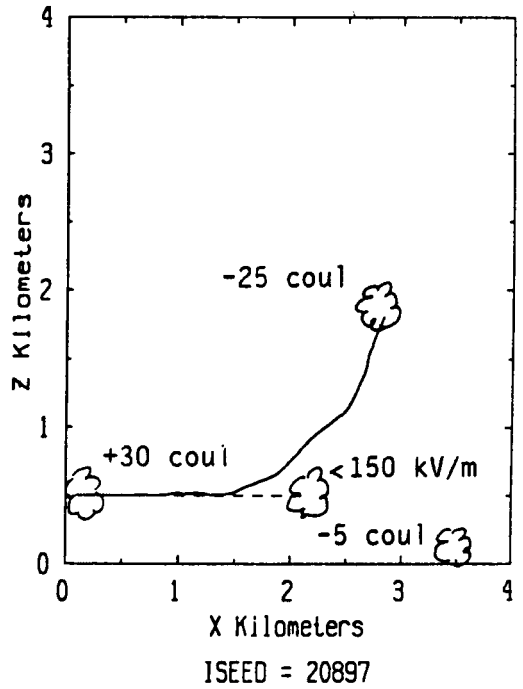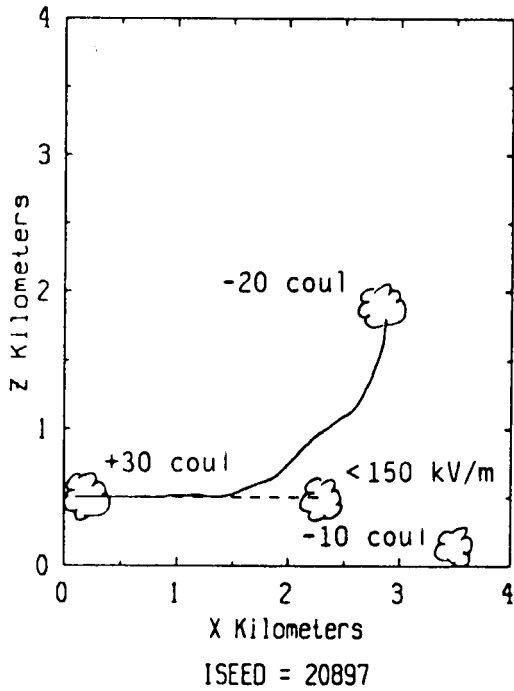
Figure 8.   EMA Electricity Model Data - Initial Discharge
in the Positively Charged Grid Cell
(Comparison of Different Ambient Electric Fields)

produced from the LDPM and the algorithm described in Helsdon[5], respectively. The four plots in Figure 6 demonstrate the effects of varying ISEED (Monte Carlo Seed for Generating Random Electron Locations).

Figure 7 shows the effects of ISEED for ambient electric fields generated from an in-house routine. This routine creates electric fields from a set of discrete charge centers. Figure 8 shows the effects of varying the charge magnitudes at specified cells. These ambient fields were computed from the in-house routine.

4.   MODEL VERSIONS AND DATA

The listings for three versions of LDPM are included in Appendix A of this report. In addition, the code used to generate ambient electric fields is included. The listings are as follows:

1.   LDPM - Subroutine
Subroutine with common statements; requires the number of x cells (NCELX), z cells (NCELZ), the initial discharge coordinate, ambient electric field components at each cell, and ISEED. Passes leader tip locations RX(I), RZ(I) and NFL, the number of total leaders back into main program.

2.   LDPM.FOR
Routine reads in ambient electric fields; requires NCELX, NCELZ, initial discharge coordinate, and ISEED. Calculates leader tip locations.

3.   LDPM - Interactive (not required by contract; used as test program)
Interactive routine; generates ambient electric field components over grid from specified cells and their charge magnitudes. Requires NCELX, NCELZ, the initial discharge coordinate, and ISEED. Routine also requires coordinates of specified charge cells. Calculates leader tip locations.

5 Helsdon, J.H., R.D. Farley and G. Wu, "A Lightning Parameterization Scheme in a Two-Dimensional, Time-Dependent Storm Electrification Model," presented at the 1986 Conference on Cloud Physics, held Sept. 22-26, 1986 in Snowmass, Colorado.

4. EFS.DT

NCAR ambient electric field data (58.5 minutes, unformatted)

FEX(K), K = 1, 9409;   FEZ(K), K = 1, 9409.

ADDITIONAL REFERENCES

1. Krider, E.P., C.D. Weidman, and R.C. Noggle, "The Electric Fields Produced by Lightning Stepped Leaders", J. Geophy. Res., 82, 1981 (pp.951-960).

2. Fleagle, R.G., J.A. Busingeil, " An Introduction to Atmospheric Physics", Academic Press, New York, 1963.

3. Golde, R.H., "Physics of Lightning - Volume 1," Academic Press, New York, 1972.

4. Hill, R.D., "Analysis of Irregular Paths of Lightning Channels," J. Geophys. Res., Vol. 73, 1968 (pp. 1897 - 1906).

APPENDIX B - CONTINUED

APPENDIX A (LDPM CODE VERSIONS) TO

REPORT EMA-86-R-55

APPENDIX A

LDPM CODE VERSIONS

LDPM -SUBROUTINE

```
      SUBROUTINE LDPM
C     DEVELOPED BY E.M.A. - AUGUST 1986
C     SUB-PROGRAM DETERMINES DIRECTION OF NEXT LEADER SEGMENT DUE TO
C     ELECTRON WHICH WILL FORM AN IONIZED PATH TO
C     THE STEPPED LEADER SEGMENT TIP IN THE LEAST TIME
C     E FIELD TOTAL = E FIELD LEADER + E FIELD PREVIOUS LEADER
C              + AMBIENT E FIELD
C
C     NCEL= # CELLS IN X AND IN Z
C     ICX,ICZ= RX,RZ COORD OF INITIAL CHARGE REGION
C     NFL= TOTAL NUMBER OF STEPPED LEADER SEGMENTS
      COMMON/MAIN/RX(0:500),RZ(0:500),FEX(9409),FEZ(9409)
      COMMON/VAR/NCELX,NCELZ,ICX,ICZ,NFL
      CHARACTER*40 OFILE1,OFILE2
C
C     ISEED=RANDOM FUNCTION INTEGER
      ISEED=30997
C
      OFILE1='LDPM.DAT'    ! BINARY PLOTFILE OF LIGHTNING PATH
      OFILE2='LDPM.PRINT'  ! PRINT VALUES OF LIGHTNING MODEL
C
C     INPUT VARIABLES
C     CL=SEGMENT LENGTH     ELAMBDA=LEADER CHARGE DENSITY
C     BDF=BREAK DOWN FIELD  EK=1/4PIEPSO        NL=LEADER #
C     DZ=Z CELL HEIGHT      DX=X CELL WIDTH
C     NE=# FREE ELECTRONS   ED=ELECTRON DENSITY (.2/m**3)
C     Q=MAX ALLOWABLE ANGLE BTW EFIELD & DIRECTION VECTORS
C
      DATA CL,ELAMBDA,BDF/50.,.001,1.5E5/
      DATA PI,EK,NL/3.1415927,9.E9,0/
      DATA DZ,DX,NE,ED,Q/200.,200.,500,.2,12.5/
      DATA EXM1,EYM1,EZM1/3*0./
      TWOPI=2.*PI
      QP=Q*PI/180.
      CONST=EK*ELAMBDA
      VOL=FLOAT(NE)/ED
      RADIUS=(.75*VOL/PI)**(1./3.)
      KTOT=NCELX*NCELZ
      XTOT=NCELX*DX
C
C     INITIALIZE STEPPED LEADER PROPAGATION
C     INPUT DATA: R1, AMBIENT E FIELD, U1
C     COORDINATES OF INITIAL POINT ON GRID PROBLEM SPACE
      RX(0)=DX*(FLOAT(ICX)-.5)
      RY=0.  ! FOR 2D CASE;  RY(0)=DY*FLOAT(ICY)-.5), FOR 3D CASE
      RZ(0)=DZ*(FLOAT(ICZ)-.5)
C
      IC=ICX+NCELX*(ICZ-1)
C     FOR 2D CASE
      ETOT=SQRT(FEX(IC)*FEX(IC)+FEZ(IC)*FEZ(IC))
C     FOR 3D CASE
C     ETOT=SQRT(FEX(IC)*FEX(IC)+FEY(IC)*FEY(IC)+FEZ(IC)*FEZ(IC))
C     DEFINE UNIT VECTOR
      UX=FEX(IC)/ETOT
      UY=0.  ! FOR 2D CASE; UY=FEY(IC)/ETOT, FOR 3D CASE
      UZ=FEZ(IC)/ETOT
C
      OPEN(1,FILE=OFILE1,FORM='UNFORMATTED',STATUS='NEW')
      OPEN(2,FILE=OFILE2,STATUS='NEW')
C
```

B-26

C - 2

```
C   START LOOP
 2000   NL=NL+1
C
C   DETERMINE CELL POSITION OF NEW LEADER SEGMENT TIP ON OVERLAY
C   USE APPROPRIATE AMBIENT E FIELD MAGNITUDE AND DIRECTION
C    K IS THE CELL NUMBER OF THE LEADER SEGMENT TIP LOCATION
        KX=ANINT((RX(NL-1)/DX)+.5)
        KZ=ANINT((RZ(NL-1)/DZ)+.5)
        K=KX+NCELX*(KZ-1)   ! NEED KY FOR 3D CASE
C   FOR 2D CASE
        EFAMB=SQRT(FEX(K)*FEX(K)+FEZ(K)*FEZ(K))
C   FOR 3D CASE
C        EFAMB=SQRT(FEX(K)*FEX(K)+FEY(K)*FEY(K)+FEZ(K)*FEZ(K))
C
C   TERMINATE IF
C   LEADER SEGMENT HAS PROPAGATED OUTSIDE THE GRID
C   LEADER SEGMENT ENTERING CELL WITH AN AMBIENT FIELD LT 1.5M V/M
        IF(K.LT.1.OR.K.GT.KTOT.OR.
     +     RX(NL-1).LT.0.OR.RX(NL-1).GT.XTOT)GOTO 3000
C
        WRITE(2,*)'LEADER SEGMENT NUMBER',NL
        WRITE(2,*)'CELL NUMBER  ',K,'     (X,Z) COORD',KX,KZ
        WRITE(2,*)'TOT E FIELD   ',ETOT,' AMB E FIELD ',EFAMB
        WRITE(2,*)'AMB EX        ',FEX(K),' AMB EZ       ',FEZ(K)
        WRITE(2,*)'X COORD       ',RX(NL-1),' Z COORD      ',RZ(NL-1)
        WRITE(2,*)'                                        '
        WRITE(1)RX(NL-1),RZ(NL-1)
C
        IF(EFAMB.LT.BDF)GOTO 3000
C
C   SHORTEST TIME OF ELECTRON TO FORM IONIZED CHANNEL
C   THIS TIME DETERMINES DIRECTION OF NEW LEADER SEGMENT
        TMIN=1.E20
C
C   USE MONTE CARLO METHOD TO GENERATE RANDOM FREE ELECTRONS
C   TO CALCULATE ELECTRON DISTRIBUTION NEAR LEADER SEGMENT TIP
        RXP=RX(NL-1)+UX*CL
        RYP=RY+UY*CL   ! USE RY(NL-1) FOR 3D CASE
        RZP=RZ(NL-1)+UZ*CL
C
        DO 100 I=1,NE
C
C   IN WORLD COORDINATES
        CALL RANDOM(ISEED,RAND)
        RE=RAND*RADIUS
C        RE=SQRT(RAND*RADIUS*RADIUS) ! FOR ACTUAL RANDOM DISTRIBUTION
        CALL RANDOM(ISEED,RAND)
        TH=RAND*PI
C        TH=ACOS((RAND*2)-1)            ! FOR ACTUAL RANDOM DISTRIBUTION
        CALL RANDOM(ISEED,RAND)
        PH=RAND*TWOPI
        RMX=RE*SIN(TH)*COS(PH)
        RMY=RE*SIN(TH)*SIN(PH)
        RMZ=RE*COS(TH)
        RM=SQRT(RMX*RMX+RMY*RMY+RMZ*RMZ)
        X=RMX+RXP
        Y=RMY+RYP
        Z=RMZ+RZP
C
C   COMPUTE E FIELD COMPONENTS FOR Ith ELECTRON
```

```
      AX=X-RX(NL-1)
      AY=Y-RY   ! USE RY(NL-1) FOR 3D CASE
      AZ=Z-RZ(NL-1)
      A=SQRT(AX*AX+AY*AY+AZ*AZ)
      IF(A.LT.1.E-6)GOTO 100
      B=AX*UX+AY*UY+AZ*UZ
      AS=A*A
      BS=B*B
      IF(AS-BS.LT.1.E-6)GOTO 100
      P=CONST/(AS-BS)
      D=CL*CL-2.*B*CL+AS
      IF(D.LE.0.)GOTO 100
      D=SQRT(D)
C
C   E FIELD COMPONENTS DUE TO LEADER SEGMENT AND AMBIENT FIELD
      EX=P*(((AX*(CL-B)+UX*(AS-B*CL))/D)-
     +    ((UX*AS-AX*B)/A))+FEX(K)
      EY=P*(((AY*(CL-B)+UY*(AS-B*CL))/D)-
     +    ((UY*AS-AY*B)/A))  !+FEY(K) FOR 3D CASE
      EZ=P*(((AZ*(CL-B)+UZ*(AS-B*CL))/D)-
     +    ((UZ*AS-AZ*B)/A))+FEZ(K)
C

      IF(NL.LE.1)GOTO 1000
      AXM1=X-RX(NL-2)
      AYM1=Y-RYM1   ! FOR 2D CASE;  RYM1=RY(NL-2), FOR 3D CASE
      AZM1=Z-RZ(NL-2)
      AM1=SQRT(AXM1*AXM1+AYM1*AYM1+AZM1*AZM1)
      IF(AM1.LT.1.E-6)GOTO 100
      BM1=AXM1*UXM1+AYM1*UYM1+AZM1*UZM1
      ASM1=AM1*AM1
      BSM1=BM1*BM1
      IF(ASM1-BSM1.LT.1.E-6)GOTO 100
      PM1=CONST/(ASM1-BSM1)
      DM1=CL*CL-2.*BM1*CL+ASM1
      IF(DM1.LE.0.)GOTO 100
      DM1=SQRT(DM1)
C
C   E FIELD COMPONENTS DUE TO PREVIOUS LEADER SEGMENT
      EXM1=PM1*(((AXM1*(CL-BM1)+UXM1*(ASM1-BM1*CL))/DM1)-
     +    ((UXM1*ASM1-AXM1*BM1)/AM1))
      EYM1=PM1*(((AYM1*(CL-BM1)+UYM1*(ASM1-BM1*CL))/DM1)-
     +    ((UYM1*ASM1-AYM1*BM1)/AM1))
      EZM1=PM1*(((AZM1*(CL-BM1)+UZM1*(ASM1-BM1*CL))/DM1)-
     +    ((UZM1*ASM1-AZM1*BM1)/AM1))
C
C   TOTAL E FIELD COMPONENTS FOR Ith ELECTRON
 1000 EX=EX+EXM1
      EY=EY+EYM1
      EZ=EZ+EZM1
      ET=SQRT(EX*EX+EY*EY+EZ*EZ)+.01
      DL=(RMX*EX+RMY*EY+RMZ*EZ)/(RM*ET)
C
C   CHOOSE APPROPRIATE ELECTRON TO FORM IONIZED CHANNEL
C   TO THE LEADER SEGMENT TIP IN SHORTEST TIME
      IF(ET.LT.(3.0E6).AND.(RM/ET).LT.TMIN.
     +  AND.ACOS(ABS(DL)).LE.QP)THEN
      TMIN=RM/ET
      ETOT=ET
      DIRX=EX
      DIRY=EY
```

```
          DIRZ-EZ
          END IF
  100     CONTINUE
C
C   CALCULATE DIRECTION FOR NEXT LEADER SEGMENT
          DRX=CL*UX
          DRY=CL*UY
          DRZ=CL*UZ
          RYM1=RY
          RY=RY+DRY  ! FOR 2D CASE, RY(NL)=RY(NL-1)+DRY, FOR 3D CASE
          RX(NL)=RX(NL-1)+DRX
          RZ(NL)=RZ(NL-1)+DRZ
C
C   NEW UNIT VECTOR
C   UNIT VECTOR IS PROJECTED ONTO X,Z PLANE FOR 2D SPACE
C   FOR 3D CASE
C       DIR=SQRT(DIRX*DIRX+DIRY*DIRY+DIRZ*DIRZ)
C   FOR 2D CASE
          DIR=SQRT(DIRX*DIRX+DIRZ*DIRZ)
          IF(DIR.GE.1.E-6)THEN
          UXM1=UX
          UYM1=UY
          UZM1=UZ
          UX=DIRX/DIR
          UY=0.  ! FOR 2D CASE; UY=DIRY/DIR, FOR 3D CASE
          UZ=DIRZ/DIR
          END IF
C
          GO TO 2000
C
 3000     NFL=NL
          IF(K.LT.1.OR.K.GT.KTOT.OR.
     +        RX(NL-1).LT.0.OR.RX(NL-1).GT.XTOT)THEN
          WRITE(2,*)'LEADER OUT OF BOUNDS'
          END IF
          IF(EFAMB.LT.BDF)THEN
          WRITE(2,*)'LEADER SEGMENT ENTERED REGION LT BREAK DOWN'
          END IF
C
          CLOSE(1)
          CLOSE(2)
          RETURN
          END
C
C
          SUBROUTINE RANDOM(ISEED,RAND)
C   RANDOM NUMBER GENERATOR
C
          DOUBLE PRECISION E31,E32,SI,SJ
          E31=2.**31
          E32=2.**32
          SI=DFLOAT(ISEED)
          SJ=MOD(69069.*SI+1.,E32)
          IF(ABS(SJ).LT.E31)THEN
          SI=SJ
          ELSEIF(SJ.GE.E31)THEN
          SI=SJ-E32
          ELSE
          SI=SJ+E32
          END IF
```

```fortran
IF(SI.GE.O.)THEN
RAND=SI/E32
ELSE
RAND=1.+SI/E32
END IF
ISEED=INT(SI)
RETURN
END
```

LDPM.FOR

```
C    DEVELOPED BY E.M.A. -  AUGUST 1986
C    PROGRAM DETERMINES DIRECTION OF NEXT LEADER SEGMENT DUE TO
C    ELECTRON WHICH WILL FORM AN IONIZED PATH TO THE SEGMENT TIP IN
C    THE LEAST TIME
C    E FIELD TOTAL = E FIELD SEGMENT + E FIELD PREVIOUS SEGMENT
C            + AMBIENT E FIELD
C
C    NCEL= # CELLS IN X AND IN Z
C    ICX,ICZ= X,Y COORD OF INITIAL CHARGE REGION
        PARAMETER(NCELX=97,NCELZ=97,ICX=86,ICZ=31)
        DIMENSION FEX(9409),FEZ(9409)
        CHARACTER*40 INFILE,OFILE1,OFILE3
C
C    ISEED=RANDOM FUNCTION INTEGER
        ISEED=20897
C    SPECIFIED CHARGED REGION CELLS (OTHER THAN INITIAL CHARGED CELL)
        DATA NC1,NC2/195,18/
C
        INFILE='EFS.DT'        ! INPUT AMBIENT E FIELDS
        OFILE1='LDPM3.DAT'     ! BINARY PLOTFILE OF LIGHTNING PATH
        OFILE3='LDPM.PRINT'    ! PRINT VALUES OF LIGHTNING MODEL
C
C    INPUT VARIABLES
C    CL=SEGMENT LENGTH     ELAMBDA= SEGMENT CHARGE DENSITY
C    BDF=BREAK DOWN FIELD  EK=1/4PIEpso        NL=LEADER SEGMENT #
C    DZ=Z CELL HEIGHT      DX=X CELL WIDTH
C    NE=# FREE ELECTRONS   ED=ELECTRON DENSITY (.2/m**3)
C    Q=MAX ALLOWABLE ANGLE BTW EFIELD & DIRECTION VECTORS
C
        DATA CL,ELAMBDA,BDF/50.,.001,1.5E5/
        DATA PI,EK,NL/3.1415927,9.E9,0/
        DATA DZ,DX,NE,ED,Q/200.,200.,500,.2,12.5/
        DATA EXM1,EYM1,EZM1/3*0./
        TWOPI=2.*PI
        QP=Q*PI/180.
        CONST=EK*ELAMBDA
        VOL=FLOAT(NE)/ED
        RADIUS=(.75*VOL/PI)**(1./3.)
        KTOT=NCELX*NCELZ
        XTOT=NCELX*DX
C
C    READ IN AMBIENT E FIELDS
        OPEN(2,FILE=INFILE,FORM='UNFORMATTED',STATUS='OLD')
        READ(2)(FEX(K),K=1,KTOT),(FEZ(K),K=1,KTOT)
        CLOSE(2)
C
C    INITIALIZE LEADER SEGMENT PROPAGATION
C    INPUT DATA: R1, AMBIENT E FIELD, U1
C    COORDINATES OF INITIAL POINT ON GRID PROBLEM SPACE
        RX=DX*(FLOAT(ICX)-.5)
        RY=0.
        RZ=DZ*(FLOAT(ICZ)-.5)
C
        IC=ICX+NCELX*(ICZ-1)
        ETOT=SQRT(FEX(IC)**2+FEZ(IC)**2)
C    DEFINE UNIT VECTOR
        UX=FEX(IC)/ETOT
        UY=0.
        UZ=FEZ(IC)/ETOT
C
```

```
            OPEN(1,FILE=OFILE1,FORM='UNFORMATTED',STATUS='NEW')
            OPEN(3,FILE=OFILE3,STATUS='NEW')
C
C     START LOOP
  2000    NL=NL+1
C
C     DETERMINE CELL POSITION OF NEW LEADER SEGMENT TIP ON OVERLAY
C     USE APPROPRIATE AMBIENT E FIELD MAGNITUDE AND DIRECTION
C     K IS THE CELL NUMBER OF THE LEADER SEGMENT TIP LOCATION
            KX=ANINT((RX/DX)+.5)
            KZ=ANINT((RZ/DZ)+.5)
            K=KX+NCELX*(KZ-1)
            EFAMB=SQRT(FEX(K)**2+FEZ(K)**2)
C
C     TERMINATE IF
C     LEADER SEGMENT HAS PROPAGATED OUTSIDE THE GRID
C     LEADER SEGMENT ENTERING CELL WITH AN AMBIENT FIELD LT 1.5M V/M
C     LEADER SEGMENT ENTERS INTO CHARGED REGION
            IF(K.LT.1.OR.K.GT.KTOT.OR.
     +        RX.LT.0.OR.RX.GT.XTOT)GOTO 3000
C
            WRITE(3,*)NL,K,KX,KZ,RX,RZ,ETOT,EFAMB,FEX(K),FEZ(K)
            PRINT*, NL,K,KX,KZ,RX,RZ,ETOT,EFAMB,FEX(K),FEZ(K)
            WRITE(1)RX,RZ
C


            IF(EFAMB.LT.BDF)GOTO 3000
C
C     SHORTEST TIME PATH OF ELECTRON TO LEADER SEGMENT TIP
C     THIS TIME PATH DETERMINES DIRECTION OF NEW LEADER SEGMENT
            TMIN=1.E20
C
C     USE MONTE CARLO METHOD FOR FREE ELECTRONS
C     TO CALCULATE ELECTRON DISTRIBUTION NEAR LEADER SEGMENT TIP
            RXP=RX+UX*CL
            RYP=RY+UY*CL
            RZP=RZ+UZ*CL
C
            DO 100 I=1,NE
C
C     IN WORLD COORDINATES
            CALL RANDOM(ISEED,RAND)
            RE=RAND*RADIUS
C           RE=SQRT(RAND*(RADIUS**2))
            CALL RANDOM(ISEED,RAND)
            TH=RAND*PI
C           TH=ACOS(RAND*2-1)
            CALL RANDOM(ISEED,RAND)
            PH=RAND*TWOPI
C           RE=RAN(ISEED)*RADIUS
C           TH=RAN(ISEED)*PI
C           PH=RAN(ISEED)*2.*PI
            RMX=RE*SIN(TH)*COS(PH)
            RMY=RE*SIN(TH)*SIN(PH)
            RMZ=RE*COS(TH)
            X=RMX+RXP
            Y=RMY+RYP
            Z=RMZ+RZP
            RM=SQRT(RMX**2+RMY**2+RMZ**2)
C
```

B-33

```
C   COMPUTE E FIELD COMPONENTS FOR Ith ELECTRON
      AX=X-RX
      AY=Y-RY
      AZ=Z-RZ
      A=SQRT(AX**2+AY**2+AZ**2)
      IF(A.LT.1.E-6)GOTO 100
      B=AX*UX+AY*UY+AZ*UZ
      AS=A**2
      BS=B**2
      IF(AS-BS.LT.1.E-6)GOTO 100
      P=CONST/(AS-BS)
      D=CL**2-2.*B*CL+AS
      IF(D.LE.0.)GOTO 100
      D=SQRT(D)
C
C   E FIELD COMPONENTS DUE TO LEADER SEGMENT AND AMBIENT FIELD
      EX=P*(((AX*(CL-B)+UX*(AS-B*CL))/D)-
     +    ((UX*AS-AX*B)/A))+FEX(K)
      EY=P*(((AY*(CL-B)+UY*(AS-B*CL))/D)-
     +    ((UY*AS-AY*B)/A)) !+FEY(K)
      EZ=P*(((AZ*(CL-B)+UZ*(AS-B*CL))/D)-
     +    ((UZ*AS-AZ*B)/A))+FEZ(K)
C
      IF(NL.LE.1)GOTO 1000
      AXM1=X-RXM1
      AYM1=Y-RYM1
      AZM1=Z-RZM1
      AM1=SQRT(AXM1**2+AYM1**2+AZM1**2)
      IF(AM1.LT.1.E-6)GOTO 100
      BM1=AXM1*UXM1+AYM1*UYM1+AZM1*UZM1
      ASM1=AM1**2
      BSM1=BM1**2
      IF(ASM1-BSM1.LT.1.E-6)GOTO 100
      PM1=CONST/(ASM1-BSM1)
      DM1=CL**2-2.*BM1*CL+ASM1
      IF(DM1.LE.0.)GOTO 100
      DM1=SQRT(DM1)
C
C   E FIELD COMPONENTS DUE TO PREVIOUS LEADER SEGMENT
      EXM1=PM1*(((AXM1*(CL-BM1)+UXM1*(ASM1-BM1*CL))/DM1)-
     +    ((UXM1*ASM1-AXM1*BM1)/AM1))
      EYM1=PM1*(((AYM1*(CL-BM1)+UYM1*(ASM1-BM1*CL))/DM1)-
     +    ((UYM1*ASM1-AYM1*BM1)/AM1))
      EZM1=PM1*(((AZM1*(CL-BM1)+UZM1*(ASM1-BM1*CL))/DM1)-
     +    ((UZM1*ASM1-AZM1*BM1)/AM1))
C
C   TOTAL E FIELD COMPONENTS FOR Ith ELECTRON
 1000 EX=EX+EXM1
      EY=EY+EYM1
      EZ=EZ+EZM1
      ET=SQRT(EX**2+EY**2+EZ**2)+.01
      DL=(RMX*EX+RMY*EY+RMZ*EZ)/(RM*ET)
C
C   CHOOSE APPROPRIATE ELECTRON TO BE DRAWN TOWARD
C   LEADER SEGMENT TIP IN SHORTEST TIME
      IF(ET.LT.(3.0E6).AND.(RM/ET).LT.TMIN.
     +   AND.ACOS(ABS(DL)).LE.QP)THEN
      TMIN=RM/ET
      ETOT=ET
      DIRX=EX
```

```
                 DIRY=EY
                 DIRZ=EZ
                 END IF
    100      CONTINUE
C
C    CALCULATE DIRECTION FOR NEXT LEADER SEGMENT
                 DRX=CL*UX
                 DRY=CL*UY
                 DRZ=CL*UZ
                 RXM1=RX
                 RYM1=RY
                 RZMZ=RZ
                 RX=RX+DRX
                 RY=RY+DRY
                 RZ=RZ+DRZ
C
C    NEW UNIT VECTOR
C        DIR=SQRT(DIRX**2+DIRY**2+DIRZ**2)
                 DIR=SQRT(DIRX**2+DIRZ**2)    ! PROJ'N ONTO 2D GRID
                 IF(DIR.LT.1.E-6)GOTO 2000
                 UXM1=UX
                 UYM1=UY
                 UZM1=UZ
                 UX=DIRX/DIR
C        UY=DIRY/DIR
                 UY=0.
                 UZ=DIRZ/DIR
C
                 GO TO 2000
C
   3000      IF(K.LT.1.OR.K.GT.KTOT.OR.
        +        RX.LT.0.OR.RX.GT.XTOT)THEN
                 PRINT*, 'LEADER SEGMENT OUT OF BOUNDS'
                 WRITE(3,*)'LEADER SEGMENT OUT OF BOUNDS'
                 END IF
                 IF(EFAMB.LT.BDF)THEN
                 PRINT*, 'LEADER SEGMENT ENTERED REGION LT BREAK DOWN'
                 WRITE(3,*)'LEADER SEGMENT ENTERED REGION LT BREAK DOWN'
                 END IF
C
                 CLOSE(1)
                 CLOSE(3)
                 STOP
                 END
C
C
                 SUBROUTINE RANDOM(ISEED,RAND)
C    RANDOM NUMBER GENERATOR
C
                 DOUBLE PRECISION E31,E32,SI,SJ
                 E31=2.**31
                 E32=2.**32
                 SI=DFLOAT(ISEED)
                 SJ=MOD(69069.*SI+1.,E32)
                 IF(ABS(SJ).LT.E31)THEN
                 SI=SJ
                 ELSEIF(SJ.GE.E31)THEN
                 SI=SJ-E32
                 ELSE
                 SI=SJ+E32
```

```
END IF
IF(SI.GE.0.)THEN
RAND=SI/E32
ELSE
RAND=1.+SI/E32
END IF
ISEED=INT(SI)
RETURN
END
```

LDPM-INTERACTIVE

```
C    INTERACTIVE VERSION OF LDPM
C
C    PROGRAM DETERMINES DIRECTION OF NEXT LEADER SEGMENT DUE TO
C    ELECTRON WHICH WILL FORM AN IONIZED PATH TO
C    THE STEPPED LEADER SEGMENT TIP IN THE LEAST TIME
C    E FIELD TOTAL = E FIELD LEADER + E FIELD PREVIOUS LEADER
C            + AMBIENT E FIELD
C
      COMMON/MAIN/FEX(9409),FEZ(9409)
      COMMON/VAR/NCX(10),NCZ(10),NCK(10),QN(10)
      COMMON/DAT/NCELX,NCELZ,ICX,ICZ,NC,QP
      CHARACTER*40 INFILE,OFILE1,OFILE3
C
      OFILE1='LDPM.DAT'    ! BINARY PLOTFILE OF LIGHTNING PATH
      OFILE3='LDPM.PRINT'  ! PRINT VALUES OF LIGHTNING MODEL
C
C
      PRINT*, 'LIGHTNING PROPAGATION - TORTUOSITY MODEL'
      PRINT*, 'DEVELOPED BY E.M.A.  -   AUGUST 1986'
      PRINT*, '        '
      PRINT*, 'SPECIFY GRID INPUT DATA'
      PRINT*, '        '
      PRINT*, 'GRID SIZE - ENTER THE TOTAL NUMBER OF CELLS'
      PRINT*, 'EACH CELL IS 200m x 200m'
      PRINT*, 'ALONG THE X (HORZ AXIS), ALONG THE Z (VERT AXIS)'
      PRINT*, 'ENTER  X,Z   (MAX IS 97,97)'
      READ*, NCELX,NCELZ
C
      PRINT*, '        '
      PRINT*, 'ENTER THE INITIAL CELL COORD (X,Z) OF DISCHARGE'
      PRINT*, 'ENTER  X,Z'
      READ*, ICX,ICZ
      PRINT*, 'ENTER THE CHARGE(+,-COUL)'
      READ*, QP
C
      PRINT*, '        '
      PRINT*, 'YOU MAY SPECIFY ANY CHARGE REGION COORDINATE '
      PRINT*, 'OTHER THAN THE INITIAL DISCHARGE COORDINATE. '
      PRINT*, 'IF YOU DONT WANT THESE REGIONS ENTER  0 '
      PRINT*, 'IT IS SUGGESTED THAT OVER THE ENTIRE GRID '
      PRINT*, 'THE SUM OF THE TOTAL CHARGE = 0  '
      PRINT*, 'ENTER THE # OF CHARGE REGIONS  (MAX IS 10)'
      PRINT*, '(NOT INCLUDING THE INITIAL DISCHARGE COORDINATE)'
      READ*, NC
      IF(NC.EQ.0)GOTO 101
      PRINT*, 'ENTER THE X,Z PAIRS AND THEIR CHARGE(-,+COUL)'
      PRINT*, 'ie:  X1,Z1,CHARGE1'
      PRINT*, '     X2,Z2,CHARGE2'
      DO 10 I=1,NC
10    READ*, NCX(I),NCZ(I),QN(I)
      DO 11 I=1,NC
11    NCK(I)=NCX(I)+NCELX*(NCZ(I)-1)
C
101   PRINT*, '        '
      PRINT*, 'THE PROGRAM USES A MONTE CARLO METHOD TO'
      PRINT*, 'GENERATE FREE ELECTRONS AROUND EACH STEPPED'
      PRINT*, 'LEADER TIP. AN ASSUMED DENSITY IS .2elec/m**3'
      PRINT*, '500 ELECTRONS IS RECOMMENDED'
      PRINT*, 'LESS THAN 100 WILL LIMIT TORTUOSITY'
      PRINT*, 'ENTER THE NUMBER OF ELECTRONS DESIRED'
```

```
        READ*, NE
C

        PRINT*, '       '
        PRINT*, 'THE MONTE CARLO ROUTINE REQUIRES A SEED INTEGER'
        PRINT*, 'ENTER ANY INTEGER UP TO 5 DIGITS & LT 32000.'
        READ*, ISEED
C

        PRINT*, '       '
        PRINT*, 'PROGRAM GENERATES A PRINT FILE OF THE MODEL'
        PRINT*, 'VALUES & A BINARY PLOTFILE IN AN X,Z OUTPUT'
        PRINT*, 'AMBIENT E FIELDS ARE PRINTED OUT'
        PRINT*, 'THESE FILES ARE  LDPM.PRINT, LDPM.DAT, AMB.DAT'
        PRINT*, '       '
        PRINT*, '*****************************************'
        PRINT*, '       '
C
C
C    CALCULATE AMBIENT E FIELDS
        CALL EGRID
C    INPUT VARIABLES
C    CL=LEADER LENGTH       ELAMBDA=LEADER CHARGE DENSITY
C    BDF=BREAK DOWN FIELD  EK=1/4PIEPso         NL=LEADER #
C    DZ=Z CELL HEIGHT       DX=X CELL WIDTH
C    NE=# FREE ELECTRONS    ED=ELECTRON DENSITY (.2/m**3)
C    Q=MAX ALLOWABLE ANGLE BTW EFIELD & DIRECTION VECTORS
C
        DATA CL,ELAMBDA,BDF/50.,.001,1.5E5/
        DATA PI,EK,NL/3.1415927,9.E9,0/
        DATA DZ,DX,NE,ED,Q/200.,200.,500,.2,12.5/
        DATA EXM1,EYM1,EZM1/3*0./
        CONST=EK*ELAMBDA
        VOL=FLOAT(NE)/ED
        RADIUS=(.75*VOL/PI)**(1./3.)
        KTOT=NCELX*NCELZ
        XTOT=NCELX*DX
C
C    INITIALIZE LEADER PROPAGATION
C    INPUT DATA: R1, AMBIENT E FIELD, U1
C    COORDINATES OF INITIAL POINT ON GRID PROBLEM SPACE
        RX=DX*(FLOAT(ICX)-.5)
        RY=0.
        RZ=DZ*(FLOAT(ICZ)-.5)
C
        IC=ICX+NCELX*(ICZ-1)
        ETOT=SQRT(FEX(IC)**2+FEZ(IC)**2)
C    DEFINE UNIT VECTOR
        UX=FEX(IC)/ETOT
        UY=0.
        UZ=FEZ(IC)/ETOT
C
        OPEN(1,FILE=OFILE1,FORM='UNFORMATTED',STATUS='NEW')
        OPEN(3,FILE=OFILE3,STATUS='NEW')
C
C    START LOOP
 2000   NL=NL+1
C
C    DETERMINE CELL POSITION OF NEW LEADER SEGMENT TIP ON OVERLAY
C    USE APPROPRIATE AMBIENT E FIELD MAGNITUDE AND DIRECTION
C    K IS THE CELL NUMBER OF THE LEADER SEGMENT TIP LOCATION
        KX=ANINT((RX/DX)+.5)
```

```
              KZ=ANINT((RZ/DZ)+.5)
              K=KX+NCELX*(KZ-1)
              EFAMB=SQRT(FEX(K)**2+FEZ(K)**2)
C
C    TERMINATE IF
C    LEADER HAS PROPAGATED OUTSIDE THE GRID
C    LEADER ENTERING CELL WITH AN AMBIENT FIELD LT 1.5M V/M
C    LEADER ENTERS INTO CHARGED REGION
              IF(K.LT.1.OR.K.GT.KTOT.OR.
         +        RX.LT.0.OR.RX.GT.XTOT)GOTO 3000
C
              WRITE(3,*)'LEADER SEGMENT NUMBER ',NL
              WRITE(3,*)'CELL NUMBER    ',K,'     (X,Z) COORD',KX,KZ
              WRITE(3,*)'TOT E FIELD V/m',ETOT,' AMB E FIELD ',EFAMB
              WRITE(3,*)'AMB EX         ',FEX(K),' AMB EZ      ',FEZ(K)
              WRITE(3,*)'X met. from 0,0',RX,' Z met. from 0,0   ',RZ
              WRITE(3,*)'                            '
              PRINT*, 'LEADER SEGMENT NUMBER ',NL
              PRINT*, 'CELL NUMBER    ',K,'     (X,Z) COORD',KX,KZ
              PRINT*, 'TOT E FIELD V/m',ETOT,' AMB E FIELD ',EFAMB
              PRINT*, 'AMB EX         ',FEX(K),' AMB EZ      ',FEZ(K)
              PRINT*, 'X met. from 0,0',RX,' Z met. from 0,0   ',RZ
              PRINT*, '                            '
              WRITE(1)RX,RZ
C
              IF(EFAMB.LT.BDF)GOTO 3000
              IF(NC.EQ.0.)GOTO 55
              DO 111 II=1,NC
  111         IF(K.EQ.NCK(II))GOTO 3000
C
C    SHORTEST TIME OF ELECTRON TO FORM IONIZATION CHANNEL
C    THIS TIME DETERMINES DIRECTION OF NEW LEADER SEGMENT
   55         THIN=1.E20
C
C    USE MONTE CARLO METHOD TO GENERATE RANDOM FREE ELECTRONS
C    CALCULATE ELECTRON POSITIONS NEAR LEADER TIP
              DO 100 I=1,NE
C
C    IN WORLD COORDINATES
              CALL RANDOM(ISEED,RAND)
              RE=RAND*RADIUS
C             RE=SQRT(RAND*(RADIUS**2))
              CALL RANDOM(ISEED,RAND)
              TH=(RAND)*PI
C             TH=ACOS((RAND*2)-1)
              CALL RANDOM(ISEED,RAND)
              PH=(RAND)*2.*PI
              X=RE*SIN(TH)*COS(PH)+RX+UX*CL
              Y=RE*SIN(TH)*SIN(PH)+RY+UY*CL
              Z=RE*COS(TH)+RZ+UZ*CL
              RMX=X-RX-UX*CL
              RMY=Y-RY-UY*CL
              RMZ=Z-RZ-UZ*CL
              RM=SQRT(RMX**2+RMY**2+RMZ**2)
C
C    COMPUTE E FIELD COMPONENTS FOR Ith ELECTRON
              AX=X-RX
              AY=Y-RY
              AZ=Z-RZ
              A=SQRT(AX**2+AY**2+AZ**2)
```

```fortran
      IF(A.LT.1.E-6)GOTO 100
      B=AX*UX+AY*UY+AZ*UZ
      AS=A**2
      BS=B**2
      IF(AS-BS.LT.1.E-6)GOTO 100
      P=CONST/(AS-BS)
      D=CL**2-2.*B*CL+AS
      IF(D.LE.0.)GOTO 100
      D=SQRT(D)
C
C   E FIELD COMPONENTS DUE TO LEADER SEGMENT AND AMBIENT FIELD
      EX=P*(((AX*(CL-B)+UX*(AS-B*CL))/D)-
     +     ((UX*AS-AX*B)/A))+FEX(K)
      EY=P*(((AY*(CL-B)+UY*(AS-B*CL))/D)-
     +     ((UY*AS-AY*B)/A))  !+FEY(K)
      EZ=P*(((AZ*(CL-B)+UZ*(AS-B*CL))/D)-
     +     ((UZ*AS-AZ*B)/A))+FEZ(K)
C
      IF(NL.LE.1)GOTO 1000
      AXM1=X-RXM1
      AYM1=Y-RYM1
      AZM1=Z-RZM1
      AM1=SQRT(AXM1**2+AYM1**2+AZM1**2)
      IF(AM1.LT.1.E-6)GOTO 100
      BM1=AXM1*UXM1+AYM1*UYM1+AZM1*UZM1
      ASM1=AM1**2
      BSM1=BM1**2
      IF(ASM1-BSM1.LT.1.E-6)GOTO 100
      PM1=CONST/(ASM1-BSM1)
      DM1=CL**2-2.*BM1*CL+ASM1
      IF(DM1.LE.0.)GOTO 100
      DM1=SQRT(DM1)
C
C   E FIELD COMPONENTS DUE TO PREVIOUS LEADER SEGMENT
      EXM1=PM1*(((AXM1*(CL-BM1)+UXM1*(ASM1-BM1*CL))/DM1)-
     +     ((UXM1*ASM1-AXM1*BM1)/AM1))
      EYM1=PM1*(((AYM1*(CL-BM1)+UYM1*(ASM1-BM1*CL))/DM1)-
     +     ((UYM1*ASM1-AYM1*BM1)/AM1))
      EZM1=PM1*(((AZM1*(CL-BM1)+UZM1*(ASM1-BM1*CL))/DM1)-
     +     ((UZM1*ASM1-AZM1*BM1)/AM1))
C
C   TOTAL E FIELD COMPONENTS FOR Ith ELECTRON
 1000 EX=EX+EXM1
      EY=EY+EYM1
      EZ=EZ+EZM1
      ET=SQRT(EX**2+EY**2+EZ**2)+.01
      DL=(RMX*EX+RMY*EY+RMZ*EZ)/(RM*ET)
C
C   CHOOSE APPROPRIATE ELECTRON TO FORM IONIZED CHANNEL
C   TO THE LEADER TIP IN THE SHORTEST TIME
      IF(ET.LT.(3.0E6).AND.(RM/ET).LT.TMIN.
     + AND.ACOS(ABS(DL)).LE.Q*PI/180.)THEN
      TMIN=RM/ET
      ETOT=ET
      DIRX=EX
      DIRY=EY
      DIRZ=EZ
      END IF
 100  CONTINUE
C
```

```
C   CALCULATE DIRECTION FOR NEXT LEADER SEGMENT
        DRX=CL*UX
        DRY=CL*UY
        DRZ=CL*UZ
        RXM1=RX
        RYM1=RY
        RZMZ=RZ
        RX=RX+DRX
        RY=RY+DRY
        RZ=RZ+DRZ
C
C   NEW UNIT VECTOR
C       DIR=SQRT(DIRX**2+DIRY**2+DIRZ**2)
        DIR=SQRT(DIRX**2+DIRZ**2)    ! PROJ'N ONTO 2D GRID
        IF(DIR.LT.1.E-6)GOTO 2000
        UXM1=UX
        UYM1=UY
        UZM1=UZ
        UX=DIRX/DIR
C       UY=DIRY/DIR
        UY=0.
        UZ=DIRZ/DIR
C
        GO TO 2000
C
 3000   IF(K.LT.1.OR.K.GT.KTOT.OR.
     +      RX.LT.0.OR.RX.GT.XTOT)THEN
        PRINT*, 'LEADER OUT OF BOUNDS'
        WRITE(3,*)'LEADER OUT OF BOUNDS'
        END IF
        IF(EFAMB.LT.BDF)THEN
        PRINT*, 'LEADER ENTERED REGION LT BREAK DOWN'
        WRITE(3,*)'LEADER ENTERED REGION LT BREAK DOWN'
        END IF
        DO 112 II=1,NC
        IF(K.EQ.NCK(II))THEN
        PRINT*, 'LEADER ENTERED CHARGED REGION'
        WRITE(3,*)'LEADER ENTERED CHARGED REGION'
        END IF
 112    CONTINUE
C
        CLOSE(1)
        CLOSE(3)
        STOP
        END
C
C
        SUBROUTINE RANDOM(ISEED,RAND)
C   RANDOM NUMBER GENERATOR
C
        DOUBLE PRECISION E31,E32,SI,SJ
        E31=2.**31
        E32=2.**32
        SI=DFLOAT(ISEED)
        SJ=MOD(69069.*SI+1.,E32)
        IF(ABS(SJ).LT.E31)THEN
        SI=SJ
        ELSEIF(SJ.GE.E31)THEN
        SI=SJ-E32
        ELSE
```

```
          SI=SJ+E32
          END IF
          IF(SI.GE.0.)THEN
          RAND=SI/E32
          ELSE
          RAND=1.+SI/E32
          END IF
          ISEED=INT(SI)
          RETURN
          END
C
C
          SUBROUTINE EGRID
C    CALCULATION OF AMBIENT ELECTRIC FIELDS
C
          DIMENSION X(9409),Z(9409)
          DIMENSION XMRN(5),B(5)
          COMMON/MAIN/FEX(9409),FEZ(9409)
          COMMON/VAR/NCX(10),NCZ(10),NCK(10),QN(10)
          COMMON/DAT/NCELX,NCELZ,ICX,ICZ,NC,QP
          DATA DX,DZ,DP,PI/200.,200.,9.E9,3.1415927/
C
          OPEN(4,FILE='AMB.DAT',STATUS='NEW')
C
          DO 10 J=1,NCELZ
          DO 10 I=1,NCELX
          K=I+NCELX*(J-1)
          X(K)=DX*(FLOAT(I)-.5)
          Z(K)=DZ*(FLOAT(J)-.5)
          K1=K
  10      CONTINUE
C
          LP=ICX+NCELX*(ICZ-1)
C   CALCULATE RESULTANT E FIELDS FROM CHARGE CENTERS
          DO 20 K=1,K1
          IF(NC.EQ.0)THEN
          IF(X(K).EQ.X(LP).AND.Z(K).EQ.Z(LP))GOTO 20
          END IF
          IF(NC.EQ.0)GOTO 23
          DO 333 I=1,NC
          IF(X(K).EQ.X(LP).AND.Z(K).EQ.Z(LP).OR.
     +       X(K).EQ.X(NCK(I)).AND.Z(K).EQ.Z(NCK(I)))GOTO 20
  333     CONTINUE
C
  23      XMRP=SQRT((X(K)-X(LP))**2+(Z(K)-Z(LP))**2)
          A=DP*QP/XMRP**3
          FEX(K)=0.
          FEZ(K)=0.
          IF(NC.EQ.0)GOTO 24
          DO 444 I=1,NC
          XMRN(I)=SQRT((X(K)-X(NCK(I)))**2+(Z(K)-Z(NCK(I)))**2)
          B(I)=DP*QN(I)/XMRN(I)**3
          FEX(K)=FEX(K)+B(I)*(X(K)-X(NCK(I)))
          FEZ(K)=FEZ(K)+B(I)*(Z(K)-Z(NCK(I)))
  444     CONTINUE
C
  24      FEX(K)=FEX(K)+A*(X(K)-X(LP))
          FEZ(K)=FEZ(K)+A*(Z(K)-Z(LP))
  20      CONTINUE
          FEX(LP)=FEX(LP+1)
```

```
      FEZ(LP)=FEZ(LP+1)
      IF(NC.EQ.0)GOTO 25
      DO 555 I=1,NC
      FEX(NCK(I))=FEX(NCK(I)-1)
      FEZ(NCK(I))=FEZ(NCK(I)-1)
555   CONTINUE
25    DO 26 K=1,K1
      WRITE(4,*)K,FEX(K),FEZ(K),X(K),Z(K)
26    CONTINUE
      CLOSE(4)
      RETURN
      END
```

AN INVESTIGATION INTO THE EFFECT OF THUNDERSTORM PARTICLES ON LIGHTNING INITIATION

Prepared by

Terence Rudolph
Rodney A. Perala

Prepared for

South Dakota School of Mines
Institute of Atmospheric Sciences
501 E. St. Joseph Street
Rapid City, SD   57701-3995

Under Contract # E02-86-001

June 1987

1.0   INTRODUCTION

The maximum observed electric fields in thunderstorms are in general smaller than is necessary to initiate corona or sparking that can lead to lightning events. Field magnitudes in the range of 1 to 2 megavolts per meter are necessary in pure air at typical thunderstorm altitudes, whereas maximum measured fields are of the order of 400 kilovolts per meter. Hence it is necessary to look for other mechanisms which can locally raise the field strength to the necessary intensity. Thunderstorm particles are one source of local field enhancement which may provide the necessary mechanism. These particles (cloud droplets, rain, ice, hail, snow, graupel), although not having large conductivities, do have small electrical relaxation times on the scale of non-lightning electric field changes in a cloud. This implies that the particles act as perfect conductors in a thundercloud, and are able to locally enhance the ambient electric field. They are also able to hold electrical charges which can alter the way in which field enhancement occurs.

The purpose of the research presented here is to attempt to determine what effect thunderstorm particles have on the lightning initiation process. Are there preferred areas within the storm where particular types of particles exist that make lightning initiation more likely? Are large particles or large particle densities more effective at producing electrical breakdown in a particular volume? To answer these questions a model has been developed to roughtly calculate the ambient field necessary to cause air breakdown in a thunderstorm in the presence of ensembles of particles. The size, shape, and density of the particles are variable inputs to the model, as is the altitude at which the model does its calculation. The altitude (or air density) is the most significant parameter in calculating the pure air electron avalanche rate [1], and the particle parameters determine how that pure air rate is altered. Using this model a table can be constructed giving the nominal air breakdown field as a function of the above parameters. The table can then be used in conjunction with large scale thunderstorm models [2] which calculate particle types and densities as a function of location in a cloud to predict the most likely regions for lightning initiation.

Electrical breakdown of air occurs because of a growth in the electron density in the air at a given location. This occurs when electrons are accelerated in an ambient electric field to energies large enough to ionize air molecules through collisions. The process is known as an electron "avalanche." The growth continues

approximately exponentially until the electron density is large enough to produce currents which neutralize the ambient field locally. These electron currents, while neutralizing a local electric field, also raise the field at other nearby locations, possibly causing the electron avalanche to propagate away from its initial location. In this way a lightning channel may be initiated.

This report investigates specifically the way in which the electron avalanche rate varies as a function of particle parameters, air density, and electric field. Nominal air breakdown fields are predicted for these variables by calculating the smallest ambient field which will produce sufficient electron density to lower that field. This involves the balancing of the electron avalanche rate with the primary loss mechanism for electrons, attachment to neutrals to form negative ions. Hence the nominal air breakdown field is that for which the avalanche rate equals the electron attachment rate.

The results, to be presented in greater detail later, show that large particles, such as snowflakes, are the most effective at altering the nominal air breakdown field, and volumes containing these particles are the most likely locations for lightning initiation. Small particles, even if large densities are present, are not nearly as effective in altering the nominal air breakdown field.

2.0   CORONA GROWTH AROUND PARTICLES IN A UNIFORM ELECTRIC FIELD

The work presented in this section has been partially published in a previous report [3] and is also presented here in the interest of completeness.

By locally redistributing the electric field energy density in a region of space, thunderstorm particles can affect the way in which electrons and ions are produced in an electron avalanche. In particular, a uniform electric field which is below breakdown intensity may be locally enhanced to a level which produces corona around the particles. This occurs because the avalanche rate is strongly nonlinear with electric field, so that small electric field changes can result in large changes in charged particle production.

As an example of this consider the case of a spherical particle in a uniform static electric field, E_o, with magnitude ninety percent of air breakdown intensity. This is shown schematically in Figure 2.1. The electrical conductivity of the particle is important only for very fast field changes (of the order of microseconds), and in general the particle acts as a perfect conductor on the time scale of large scale thunderstorm fields. Because of this the well-known analytic development for the altered field distribution around a conducting sphere in a uniform electric field may be used. Figure 2.1 shows the regions around the particle in which fields larger and smaller than the ambient field exist. In addition the regions in which the field magnitude exceeds air breakdown level, E_b, are shown. These latter regions depend on the magnitude of the ambient field with respect to breakdown field. That is, if the ambient field drops, the breakdown region will shrink, finally disappearing altogether when the ambient field goes below one-third of the breakdown field. The other regions, those of enhanced and decreased field, are not dependent on ambient field strength.

The preceding discussion was based on a spherical particle. The situation for more irregular particles such as ice crystals or snow flakes is more complicated. Analytic solutions for these shapes do not exist, so approximations must be made in specifying the local field distribution around the particle. In general, however, a polarized particle will behave like an electric dipole to some level of approximation. The assumption used in the development presented here is to treat the local field distribution as the same as that around a spherical particle, but to raise the maximum field enhancement to that determined from a previous study [4] (e.g., enhancement of five for columnar ice crystals and nine for a typical snowflake).

The importance of Figure 2.1 is that it shows that a conducting particle can cause electron avalanching to occur in a region of space which would have no avalanching in the particle's absence. The details of how much avalanching occurs because of the particle and the effects of irregularly shaped particles and particle density are left for the mathematical development of the next section.
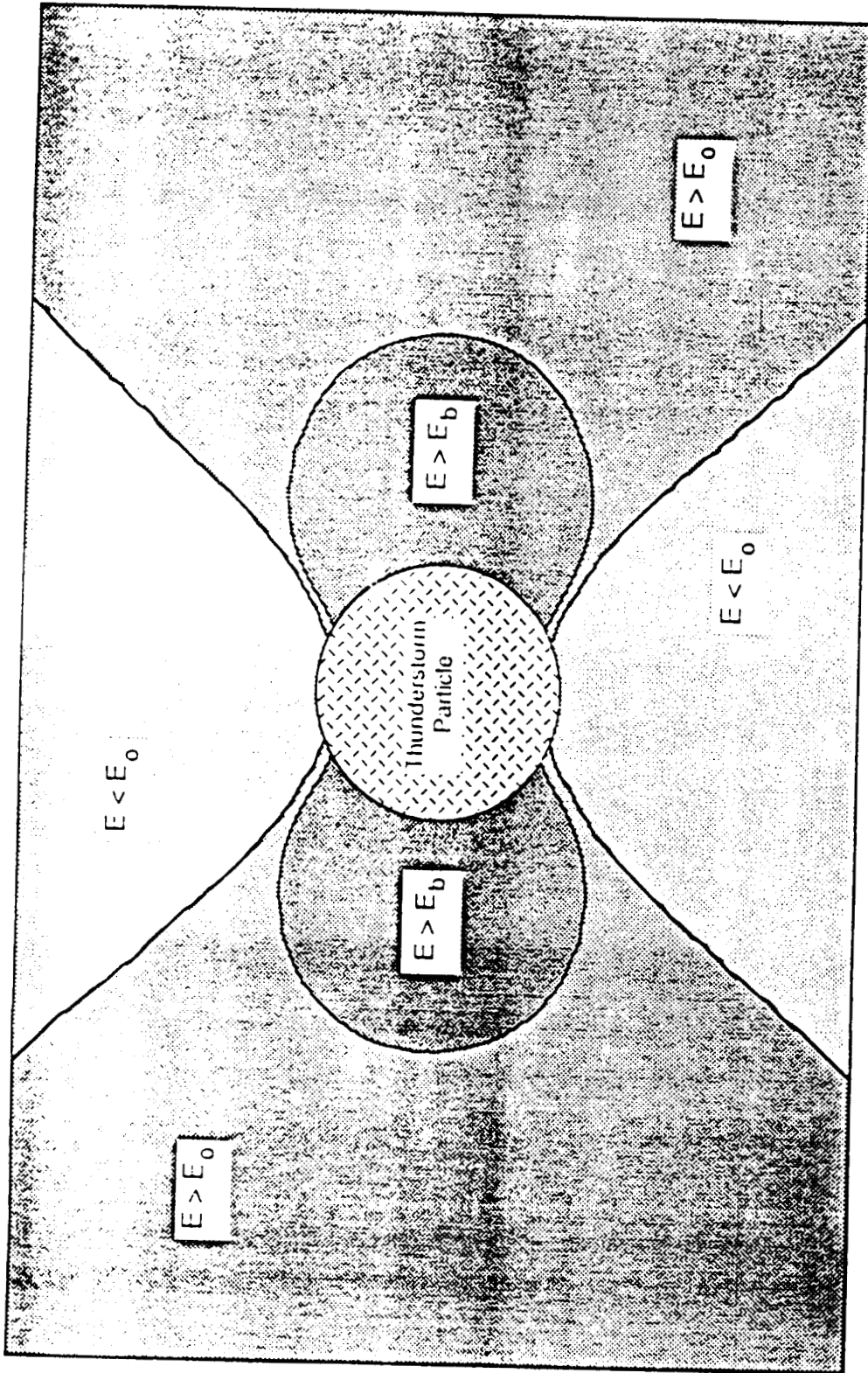
Figure 2.1 Electric Field Distribution Around a Typical Spherical Thunderstorm Particle. E_o Is Ambient Field, Oriented Horizontally E_b Is the Field Required for Air Breakdown

2.1   Mathematical Development

To facilitate the mathematical development to follow, some symbols will first be defined. The development will be done in a spherical coordinate system, assuming no azimuthal variation. The ambient field is assumed to be oriented along the polar axis. The assumption of no azimuthal variation is strictly true only for spherical particles or cylindrical particles oriented with their axis along the polar axis. Particles not satisfying this criterion will be included in an approximate sense.

Table 2.1
Definition of Symbols Used in Section 2.3

a	-	approximate half size of particle (radius in the case of a spherical particle)
E_o	-	ambient electric field intensity
E_b	-	breakdown electric field intensity
E_r	-	radial electric field intensity
E_θ	-	theta component of electric field intensity
E_z	-	component of electric field intensity along polar axis
f_{max}	-	maximum electric field enhancement factor (particle dependent)
n	-	density of thunderstorm particles
N	-	number of thunderstorm particles in a finite difference cell
ρ	-	air density relative to sea level density
ΔV	-	volume around a particle in which field is above E_b

The objective of the analysis to follow is to develop a modified electron avalanche rate which accounts for the presence of thunderstorm particles. Previous work has assumed that corona formation occurs in clear air only. To include particles, it is necessary first to calculate the avalanche occurring around a single particle and then to consider the effects of a particle density in a given region of space. The electric field around a single particle is investigated first.

The field distribution outside of a spherical conducting particle placed in a uniform electric field is given by,

$$E_r(r,\theta) = E_0 \left(1 + 2\frac{a^3}{r^3}\right) \cos\theta \qquad (2.1)$$

$$E_\theta(r,\theta) = -E_0 \left(1 - \frac{a^3}{r^3}\right) \sin\theta$$

Figure 2.2 shows the spherical coordinate system used in the analysis. For use here this expression is generalized to approximate the field distribution around irregularly shaped particles as follows,

$$E_r(r,\theta) = E_0 \left[1 + (f_{max} - 1)\frac{a^3}{r^3}\right] \cos\theta \qquad (2.2)$$

$$E_\theta(r,\theta) = -E_0 \left(1 - \frac{a^3}{r^3}\right) \sin\theta$$

Note that the only difference between Equations 2.1 and 2.2)is that the 2 in the first of Equations 2.1 has been replaced by the term f_{max} -1 in Equation 2.2. This reduces to Equation 2.1 in the case of a sphere (for which f_{max} = 3). The justification for using Equation 2.2 in the present model is not rigorous. Any conducting particle placed in a uniform electric field must polarize, and the resulting field distribution must in some sense resemble a dipole field. The assumption is made here, mainly for the purpose of making further analytic progress on particles in general, that the distribution
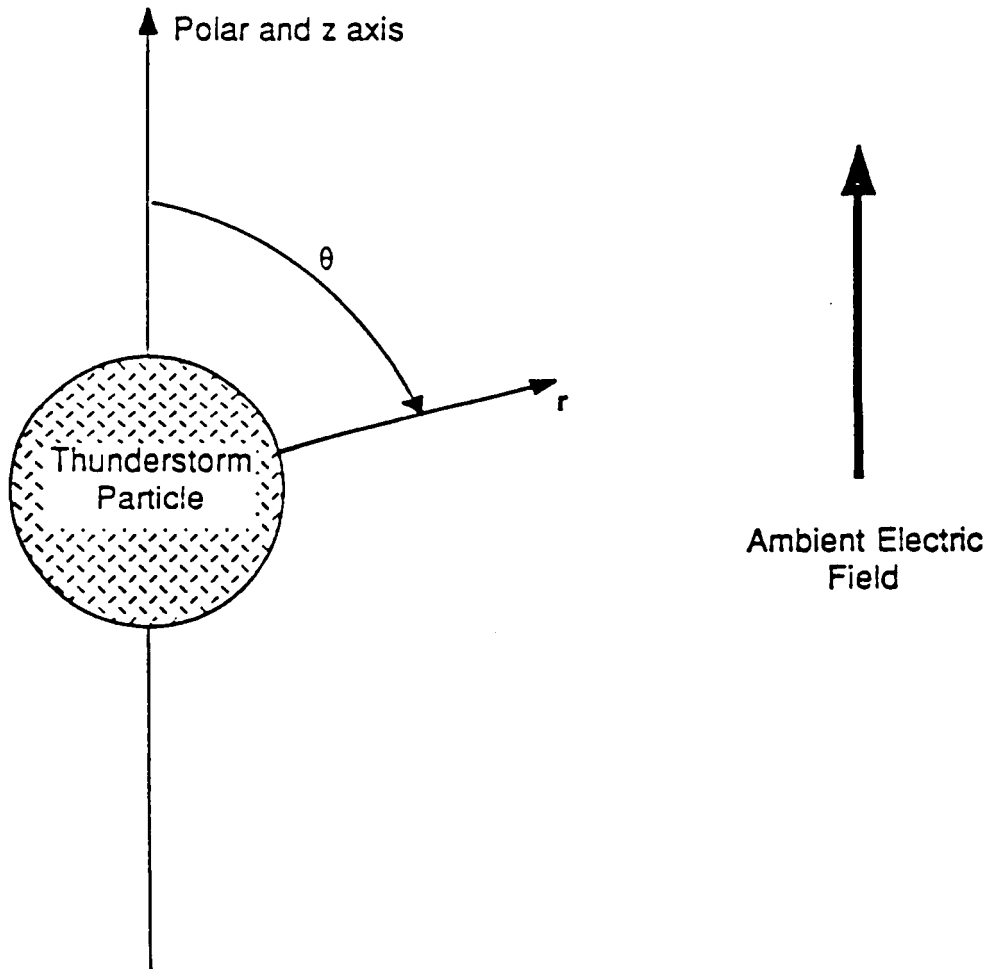
Figure 2.2   Spherical Coordinate System Used in Analysis of Thunderstorm Particles

is similar to that around a spherical particle, but with differing maximum field enhancements.

In addition, the electric field used in the calculations to follow is the component along the polar axis of the coordinate system. Strictly speaking, the total electric field is more appropriate. However, the form of the polar component is much easier to work with analytically, and introduces only a small error. The error is small because the axial oriented field is a good approximation to the total field at most locations. The axial field is easily calculated from Equation 2.2 and is shown below.

$$E_z(r,\theta) = E_o\left[1 + (f_{max}\cos^2\theta - 1)\frac{a^3}{r^3}\right] \tag{2.3}$$

This expression involves three physical quantities of interest, the ambient electric field, the size of the particle, and its shape (included in f_{max}). These three quantities, along with the breakdown field strength at a particular altitude and the particle density, completely determine the altered avalanche rate from the clear air expression. The next step in the analysis is to specify the volume around the particle over which avalanching occurs. In other words, over what volume is E_z larger than E_b? The condition for this is expressed in equation (2.4).

$$E_o\left[1 + (f_{max}\cos^2\theta - 1)\frac{a^3}{r^3}\right] \geq E_b \tag{2.4}$$

There are three possible regimes for Equation 2.4. If E_o is larger than E_b, then Equation 2.4 is satisfied in all of space. This is of course the trivial case in which air breakdown would occur in the absence of particles. A second regime is one in which Equation 2.4 is satisfied nowhere in space. This occurs when f_{max} is not large enough to raise the maximum enhanced field above E_b. In this case air breakdown is absent even in the presence of particles. The middle regime in which Equation 2.4 is satisfied in a limited region of space is the most interesting. The conditions $f_{max} \geq \frac{E_b}{E_o}$ and $E_o < E_b$ define this regime. Here air breakdown occurs when particles

are present but not when they are absent. From Equation 2.4 the volume over which this occurs can be specified as below.

$$0 \leq \theta \leq \cos^{-1} \sqrt{\frac{E_b}{f_{max}E_o}} \equiv A \qquad (2.5)$$

$$a \leq r \leq a \sqrt[3]{\frac{f_{max}\cos^2\theta - 1}{\frac{E_b}{E_o} - 1}} \equiv Ba$$

Equation 2.5 represents a two dimensional projection of a three dimensional volume. The full volume is obtained by rotating the area specified in Equation 2.5 around the polar axis of the particle. Note also that there are two of these volumes, one on either end of a symmetrically shaped particle. An expression for the volume over which the enhanced electric field is above E can now be derived by integrating over the limits of Equation 2.5 and multiplying by two to account for both ends of the particle. Formally this is written,

$$\Delta V = 2 \int_o^{2\pi} \int_o^A \int_a^{Ba} r^2 \sin\theta \, dr d\theta d\varphi \qquad (2.6)$$

The details of the integration are straightforward, and the final expression for the avalanche volume is,

$$\Delta V = \frac{4\pi a^3}{9} \frac{E_o f_{max}}{E_b - E_o} \left[1 + 2 \left(\frac{E_b}{E_o f_{max}} \right)^{3/2} - 3 \left(\frac{E_b}{E_o f_{max}} \right) \right] \qquad (2.7)$$

The most important thing to notice about Equation 2.7 is the way in which ΔV depends on various quantities. A large ΔV implies that the particle has a significant effect on electron avalanching, and a small ΔV implies very little effect. Therefore it is clear that larger particles (large a) are most effective at altering the avalanche rate,

C-10

since ΔV varies as the cube of the particle dimension. The shape is also involved, but is less important, in the sense that ΔV is nearly linearly dependent on f_{max}. Of course it must be remembered that f_{max} is quite important in determining whether there will be any avalanching at all around the particle.

Equation 2.7 gives the volume around a single particle in which avalanching will occur. To implement this concept in a numerical model, it is necessary to include the density of particles which is present in the region of interest. Hence it is necessary to calculate how much of a given volume has fields above breakdown level. The total volume with field above breakdown strength in a given volume is then,

$$\Delta V_T = N \Delta V \qquad (2.8)$$

where N is the number of particles in the given volume and is numerically equal to the particle number density multiplied by that volume. In Equation 2.8 the assumption has been made that the particles are noninteracting in the sense that none of the individual enhanced field volumes overlap. This appears to be a reasonable approximation for typical particle densities in thunderstorms.

The next step in the analysis is to calculate the number of electron-ion pairs produced in ΔV_T per unit time. This is essentially the desired avalanche rate from particles. The rigorous method to find this quantity is to integrate the (strongly electric field dependent) avalanche rate over ΔV. This is computationally inefficient for large scale air breakdown codes, however, so the method used here is somewhat different. The alternate method is to define an average electric field in the breakdown volume and to simply evaluate the altered avalanche rate for that electric field. One possible choice of this average field is to set it equal to the arithmetic average of the smallest and largest fields in the volume. These fields are E_b and $f_{max}E_o$, respectively. However, because the largest field exists only in a very small subvolume of ΔV it would be better to favor the lower fields in any average. Therefore the geometric mean is used, as shown below.

$$\text{Average field} = \sqrt{E_b f_{max} E_o} \qquad (2.9)$$

The geometric mean is always less than or equal to the arithmetic mean, so this should be a more appropriate value to use in the model.

Finally the avalanche rate from particles may be formally written,

$$G_{particles} = G_{pure\ air}(average\ field)\frac{\Delta V_T}{V_{given}} \tag{2.10}$$

The last matter to be considered is the issue of irregularly shaped particles which may not be aligned with their axis along the ambient electric field. Although electrostatic forces would tend to align these particles, it is likely that hydrodynamic forces from winds and small scale turbulence would overwhelm the electrostatic force. Hence the particles are probably randomly oriented with respect to the field direction. This is taken into account in the present model by assuming that on the average half of the particles are aligned along the field and half are aligned across the field. The particles across the field make no contribution to the particle dependent avalanche rate. In the model this is accomplished simply by dividing the true particle density by two to arrive at an effective density. It should be understood that this is done only for the case of nonspherical particles ($f_{max} \neq 3$), because for spherical particles alignment is unimportant.

3.0 RESULTS

The immediate result which can be calculated from the thunderstorm particle model is the effective ambient field which causes air breakdown to occur. This should be lower in the presence of thunderstorm particles than in their absence. An approximation to the breakdown field is achieved by finding the field level at which the avalanche rate becomes larger than the electron attachment rate. Although this is not a strict criterion for air breakdown it does serve to illustrate the difference in corona growth caused by particles. Table 3.1 shows the nominal air breakdown field at various altitudes for a number of typical thunderstorm particle environments.

It should be noted that not all altitudes shown in Table 3.1 are appropriate for each of the environments. For instance, the ice particles and snowflakes of Cases 6-14 would not be expected below the freezing level in a thunderstorm.

Table 3.1
Nominal Air Breakdown Field (MV/m) as a Function of Air Density and Particle Parameters
(Note: Not All Air Densities Are Appropriate for Particular Particles)

ρ / Case	.3	.4	.5	.6	.7	.8	.9	1.0
1	.64	.86	1.07	1.29	1.50	1.72	1.93	2.15
2	.64	.86	1.07	1.29	1.50	1.72	1.93	2.15
3	.64	.86	1.07	1.29	1.50	1.72	1.93	2.15
4	.64	.86	1.07	1.29	1.50	1.72	1.93	2.15
5	.64	.86	1.07	1.29	1.50	1.72	1.93	2.15
6	.64	.86	1.07	1.29	1.50	1.72	1.93	2.15
7	.64	.96	1.07	1.29	1.50	1.72	1.93	2.15
8	.64	.86	1.07	1.29	1.50	1.72	1.93	2.15
9	.64	.86	1.07	1.29	1.50	1.72	1.93	2.15
10	.64	.86	1.07	1.29	1.50	1.72	1.93	2.15
11	.64	.86	1.07	1.29	1.50	1.72	1.93	2.15
12	.64	.86	1.07	1.29	1.50	1.72	1.93	2.15
13	.64	.85	1.07	1.28	1.50	1.71	1.93	2.14
14	.62	.83	1.04	1.25	1.45	1.66	1.87	2.08

ρ = relative air density

Key to cases:

1 - pure air
2 - $r = 2.5\ \mu$, $n = 10^8 m^{-3}$, $f_{max} = 3$
3 - $r = 10\ \mu$, $n = 10^8 m^{-3}$, $f_{max} = 3$
4 - $r = 2.5\ \mu$, $n = 10^9 m^{-3}$, $f_{max} = 3$
5 - $r = 10\ \mu$, $n = 10^9 m^{-3}$, $f_{max} = 3$
6 - $r = 50\ \mu$, $n = 10^4 m^{-3}$, $f_{max} = 5$
7 - $r = 500\ \mu$, $n = 10^4 m^{-3}$, $f_{max} = 5$

8 - $r = 50\ \mu$, $n = 10^5 m^{-3}$, $f_{max} = 5$
9 - $r = 500\ \mu$, $n = 10^5 m^{-3}$, $f_{max} = 5$
10 - $r = 50\ \mu$, $n = 10^4 m^{-3}$, $f_{max} = 9$
11 - $r = 500\ \mu$, $n = 10^4 m^{-3}$, $f_{max} = 9$
12 - $r = 50\ \mu$, $n = 10^5 m^{-3}$, $f_{max} = 9$
13 - $r = 500\ \mu$, $n = 10^5 m^{-3}$, $f_{max} = 9$
14 - $r = 1\ cm$, $n = 100\ m^{-3}$, $f_{max} = 9$

r = particle radius
n = particle density

Although the contents of Table 3.1 are rather dull, they illustrate the principle that small particles do not significantly change the air breakdown field, even when present at high densities. Only the very largest particles with large enhancement factors, such as snowflakes, are able to change the breakdown field by more than 1%. Hence, if e ectric fields everywhere in the cloud were equal, it is slightly more likely that regions having this type of particle will initiate lightning. However, the field variation throughout a typical cloud will certainly swamp the small selection effect toward large particles shown in Table 3.1, so in practice the large particle regions are probably no more or less likely to initiate lightning than any other regions.

4.0   CHARGED PARTICLE CONSIDERATIONS

The previous analysis assumed that the thunderstorm particles were uncharged. A net charge on the particles introduces several complicating factors. The total electric field around the particle can be represented as the sum of the field from the analysis of Section 2.1 and the field from the net charge. For spherical particles the field from the charge is just the well known field from a point charge. For more complicated shapes such as ice columns and snowflakes the field distribution becomes much more complex. For instance, for an ice column with a net charge the field is likely to be more characteristic of two point charges separated by the length of the column. For snowflakes sharp points are likely to behave as point charges, each comprising a fraction of the total charge. Hence the field from a net charge around a point where corona may occur may be roughly characterized as that around a point charge carrying a fraction of the total charge on the particle. That fraction may be estimated by the number of potential corona points on the particle: one for spheres, two for columns, and possibly six for undamaged snowflakes.

The maximum total charge on the object is also a function of the type of particle and its size. Corona growth bleeds charge into the surrounding atmosphere when the total charge is large enough to produce air breakdown level fields around the particle. Clearly larger particles can hold larger charges, and spheres, because of their low enhancement factor, can hold larger charges than equally sized particles of other types. The upper limit on total charge for a particle is then the quantity which produces breakdown around a sphere of roughly equal size, as given below.

$$Q \leq 4\pi\varepsilon_0 a^2 E_b \tag{4.1}$$

Here E_b is the breakdown field at the altitude of interest, and a the nominal radius of the particle. This is roughly 2 picocoulombs for a particle of radius 100 μ at an altitude for which the air breakdown field is 1.5 megavolts per meter.

The interaction of a net charge and an ambient field on the possible air breakdown around the particle is interesting. An uncharged particle has volumes of equal electric field levels on either side as was shown in Figure 2.1. When a net charge of either sign is placed on the particle, the field on one side of the particle is lowered and on the other side elevated. Qualitatively, this tends to suppress potential air breakdown on one side and enhance it on the other. While this effect reduces the net volume over which corona occurs by roughly a factor of two, the ambient field required to initiate corona on the enhanced side can be significantly reduced. This can be seen by writing down the total field component in the axial direction, in analogy with Equation 2.3.

$$E_z(r,\theta) = E_0 \left[1 + (f_{max} \cos^2\theta - 1)\frac{a^3}{r^3} \right] + \frac{q_f}{4\pi\varepsilon_0 r^2} \cos\theta \qquad (4.2)$$

Here q_f is the absolute value of the fraction of the total charge on the particle which contributes to the field at the point in question. Unfortunately this expression is no longer a very good approximation to the total field in the enhanced volume as in Equation 2.3, because of the spherical nature of the field from the charge. Because of this and the relatively complicated nature of Equation 4.2, a detailed analysis of the breakdown volume as was done in Section 2.1 is beyond the scope of this effort. However, a qualitative feel for the reduction in ambient field necessary to cause breakdown can be gained by investigating the maximum fields in Equation 4.2 in the cases of a particle with and without a net charge. The maximum field in each case occurs at $\theta = 0$, and $r = a$. Equation 4.2 becomes for this case,

$$E_z^{max}(a,0) = E_0 f_{max} + \frac{q_f}{4\pi\varepsilon_0 a^2} \qquad (4.3)$$

Next assume that this maximum field is exactly the breakdown field E_b. The ambient field needed to produce this breakdown field is given by

$$E_o = \frac{1}{f_{max}} \left(E_b - \frac{q_f}{4\pi\varepsilon_o a^2} \right) \qquad (4.4)$$

Then the ratio of the necessary ambient field needed to produce a breakdown in the charged and uncharged case is given by,

$$E_o{}^{charged}/E_o{}^{uncharged} = 1 - \frac{q_f}{4\pi\varepsilon_o a^2 E_b} \qquad (4.5)$$

Hence, as one would expect, the reduction in ambient field necessary to produce air breakdown is linearly dependent on the net charge of the particle.

This analysis, admittedly crude, can be used in conjunction with Table 3.1 to estimate the ambient field necessary to initiate lightning in a region of particles having net charge.

5.0 EXPERIMENTAL INITIATION CRITERION

In addition to the requirement that the absolute electric field magnitude exceed air breakdown in a volume for lightning initiation to occur, there is some experimental evidence, documented by Ruhnke [5], of a ceiling on the allowable field gradient. For field gradients above an absolute magnitude of 2.5×10^8 V/m^2 only corona will occur and no spark or lightning leader will be initiated. Field gradients below this level allow the initiation of a spark which may grow into a full leader. It is therefore of interest to evaluate the expressions for the electric field distribution around thunderstorm particles to determine whether this criterion is satisfied.

The expression for the axially oriented field around a particle was derived in Equation 4.2.

$$E_z(r,\theta) = E_o \left[1 + (f_{max} \cos^2\theta - 1)\frac{a^3}{r^3} \right] + \frac{q_f}{4\pi\varepsilon_o r^2} \cos\theta \qquad (5.1)$$

The largest electron avalanche and therefore the largest corona growth will occur at the point where the largest electric field exists. This is at the $\theta = 0$, $r = a$ point. This is also the point at which the largest electric field gradient exists. Hence to satisfy the above criterion in the entire breakdown volume, it must be satisifed at this point. Because propagation of any potential spark will occur in the direction of the field, it is the radial derivative which is of most interest. This derivative is shown below.

$$\frac{\partial E_z}{\partial r} = -\frac{3E_0}{r} (f_{max} \cos^2\theta - 1) \frac{a^3}{r^3} - \frac{q_f}{2\pi\epsilon_0 r^3} \cos\theta \qquad (5.2)$$

Evaluating this expression at the point of maximum field gives,

$$\frac{\partial E_z}{\partial r} (r=a, \theta=0) = \frac{3E_0}{a} (f_{max} - 1) - \frac{q_f}{2\pi\epsilon_0 a^3} \qquad (5.3)$$

Note here that E_0, q_f, and f_{max} all contribute in a linear fashion to the gradient. Hence particles with low net charges and small enhancement factors would appear to be more likely to satisfy the criterion. However, this is not really the case, because a decrease in q_f on a particle results in a corresponding increase in E_0 in order to achieve a field of breakdown magnitude. The same is true of f_{max}. E_0 is not an independent variable in the equation. In effect Equation 5.3 can be evaluated with $q_f = 0$, and $f_{max} = 3$ to set order of magnitude values for field gradients of typical thunderstorm particles.

The size of the particle, a, enters Equation 5.3 in an inverse fashion. Hence larger particles are more likely to satisfy the maximum gradient criterion. Evaluating Equation 5.3 for the largest particles in Table 3.1 and for the breakdown fields given there shows that nowhere is the criterion satisfied. The closest approach occurs for Case 14 with relative air density .3, for which the gradient is 3.72×10^8 V/m^2. This is close enough to the experimental value that it is conceivable that an occasional larger particle may exist which could sustain the spark discharge.

6.0   MULTIPLE PARTICLE EFFECTS

The discussion of the last section was confined to the field distribution around single particles. It was found that it is relatively easy to produce breakdown fields around a typical thunderstorm particle, but only for the very largest particles is the criterion of maximum field gradient satisfied. However, if one allows the possibility of interacting particles, the situation becomes much more favorable for spark initiation. By interaction of particles is meant the close approach of two or more particles such that the field distributions around the particles are altered from what they would be in the individual particle case. In principle, by bringing two particles together closely enough, it is possible to achieve as low a field gradient as desired, while still maintaining breakdown field intensities. This allows the initiation of a spark between the particles. The problem is then to determine what happens to that spark when it attempts to propagate away from the two particle system. In effect what has been created by the spark between the two particles is a larger elongated particle which may have properties more conducive to the initiation of a real lightning leader.

Systems of particles have not been investigated in detail in this study. To do so realistically requires the use of statistical descriptions of particle sizes, densities, and motions within a thundercloud. For the scenario described above, however, it may be possible to apply the analysis of Sections 2 and 3 to the multiple particle interactions. It may be possible to derive information on the density of interacting systems of particles necessary to produce a reduction in the ambient field needed to produce lightning initiation. This, along with measured and calculated data from actual thunderstorms, may allow a statistical prediction of the locations for lightning initiation in a cloud.

7.0   SUMMARY

In this report, the effect of thunderstorm particles on lightning initiation has been studied. The following major points may be summarized.

(1)   A model has been developed to roughly predict breakdown field as a function of particle size, shape, and density.

(2) The model has been applied to typical thunderstorm particle environments. The results show that only the largest particles may be expected to have much effect on the threshold initiation field.

(3) The effect of net charge on the particles is to lower the effective breakdown field. It also makes the local corona breakdowns around particles one-sided.

(4) An experimental criterion on electric field gradient has been applied to the fields around thunderstorm particles. Once again, only the largest particles were seen to satisfy this criterion.

(5) Although interactions between particles were not investigated in detail, it is clear that close approaches between two or more particles more easily satisfy the two criteria on field magnitude and gradient for spark initiation.

(6) Statistical approaches are necessary to investigate the likelihood that particle systems are responsible for the initiation of lightning discharges.

REFERENCES

1.   Radasky, W.A., "An Examination of the Adequacy of the Three Species Air Chemistry Treatment for the Prediction of Surface Burst EMP," DNA 388-T, Dec., 1975.

2.   Helsdon, J.H., Farley, R.D., and Wu, G., "A Lightning Parameterization Scheme in a Two-Dimensional Time-Dependent Storm Electrification Model," Conf. on Cloud Physics, Sept., 1986.

3.   Rudolph, T., C.C. Easterbrook, P.H. Ng, R.W. Haupt, and R.A. Perala, "Experimental and Analytic Studies of the Triggered Lightning Environment of the F106B," EMA-87-R-37, May 1987.

4.   Rudolph, T., R.A. Perala, C.C. Easterbrook, S.L. Parker, "Development and Application of Linear and Nonlinear Methods for Interpretation of Lightning Strikes to In-Flight Aircraft," NASA Contractor Report 3974, Sept., 1986.

5.   Ruhnke, L.H., "Design of a Rocket to Trigger Lightning Strokes," Technical Note Prepared for NASA, Kennedy Space Center, Florida, under Contract CC-88025, June, 1970.

1. Report No.	2. Government Accession No.	3. Recipient's Catalog No.
NASA CR-181639		

4. Title and Subtitle	5. Report Date
Atmospheric Electrical Modeling in Support of the NASA F-106 Storm Hazards Project	March 1988
	6. Performing Organization Code

7. Author(s)	8. Performing Organization Report No.
John H. Helsdon, Jr.	SDSMT/IAS/R-87/02
	10. Work Unit No.
	505-68-01-01

9. Performing Organization Name and Address	11. Contract or Grant No.
South Dakota School of Mines and Technology Institute of Atmospheric Sciences Rapid City, SD 57701-3995	NAG1-463
	13. Type of Report and Period Covered

12. Sponsoring Agency Name and Address	
National Aeronautics and Space Administration Langley Research Center Hampton, VA 23665-5225	Contractor Report
	14. Sponsoring Agency Code

15. Supplementary Notes
Langley Technical Monitor: Bruce D. Fisher Final Report March 15, 1984 - June 14, 1987

16. Abstract

A recently developed storm electrification model (SEM) has been used to investigate the operating environment of the F-106 airplane during the NASA Storm Hazards Project. The model is two dimensional, time dependent and uses a bulk water microphysical parameterization scheme. Electric charges and fields are included, and the model is fully coupled dynamically, microphysically and electrically. An analysis of one flight showed that a high electric field was developed at the aircraft's operating altitude (28 kft) and that a strong electric field would also be found below 20 kft; however, this low-altitude, high-field region was associated with the presence of small hail, posing a hazard to the aircraft. An operational procedure to increase the frequency of low-altitude lightning strikes was suggested. To further the understanding of lightning within the cloud environment, a parameterization of the lightning process was included within the SEM. It accounted for the initiation, propagation, termination and charge redistribution associated with an intracloud discharge. Finally, under a subcontract to this grant, Electro Magnetic Applications, Inc., developed a randomized lightning propagation scheme and investigated the effects of cloud particles on the initiation of lightning.

17. Key Words (Suggested by Author(s))	18. Distribution Statement
Triggered Lightning F-106B airplane Storm electrification Thunderstorm electrical modeling	Unclassified - Unlimited Subject Category 47

19. Security Classif. (of this report)	20. Security Classif. (of this page)	21. No. of pages	22. Price
Unclassified	Unclassified	136	A07